

**Università degli Studi di Padova**  
**Dipartimento di Ingegneria Civile, Edile e Ambientale**  
*Department of Civil, Environmental and Architectural Engineering*

**Corso di laurea magistrale in Environmental Engineering**



Tesi di laurea

**High resolution geomatics techniques for coastline  
detection and monitoring: Boccasette and Barricata  
case studies (Po River Delta, Rovigo, Italy).**

**Relatore: Prof. Ing. Massimo Fabris**

**Laureando: Mirco Balin  
M: 2019272**

**Anno accademico 2021 – 2022**



Università degli Studi di Padova  
Laboratorio di Rilevamento e Geomatica  
Master's thesis *Land Planning and Management* course  
Environmental Engineering

High resolution geomatics techniques for coastline  
detection and monitoring: Boccasette and Barricata  
case studies (Po River Delta, Rovigo, Italy).

Thesis advisor: Massimo Fabris  
Student: Mirco Balin  
July 2022



## **Abstract**

The topic studied in this thesis aims to analyze an experimental approach for the definition of a methodology that allows the identification of the coastline, or instantaneous coastline, perceived as a land-sea-air interface. As we will see its geographical boundaries are not easily defined in a universal way, we will see through the comparison between three different methodologies, including the GNSS system the classical topography and the methodology of photogrammetric survey SfM (Structure from Motion), the difficulties encountered in defining an extension to land and sea that delimits the coastline in a unique way.

The treated area concerns areas on the Po delta, specifically the beaches of Boccasette and Barricata.

In the chapters will be addressed the various aspects, first analyzing the context of reference, identifying the location, with an introduction to the coastal reality in question, characterized by phenomena such as subsidence, a worrying phenomenon for the Po delta area, monitored by several studies over the years.

The various methodologies applied in the context will be explained, exposing the characteristics of the same to understand their potential in the case study, then passing to the software used to process data and obtain the output. The data obtained with the various methodologies have been compared with each other in GIS thanks to the potential that the software offers, proving practical and fast.

The approach of the study mainly uses the distance and the area between the segments joining the points detected, evaluating the differences in terms of mean and standard deviation, to establish, also on the basis of the operator's interpretation, which of the following methodologies is the most practical, precise and fast for monitoring purposes.

We then went on to compare and discuss the results obtained with the various methods, highlighting the more or less significant variations. As we will see, there is a certain difference between the methodologies used directly in the

field, by measuring the physical points and the SfM technique, influenced as we will see by many factors.

The coastline at zero level obtained through a DTM (Digital Terrain Model) was subsequently superimposed and compared with the coastline extracted from a LiDAR survey performed in 2018. This second activity allowed, through appropriate processing, a four-year multi-time analysis of coastline changes and the identification and classification of areas of expansion and erosion. The research thus made it possible to:

- A comparison between the different methodologies comparing their applicability and limits;
- Evaluate and define the most appropriate relevant technique to study and identify the coastline;
- Define the accuracy parameters for modelling the detected elements;
- The creation of a database for possible future comparisons of coastal variations;
- The possibility of conducting a multi-temporal analysis with available LiDAR data.

High resolution geomatics techniques for coastline detection and monitoring:  
Boccasette and Barricata case studies (Po River Delta, Rovigo, Italy).

High resolution geomatics techniques for coastline detection and monitoring:  
Boccasette and Barricata case studies (Po River Delta, Rovigo, Italy).



## Acknowledgements

In this space I would like to take the opportunity to thank all those who, even in a small way, have helped me throughout my studies.

In particular, I want to thank the professors of the Laboratory of Surveying and Geomatics at the University of Padova, for having kept alive during the lessons the passion for the topographic field, for having followed me in completing the thesis with personal satisfaction. First of all I would like to thank the Engineer Massimo Fabris, thesis advisor, who immediately made himself available to help me, proposing various themes of thesis to facilitate my choice according to my interests, also offering me the opportunity to participate in the survey of Barricata treated in the thesis theme, he was able to advise me and provided me with the missing skills, following me patiently in the development of the thesis to achieve this result.

A thank you also goes to Engineer Andrea Menin, who at the end of the three-year engineering course convinced me to continue my studies, and was always available to help and advise me.

I would also like to thank the Geologist Michele Monego, who followed me, helped me and provided me with the necessary material to complete my work, always proving to be attentive and helpful.

I also thank the teammates who shared the experience of the 25/02/2022 in the Barricata coast.

Thanks to my family that has always been close to me and has supported me unconditionally in good and bad times, never letting me lack anything and leaving me full freedom to choose my own path, giving me all the means to achieve this result. I could never have achieved this without their teachings.

Thanks to all my classmates, who have enriched and made the tortuous path less hard during these years, marked by dark moments like the pandemic in which it was not easy to even meet each other.

Thanks again to all the friends and life companions in whom I have always felt their support.

High resolution geomatics techniques for coastline detection and monitoring:  
Boccasette and Barricata case studies (Po River Delta, Rovigo, Italy).

# Index

<b>1</b>	<b>Introduction.....</b>	<b>1</b>
<b>2</b>	<b>The context of reference .....</b>	<b>5</b>
2.1	Land subsidence in the Po River Delta .....	6
2.2	Historical evolution of sites .....	10
2.3	The coasts of Boccasette and Barricata.....	16
<b>3</b>	<b>Techniques and methodologies for the survey .....</b>	<b>19</b>
3.1	The approach to the study of the coastal area .....	20
3.2	Survey methods.....	21
3.2.1	<i>Classical instrumentation (Total Station).....</i>	<i>23</i>
3.2.2	<i>GNSS (Global navigation satellite system) .....</i>	<i>28</i>
3.2.3	<i>Photogrammetry (Drone).....</i>	<i>45</i>
3.3	Software used.....	53
3.3.1	<i>Agisoft Metashape .....</i>	<i>54</i>
3.3.2	<i>AutoCAD.....</i>	<i>55</i>
3.3.3	<i>QGIS.....</i>	<i>55</i>
3.3.3.1	Reference Systems .....	56
<b>4</b>	<b>Acquisition processing and data return .....</b>	<b>63</b>
4.1	The objectives .....	64
4.2	In situ data acquisition .....	66
4.3	Image processing with SfM technique .....	71
4.4	Geomatic data processing for coastline definition with AutoCAD .....	82
4.5	Geomatic data processing for coastline definition with QGIS.....	86
4.5.1	<i>Methodology for comparing classical topography (Total Station) and GNSS .....</i>	<i>88</i>
4.5.1.1	Calculation with distances.....	89
4.5.1.2	Calculation with areas .....	92
4.5.2	<i>Methodology for comparing photogrammetry and GNSS.....</i>	<i>94</i>
4.5.2.1	Calculation with distances.....	95
4.5.2.2	Calculation with areas .....	96
4.6	Multi-temporal study for the estimation of coastline changes in GIS. ....	98
4.6.1	<i>Methodology for comparing Photogrammetry and LiDAR.....</i>	<i>98</i>
4.6.1.1	Multi-temporal comparison with area analysis.....	99

<b>5</b>	<b>Monitoring results and discussion.....</b>	<b>101</b>
5.1	General background on the results .....	102
5.2	Comparison of results between different methodologies .....	102
5.2.1	<i>Boccasette results</i> .....	104
5.2.1.1	GNSS and PHOTOGRAMMETRIC RESTITUTION (distances)...	104
5.2.1.2	GNSS and PHOTOGRAMMETRIC RESTITUTION (areas) .....	109
5.2.1.3	GNSS and CLASSICAL TOPOGRAPHY (distances).....	111
5.2.1.4	GNSS and CLASSICAL TOPOGRAPHY (areas).....	115
5.2.2	<i>Barricata results</i> .....	117
5.2.2.1	GNSS and PHOTOGRAMMETRIC RESTITUTION (distances)...	117
5.2.2.2	GNSS and PHOTOGRAMMETRIC RESTITUTION (areas) .....	124
5.2.2.3	GNSS and CLASSICAL TOPOGRAPHY (distances).....	126
5.2.2.4	GNSS and CLASSICAL TOPOGRAPHY (areas).....	129
5.3	Evaluation multitemporal analysis .....	131
<b>6</b>	<b>Conclusions and Future Developments.....</b>	<b>135</b>
<b>7</b>	<b>Bibliography .....</b>	<b>139</b>

## Figure index

Figure 1 Location of the PRD area in northern Italy, branches of the river, and main areas of interest (Boccasette and Barricata). Coordinates are in the RDN2008 / Zone 12 (N-E) reference system, orthophoto 2018. ....	6
Figure 2 Graphic illustration of different types of land subsidence (source: Wikipedia). ....	7
Figure 3 Subsidence rate changes from 1950 to 2017 based on the available data (source: Monitoring the Coastal Changes of the Po River Delta (Northern Italy) since 1911 Using Archival Cartography, Multi-Temporal Aerial Photogrammetry and LiDAR Data: Implications for Coastline Changes in 2100 A.D.).....	12
Figure 4 Overlays using old datasets for erosion study, (a) detail related to subarea 3 (Bonelli Levante Basin) is also shown (b) together with orthophotos obtained from the 1955 (c), 1977 (d), and 2014 (e) surveys, highlighting the large surface deformations that emerged in the 1955-1977 comparison.1977 (source: Monitoring the Coastal Changes of the Po River Delta (Northern Italy) since 1911 Using Archival Cartography, Multi-Temporal Aerial Photogrammetry and LiDAR Data: Implications for Coastline Changes in 2100 A.D.).....	13
Figure 5 Coastlines obtained from aerial photogrammetric surveys performed in 1944 (green), 1955 (red), 1962 (magenta), 1977 (yellow), 1999 (cyan) and 2008 (blue) overlapped on the orthophoto generated from the 2014 one. Details A, B, C show relevant changes in multi-temporal analysis (source: Coastline evolution of the Po River Delta (Italy) by archival multi-temporal digital photogrammetry). ....	14
Figure 6 Sequence related the ascent of the salt wedge in the Po Delta at the years: a) Fifties-Sixties; b) Seventies-Eighties; c) 2000s. ....	16
Figure 7 Barricata beach seen from multiple angles. ....	17
Figure 8 Boccasette beach seen from multiple angles.....	18
Figure 9 Total Station for measuring angles and distances (source: faradsrl.it).....	23
Figure 10 From left to right we have first the tripod, second case we can clearly see the plate with the screw in the middle, in the third case view from above (source: slide for GIS course by M. Fabris). ....	23
Figure 11 Details previous image. ....	23
Figure 12 On the left we have the image related to the base screws for centering the bubbles of the spherical and toric levels, on the right the optical (or digital) lead for centering the point in the ground (source: slide for GIS course by M. Fabris). ....	24
Figure 13 Spherical level on the left and toric on the right (source: slide for GIS course by M. Fabris).....	25
Figure 14 Azimuth angle (source: slide for GIS course by M. Fabris). ....	25
Figure 15 Zenith angles (source: slide for GIS course by M. Fabris).....	26
Figure 16 Characteristics of signals for the precise collimation of the points.....	27

Figure 17 TOPCON GNSS Receiver (source: geoshack.com). .....	28
Figure 18 WGS84 system diagram (source: author). .....	29
Figure 19 GPS Constellation (source: code7700.com). .....	31
Figure 20 Position of the satellite relative to the Earth and its center. (source: author). .....	31
Figure 21 One satellite (source: code7700.com).....	32
Figure 22 Two satellite (source: code7700.com). .....	32
Figure 23 Three satellite (source: code7700.com). .....	33
Figure 24 Four satellite (source: code7700.com). .....	33
Figure 25 GPS system control stations (source: slide for GIS course by M. Fabris).....	34
Figure 26 Signals emitted by satellite and receiver, respectively (source: author). .....	37
Figure 27 Types of positioning (source: author).....	38
Figure 28 Types of measurement (source: author).....	39
Figure 29 Disruption Ionosphere and Troposphere. ....	40
Figure 30 Difference in the disturbance according to receiver and satellite position (source: electroyou.it). .....	40
Figure 31 Cut off angle (source: author). .....	41
Figure 32 GPS-based altitude measurement (source: mondogeo.it). .....	42
Figure 33 Differential GNSS. ....	43
Figure 34 Networked Transport of RTCM via Internet Protocol (source: www.swisstopo.admin.ch). .....	44
Figure 35 Drone used for surveying (source: parrot.com).....	45
Figure 36 Grip pattern between two frames (source: Zanichelli). .....	46
Figure 37 Land-covering scheme with a photogrammetric flight organized into straight, parallel trajectories during which a certain number of frames called a swipe is taken (source: Zanichelli).....	47
Figure 38 Overlap between different frames and swipes (source: Zanichelli).....	47
Figure 39 Schematic example photogrammetric camera (source: slide for GIS course by M. Fabris).....	48
Figure 40 Image plane diagram and acquisition center (source: slide for GIS course by M. Fabris).....	48
Figure 41 On the left geoid and ellipsoid representation, on the right earth surface and reference surfaces (source: openoikos.com). .....	57
Figure 42 Local and global datum comparison with geoid (source: 3dmetrica.it).....	58
Figure 43 Conical, cylindrical and tangent plane projection (source: openoikos.com). .....	58
Figure 44 Zones and bands in the UTM system (source: openoikos.com).....	59
Figure 45 Main projected SRs used in Italy and their EPSG codes (source: openoikos.com). ..	60
Figure 46 Measurement scheme carried out with Total Station (source: software QGIS). .....	66
Figure 47 Measurement acquisition with Total Station in Boccasette.....	67
Figure 48 Measurement scheme carried out with GNSS (source: software QGIS).....	67
Figure 49 Measurement acquisition with GNSS in Boccasette. ....	68

Figure 50 Target for the Drone. ....	68
Figure 51 Photogrammetric acquisition scheme in Barricata. ....	69
Figure 52 Measurement acquisition with Drone in Barricata. ....	70
Figure 53 Image block after photogrammetric survey. ....	70
Figure 54 Loading images within the Agisoft Metashape software. ....	72
Figure 55 Screenshot of Metashape with photo alignment setting. ....	73
Figure 56 Sparse cloud. ....	73
Figure 57 Screenshot of Metashape with the dense cloud setting. ....	74
Figure 58 Dense cloud. ....	74
Figure 59 Screenshot of Metashape with the mesh setting. ....	75
Figure 60 Mesh of Barricata. ....	76
Figure 61 Screenshot of Metashape with the texture setting. ....	76
Figure 62 Final product following texture mesh dressing for Boccasette. ....	78
Figure 63 Final product following texture mesh dressing for Barricata. ....	79
Figure 64 Screenshot of Metashape with the DEM setting. ....	80
Figure 65 Product processing DEM for Barricata. ....	81
Figure 66 Geomatic data in text format. ....	82
Figure 67 Plug-in DxfF_Coo setting. ....	83
Figure 68 Algorithm created on Grasshopper for Rhino 7. ....	84
Figure 69 Algorithm details first box at left image 68. ....	84
Figure 70 Result with AutoCAD software for distances and areas. ....	85
Figure 71 Points exported to QGIS from csv. format Excel files related to Total Station and GNSS. ....	87
Figure 72 Reference system display from notepad. ....	88
Figure 73 QGIS field calculator setting for line point distance. ....	89
Figure 74 Setting the QGIS field calculator to obtain the distance value. ....	90
Figure 75 Result processing with distances in meters. ....	90
Figure 76 With field calculator. ....	91
Figure 77 With expression. ....	91
Figure 78 Layer union with positive and negative distances for calculating mean and standard deviation. ....	92
Figure 79 Area created between the two lines as a result of the polygonize command. ....	93
Figure 80 Setting to cut polygons. ....	93
Figure 81 Layer union with positive and negative areas for calculating mean and standard deviation. ....	94
Figure 82 Plotting the coastline from the orthophoto. ....	95
Figure 83 Result processing with distances in meters. ....	96
Figure 84 Line photogrammetry and GNSS on Boccasette. ....	97
Figure 85 Area created between the two lines as a result of the polygonize command. ....	97
Figure 86 Zero-line cleaning produced by QGIS. ....	99

Figure 87 Local expansion and erosion, zero line in the Boccasette multitemporal comparison. ....	100
Figure 88 Po delta area as seen from satellite (Kosmosnimki.ru).....	103
Figure 89 Boccasette weather conditions January 27, 2022. ....	104
Figure 90 Difficulty in drawing the line (green) directly from Orthophoto for Boccasette. ....	105
Figure 91 Total GNSS and photogrammetry comparison. ....	106
Figure 92 Variation between GNSS and photogrammetry in the area covered by the orthophoto. ....	106
Figure 93 Comparison of GNSS and photogrammetry in unproblematic areas. ....	107
Figure 94 Very low correspondence between GNSS and photogrammetry. ....	108
Figure 95 Positive and negative areas between GNSS line and photogrammetric restitution. ....	110
Figure 96 GNSS beach/sea boundary line. ....	110
Figure 97 Considerable variations between the two lines. ....	111
Figure 98 Variation between GNSS and Total Station. ....	112
Figure 99 Cover length of different methods. ....	113
Figure 100 Excellent tracking between GNSS and Total Station. ....	113
Figure 101 Localized points where deviation error increases. ....	114
Figure 102 Positive and negative areas between GNSS line and classical topography. ....	116
Figure 103 Small variations between the two lines. ....	116
Figure 104 Different land-sea boundary geometry between Boccasette and Barricata, using GNSS points. ....	117
Figure 105 Barricata weather conditions February 25, 2022. ....	118
Figure 106 Maximum distance in restitution from photogrammetry to GNSS line. ....	118
Figure 107 General framing coastline restitution lines (GNSS and photogrammetric restitution). ....	119
Figure 108 Wave behavior in line identification. ....	120
Figure 109 Wave behavior in line identification. ....	121
Figure 110 Good coastline identification. ....	122
Figure 111 Areas with more intense wave motion. ....	124
Figure 112 Areas with milder wave motion. ....	125
Figure 113 Excellent tracking between GNSS and Total Station. ....	126
Figure 114 Localized points where deviation error increases. ....	127
Figure 115 Negative area zone. ....	129
Figure 116 Area with good restitution. ....	130
Figure 117 Multi-temporal study result for Boccasette. ....	131
Figure 118 Multi-temporal study result for Barricata. ....	132



## **Graph index**

Graph 1 Comparison between GNSS and photogrammetric restitution (Boccasette). .....	109
Graph 2 Comparison between GNSS and Total Station (Boccasette). .....	115
Graph 3 Comparison between GNSS and photogrammetric restitution (Barricata). .....	123
Graph 4 Comparison between GNSS and Total Station (Barricata).....	128

High resolution geomatics techniques for coastline detection and monitoring:  
Boccasette and Barricata case studies (Po River Delta, Rovigo, Italy).

## **Acronyms**

LRG: Laboratorio di Rilevamento e Geomatica

GPS: Global Positioning System

GNSS: Global Navigation Satellite System

DGNSS: Differential Global Navigation Satellite System

PRD: Po River Delta

CTP: Conventional Terrestrial Pole

BIH: Bureau International de l'Heure

APR: Aeromobile a Pilotaggio Remoto

IMU: Inertial Measurement Unit

HDOP: Horizontal Dilution Of Precision

CAD: Computer Aided Design

GIS: Geographic Information System

GNU: General Public License

DBMS: Data Base Management System

CRS: Coordinate Reference Systems

SRS: Spatial Reference System

SR: Reference System

WGS84: World Geodetic System 1984

EPSG: European Petroleum Survey Group

RMS: Root Mean Square

DTM: Digital Terrain Model

RTK: Real Time Kinematic

DEM: Digital Elevation Model

DTM: Digital Terrain Model

DSM: Digital Surface Model

SfM: Structure from Motion

UTM: Universal Transverse of Mercator

OGC: Open Geospatial Consortium

High resolution geomatics techniques for coastline detection and monitoring:  
Boccasette and Barricata case studies (Po River Delta, Rovigo, Italy).

# 1 Introduction

On January 27th and February 25th, 2022, the Laboratory of Surveying and Geomatics (LRG) of the University of Padua was engaged in a series of survey campaigns in the area of the Po Delta. It is well known from several studies the fragility of the area, characterized in particular by the phenomenon of subsidence. Specifically, the objective of the study focuses on the beaches of Boccasette and Barricata. The choice of methodologies and instrumentation to be used was, first, linked to the extent of the details that we want to highlight and consequently to the precisions that we want to achieve in the measures, considering a high scale of detail. The coastal strip represents the transitional border between land and sea, characterized by geographical boundaries not universally definable, depending on the scale of the analysis. It is a natural and economic resource of great value, which due to various factors is subject to a continuous and incessant transformation.

We can define it as a highly dynamic system, characterized by phenomena of erosion or expansion of the coastline, led by numerous meteorological, geological and anthropic factors. We can therefore say that the waterline is the most evident state of how this branch is particularly dynamic, showing more or less immediately the evolutionary trends in progress.

An important aspect in the evaluation of erosive processes defined as "chronic", that is linked to the fluctuations of forcing that develop on long temporal scales (solid transport, subsidence, sea level rise), is that the phenomena must be analysed in an integrated way with the various dynamics.

For example, high rates of subsidence, or sea level rise, lead to a high demand for sedimentary input from rivers, which, if not met, activate irreversible erosion processes. Moreover, in our case both coasts are sandy, territories more subject to these evolutions and more vulnerable.

In the evaluation of erosive phenomena, therefore, all these factors must be known and properly monitored. It is important to know these aspects although the thesis is aimed at determining the most suitable methodology for the identification of the

coastline, to highlight the complexity of the phenomenon and therefore the importance of good monitoring.

Many studies have taken care and are generally concerned with the definition of the coastline, and the related problems, to obtain a return as reliable and truthful as possible. Assessing the location and changes of the coastline is an important consideration in coastal management, design and engineering. The location of the coast and its historical change is able to provide important information for the design of coastal protection works, plans for coastal development, and the calibration and verification of numerical models. In addition to the growing interest in coastal areas, there is also growing concern about the risks and consequences of increasing anthropogenic pressures. The set of needs and problems reported makes us understand the complexity and need, to carry out studies in order to better define these areas, also through surveys close in time. It is therefore necessary to identify effective methods for the extrapolation of the same, which are a good compromise between accuracy, time and cost. As we will see in the thesis, the time factor in these areas plays an important role, in fact, for both areas studied the measurements were taken at low tide, so for a limited time interval.

Effective detection involves the development of technologies and appropriate approaches to provide knowledge over time useful for safeguarding, prevention, intervention and management. As we will see, there is no unique way to draw the coastline, we can in fact use different technologies, which offer different results and precisions. Specifically, we will deal basically with two blocks of investigation:

- Traditional topographies (with Total Station) and GNSS (differential mode), which allow to obtain high precisions, on the order of millimeters/centimeters, and provide a relief for points;
- Aerial images (drone) that then need to be orthorectified and mosaic, in this case we do not have a punctual relief, and we get the entire area detected at the time of shooting.

In this way, we have obtained comparable datasets for both studied areas that, in addition to providing a database for possible future studies, allow us to define the fastest methodology in the interest of obtaining a detailed scale. The comparison of the methodologies also allows through the results to obtain a perception on the influence of the operator in the acquisition of the points. We will see in fact that in

addition to the speed of relevant methodologies such as GNSS in differential mode is much more practical than a Total Station, which requires two operators, and a point acquisition in a partially static way. Regarding SfM, we can not say that it is not accurate, but as we will see it did not provide excellent results for the chosen scale of study, due to problems related to the site, and the constraints of the method in some climatic conditions. However, it should be remembered that the choice of the most suitable methodology must be made on the basis of the detail that is intended to be reached in this discussion, we do not indicate the best methodology ever but for the object of study.

High resolution geomatics techniques for coastline detection and monitoring:  
Boccasette and Barricata case studies (Po River Delta, Rovigo, Italy).



## **2 The context of reference**

## 2.1 Land subsidence in the Po River Delta

River deltas, such as the Po River Delta (PRD) in the present case, are areas that host a large population and widespread economic activities and are among the most vulnerable areas to land subsidence. The PRD area is located in the east of northern Italy, washed by the waters of the Adriatic Sea (Figure 1), covers about 400 km<sup>2</sup>, and extends seaward for about 25 km. The geology is mainly composed of terrigenous sediments up to 2000 m thick and has a complex multi-falदे freshwater system<sup>1</sup>.

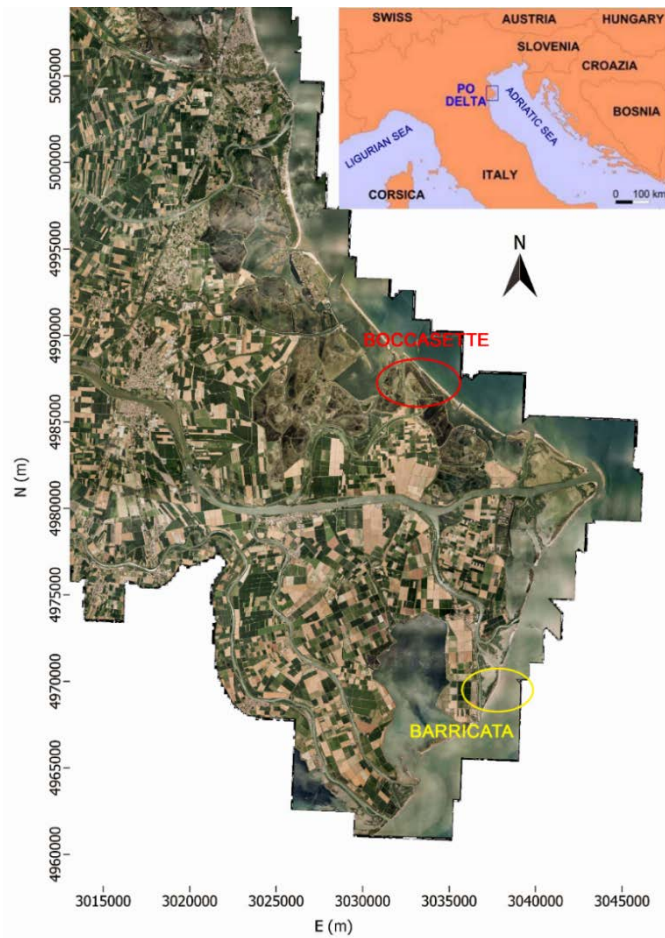


Figure 1 Location of the PRD area in northern Italy, branches of the river, and main areas of interest (Boccasette and Barricata). Coordinates are in the RDN2008 / Zone 12 (N-E) reference system, orthophoto 2018.

---

<sup>1</sup> It forms the largest floodplain in Western Europe.

Researches aimed at studying the phenomenon of subsidence in these areas are in continuous development especially in recent years in order to identify the temporal trend of the phenomenon and thus obtain a chronology of data to keep well monitored the behavior, which characterizes the whole area, including Boccasette and Barricata treated in the thesis. These areas are historically known for this problem, which we can see schematically in Figure 2.

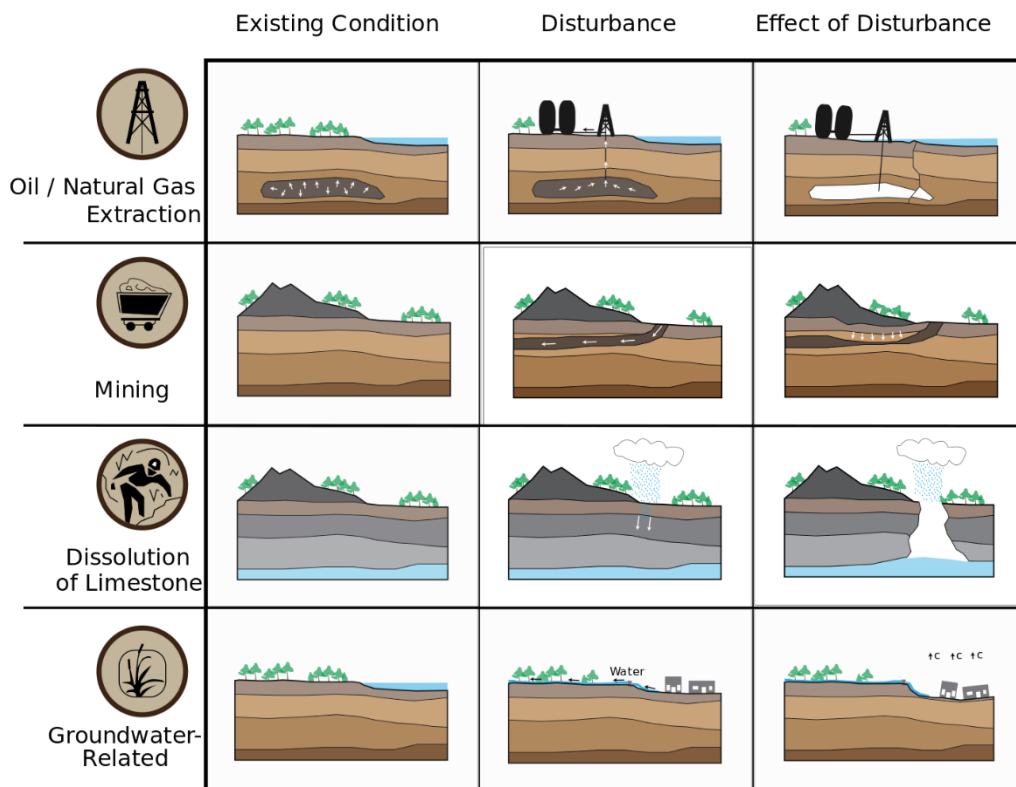


Figure 2 Graphic illustration of different types of land subsidence (source: Wikipedia).

Subsidence is defined as a vertical lowering of the earth's surface, independent of the cause that produced it. It is mainly due to natural processes and human activities and leads to considerable pressure on the stability of natural ecosystems as well as socio-economic consequences. These fragile territories that are vulnerable to subsidence are subject to various complications over time, such as progressive environmental degradation, morphological changes of coastlines and land areas, damage to buildings, and disruption of services. Areas affected by this issue are coastlines

characterized by a certain amount of moisture, such as in the present case the lagoon, which are increasingly vulnerable to flooding, in the most severe cases permanent.

What leads to the formation of this phenomenon in these areas is related to the complex combination of several factors, which can be natural and anthropogenic. Natural factors include, holocene sediment compaction<sup>2</sup>, tectonic movements, sinkhole formation<sup>3</sup>, volcanism, permafrost<sup>4</sup> thaw, and glacial isostatic adjustment (GIA).

In addition to all this, sea level rise, caused by climate change, can dramatically increase subsidence issues, thus resulting in severe impacts on both ecosystems and human activities in these areas.

We have introduced two basic causes, we can say that human-introduced subsidence generally occurs within a short period of time, on the order of a decade or so. On the other hand, among the anthropogenic factors, thus related to human activity we have; compaction of the aquifer system associated with depletion and storage of groundwater/oil/natural gas from quaternary deposits of medium depth (200-600 m), drainage of organic soils, underground mining, hydro-compaction and stress given by new construction.

Thus, there is a significant footprint in the loss of soil elevation relative to sea level in these ecosystems now considered increasingly vulnerable.

The risks to this area considered precisely vulnerable involve the intrusion of the sea into the land, which can lead to flooding and desertification.

To clarify the treatment and complexities on the area I quote a part of the scientific article "Monitoring of Land Subsidence in the Po River Delta (Northern Italy) Using Geodetic Networks."<sup>5</sup>:

---

<sup>2</sup> Holocene sediments consist of clays, varying in color from dark gray or light gray to yellow- stro, sometimes light green, and dark gray to light gray silts.

<sup>3</sup> Cavity of karst origin, due directly to erosion of limestone rocks by meteoric water filtering through fissures, or to subsidence of limestone as a result of dissolution of limestone by water circulating underground.

<sup>4</sup> Designates a terrain typical of cold regions where the soil is perpetually frozen (not necessarily with the presence of frozen water masses).

<sup>5</sup> Nicola Cenni, Simone Fiaschi, and Massimo Fabris. Department of Geosciences, University of Padova; UCD School of Earth Sciences, University College Dublin; Department of Civil, Environmental and Architectural Engineering—ICEA, University of Padova. Published: 13 April 2021.

«The formation of the modern delta is the result of natural processes and human interactions, such as the filling of the wetlands area and engineering endeavors. The eastern part of the delta is mainly characterized by reclaimed territories. At present day, the reclamation in the PRD area is strongly reduced and part of the territory (about 200 km<sup>2</sup>) is characterized by a large system of shallow water bodies. Most of the reclaimed territories are actually below the mean sea level and are poorly supplied by sediments because all its river branches have major artificial levees. The complex-wide sandy beach ridges elongating from south to north can be considered as the natural western border of the reclaimed territories. The compaction of the Plio-Quaternary alluvial deposits in the PRD area is an important driver of the natural ground settlement in these territories: in particular, suggests that the land subsidence rates in the delta area are significantly correlated with the age of the highly compressible Holocene deposits that compose the shallowest 30–40 m of the sedimentary sequence. Other authors obtained similar results by analyzing the correlation between the age of the Holocene sediments and the compaction rate observed in the Southern Louisiana Mississippi delta. Their results show land subsidence rates of about 4–5 mm/year for deposit of ages and thicknesses similar to those present in the PRD. An additional contribution to the natural land subsidence can be related to tectonic movements: some authors (e.g. suggest a contribution of about 1 mm/year due to a crustal flexing induced by the south-westward subduction of the Adriatic plate under the Apennine belt. This subduction model seems to be not compatible with the evidence provided by seismic surveys, which do not show an evident and well-developed slab, and with a maximum depth of more than 90 km of the earthquakes occurring in the Northern Apennines. An alternative model suggests that the present deformation pattern observed in the Apennine belt and the Po Plain is driven by the northward motion of the Adriatic plate, instead of the rollback of the Adriatic subducted margin. The sedimentary basin of the Po Plain is also characterized by a complex system of non-

confined, semi-confined, and confined aquifers. The extensive exploitation of these aquifers can be considered as one of the principal causes of the anthropogenic land subsidence observed in both the plain and the delta areas. Because of the important historical and natural patrimony located in the Po Plain and the large concentration of industrial facilities as well as the intensive farming in this area, it is necessary to systematically monitor the occurrence and development of the land subsidence phenomenon.»

An additional factor of concern nowadays that is becoming increasingly topical is the eustasy<sup>6</sup> of the Adriatic Sea, which could further increase the vulnerability of coastal areas.

## **2.2 Historical evolution of sites**

The Po Delta area has been the subject of study for more than fifty years, the land consumption data increased during Italy's economic growth after the end of World War II. In those years, the multi stratum system of the Po Valley was widely exploited for anthropogenic uses, including industrial and agricultural. To all this must be added the withdrawal of water and methane from onshore and offshore reservoirs, which increased the problems related to land subsidence, in addition to the natural phenomena already mentioned. In this discussion we will go over past results, which have led to the need for repeated monitoring. Soil deformation zones can be monitored with geometric methodologies that provide high-precision, high-resolution data. Initially, the most widely used methodology was geometric levelling for elevation changes, and photogrammetry to reconstruct soil deformation over long periods with multi-temporal surveys to show changes at the planimetric level. Photogrammetry, in fact, makes it possible to acquire the coordinates of a large number of points, for the construction of useful models to quantify the intensity of the phenomenon.

---

<sup>6</sup> Eustasy is the phenomenon of global-scale rise or fall in mean sea level, that is, not dependent on local phenomena such as subsidence. Along coastlines it causes backward and forward movement of the sea relative to the coast.

Thus, the imprint of man and his activities on fragile territories such as the Po River Delta (PRD) is well known. A time mirror that clearly summarizes the historical trend is again reported by the scientific article "Monitoring of Land Subsidence in the Po River Delta (Northern Italy) Using Geodetic Networks," which reports the following:

« The land subsidence rates increased during the Italian economic growth, after the end of the Second World War: in that period, the multi-aquifers system of the Po Plain was extensively exploited for anthropic uses (industrial and agricultural).

The methane-water withdrawals from onshore and offshore reservoirs have also contributed to the increase of the land subsidence values. Used precise leveling surveys performed in the 1950–1957 in the PRD and Po Plain to measure land subsidence rates up to 300 mm/year. Subsequently, leveling data obtained from 1962 to 1974, highlighted a progressive reduction of the rates with values of about 30 mm/year, in agreement with the progressive reduction of the anthropogenic withdrawals.

During the late 1970s and at the beginning of the 1980s, the construction of new public aqueducts exploiting surface waters significantly reduced the aquifer overdraft and yielded a general progressive head recovery with a significant decrease of the land subsidence rate. Recent studies indicate a decrease of the land subsidence rates with values less than 10 mm/year, probably as a consequence of the successful policies applied 40 years ago to reduce the anthropogenic deformations in the PRD.»

It follows that since 1950 the Military Geographic Institute (IGMI) has carried out frequent measurements, which have also involved local agencies, companies and institutions. If we go to consider the graph (Figure 3) related to the monitoring of

coastal changes in the Po Delta, using archival cartography, we can see the following.

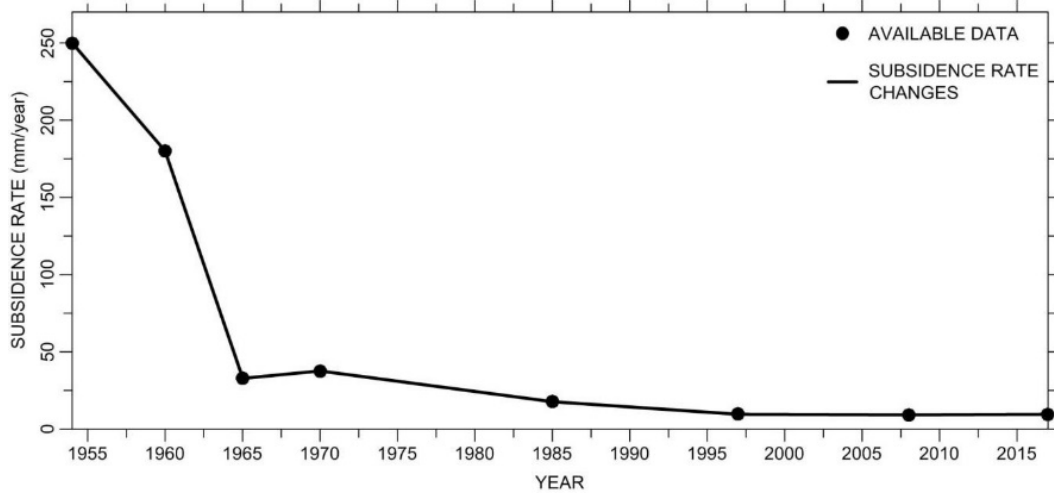


Figure 3 Subsidence rate changes from 1950 to 2017 based on the available data (source: Monitoring the Coastal Changes of the Po River Delta (Northern Italy) since 1911 Using Archival Cartography, Multi-Temporal Aerial Photogrammetry and LiDAR Data: Implications for Coastline Changes in 2100 A.D.).

At the planimetric level these variations are well known from the restitution of archival cartography, which allows us a century-long time comparison, significantly highlighting the variations along the coast.

In the following image (Figure 4), therefore, we see that the 2014 orthophotos were overlaid with all available returns from archival cartography (1911-1924), photoplans (aerophotogrammetric surveys carried out in 1933, 1944 and 1949) and photogrammetric models (surveys carried out in 1955, 1962, 1969, 1977, 1983, 1990, 1999 and 2008) using stereoscopic devices.



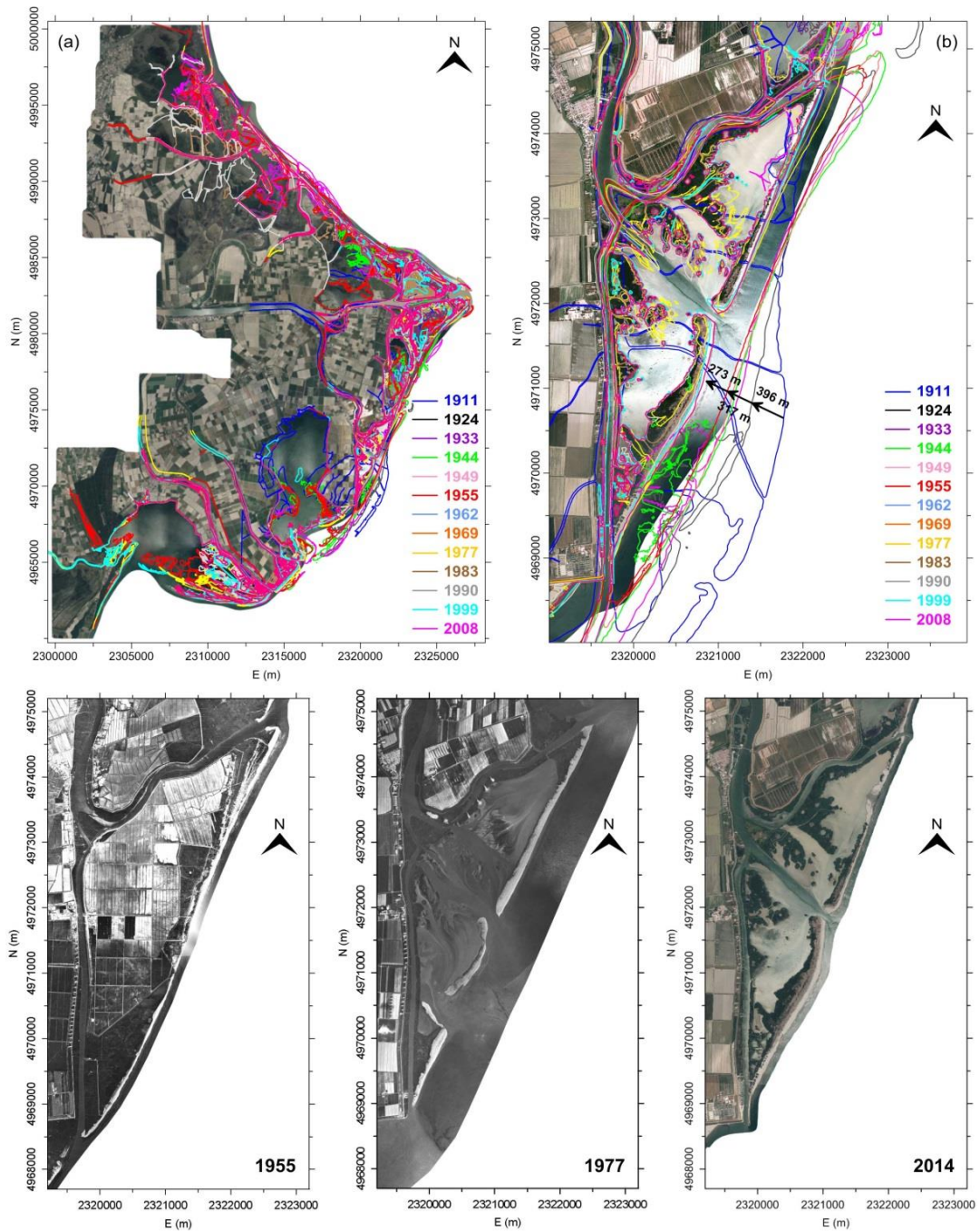


Figure 4 Overlays using old datasets for erosion study, (a) detail related to subarea 3 (Bonelli Levante Basin) is also shown (b) together with orthophotos obtained from the 1955 (c), 1977 (d), and 2014 (e) surveys, highlighting the large surface deformations that emerged in the 1955-1977 comparison. 1977 (source: Monitoring the Coastal Changes of the Po River Delta (Northern Italy) since 1911 Using Archival Cartography, Multi-Temporal Aerial Photogrammetry and LiDAR Data: Implications for Coastline Changes in 2100 A.D.).

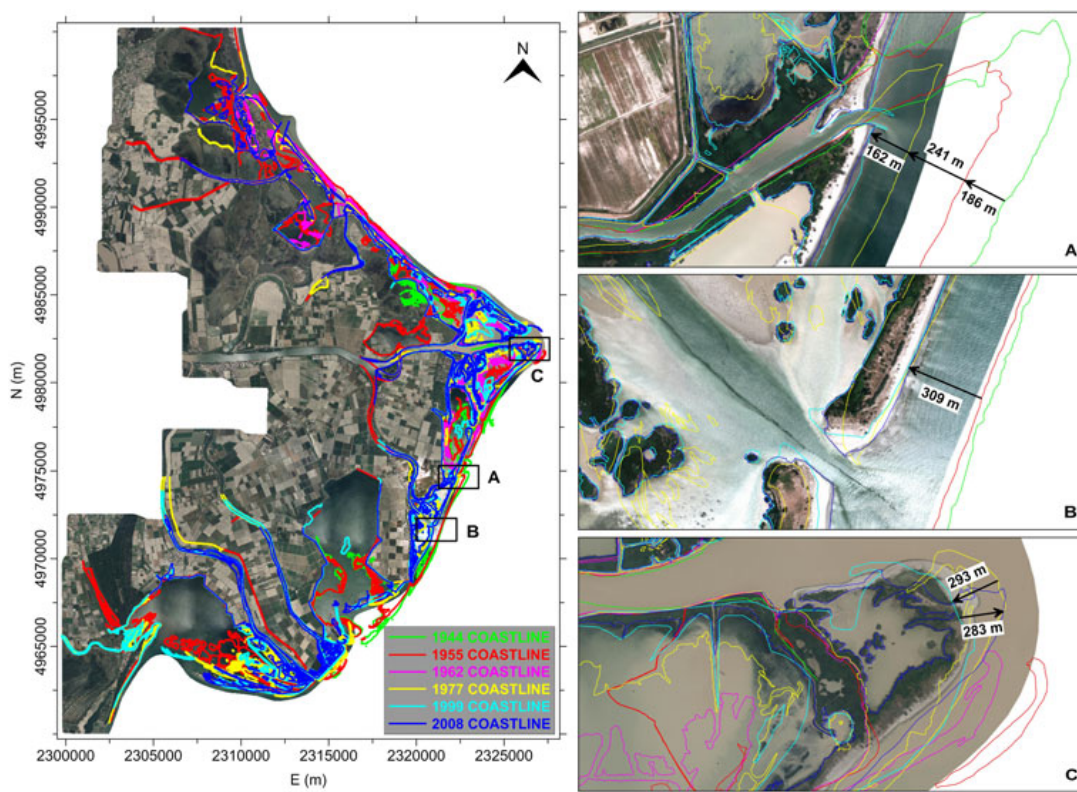


Figure 5 Coastlines obtained from aerial photogrammetric surveys performed in 1944 (green), 1955 (red), 1962 (magenta), 1977 (yellow), 1999 (cyan) and 2008 (blue) overlapped on the orthophoto generated from the 2014 one. Details A, B, C show relevant changes in multi-temporal analysis (source: Coastline evolution of the Po River Delta (Italy) by archival multi-temporal digital photogrammetry).

Without going into too much detail, the complexity of the area and the extent of the phenomenon is already known.

One encouraging fact is that the various studies conducted converge that the subsidence rate with time has decreased, through the mitigation actions implemented by the government and local organizations. On the other hand, however despite the fact that in recent decades it has significantly reduced, it is still high compared to natural values, and has affected the coastline of areas not protected by embankments. From the dynamics of the facts, it follows that most of the PRD is now below sea level, with the edges elevated to the sea and an immense depression in the middle, due to the exaggerated elongation of delta branches, anthropogenic stabilization of the hydrographic network and soil subsidence. The combination of issues, can lead to

serious environmental problems, leading to changes on the drainage of the secondary hydraulic network, increasing the expansion of the salt wedge for many kilometers inland.

The salt wedge is a characteristic feature of coastal areas and especially of deltaic mouths. The Po delta represents an optimal case study for the analysis of this process, which develops at riverbeds, coastal aquifers and soils facing the coast. This results in the transformation of fresh water from the land into water characterized by high degrees of salinity, as a result of the mixing phenomenon between fresh and salt water (Figure 6). This results from the velocity of the current, the inclination of the seabed, the distribution of density present within the water column, seasonality, and the alternation of water flow rates within the riverine area. Thus, saline intrusion occurs according to different mechanisms, particularly in the event that freshwater inflow is reduced relative to tides. As a result, some branches of water previously used for irrigation can no longer be used, or rather reduction of usable fresh water.

This phenomenon has also led to the disappearance of morphological elements typical of coastal wetlands and lagoons. For all these reasons, constant monitoring of changes throughout the complex ecosystem of the PRD is necessary in order to provide information to implement territorial defense systems against flooding.

All the measurements to monitor and sample the different areas will support the Veneto Region GNSS network and the PODELNET<sup>7</sup> (PO DELta NETwork) geodetic network designed to study subsidence in the Po Delta area. It is important to continue the study in these areas through approaches to acquire increasingly detailed data.

---

<sup>7</sup> Infrastructure materialized in June 2016 is a network consisting of 46 vertices, the location of which will be monitored every two years, and spatially extends from Porto Caleri (Rovigo) to Lido di Volano (Ferrara) in a north-south direction and west to the town of Adria (Rovigo).

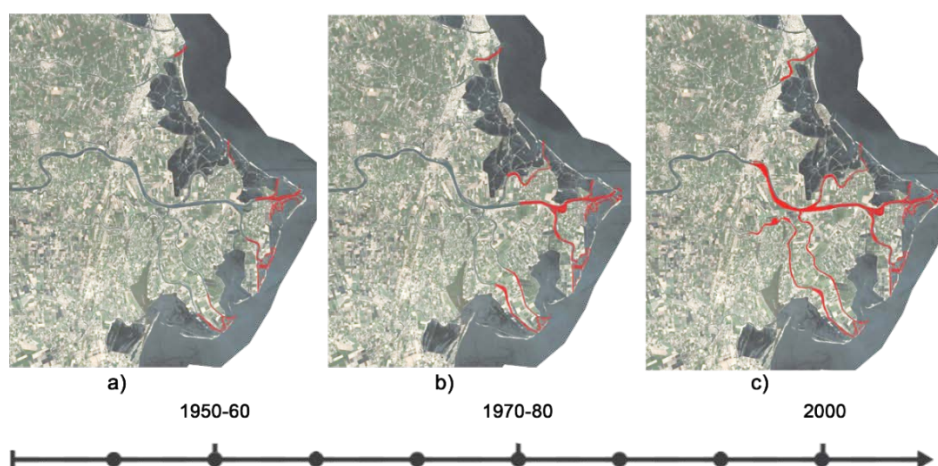


Figure 6 Sequence related the ascent of the salt wedge in the Po Delta at the years: a) Fifties-Sixties; b) Seventies-Eighties; c) 2000s.

### **2.3 The coasts of Boccasette and Barricata**

The Po delta is one of Europe's largest wetland natural areas, considered a National Park since 2006, and in 2015 obtained recognition as a Biosphere Reserve under the UNESCO MAB Program.

The beaches of Boccasette and Barricata are typical Venetian beaches reside in the outer part of the Po delta, directly facing the Adriatic Sea, with long tongues of sand called 'scanni'<sup>8</sup>. They are natural barriers created by the ebb and flow of the tides and the sandy material carried by the great river, and are often completely overridden by storm surges that flow into the first channels or pockets behind. They curb the violence of the waves that would otherwise break over the levees of the fishing valleys or create problems in the inland lagoons. They are formed of very unstable sand, therefore subject to constant change and evolution; only marsh reeds and sparse pioneer shrubs grow there, the only ones able to withstand the extreme conditions of wind and salt. For both, man's "rehabbing" has not led to significant changes, as it has for high Venetian littorals. In these areas, in fact, typical factory workings are not carried out. They are therefore places in which the physical variations of the coastline

---

<sup>8</sup> Accumulation of minute alluvial deposits in littoral or deltaic formations.

are not altered by repetitive anthropogenic workings. All this makes them natural places, suitable for measurements, to be able to study and obtain the multi-temporal behavior of the coast. In Barricata locality there are two equipped beaches. The first, "Barricata" island or scanno, can be reached during the summer season by crossing a characteristic mobile pedestrian bridge over the river (Figure 7); the other, Conchiglie Beach, is accessible year-round. The survey phase covered concerns the first beach, in fact given the survey period and the lack of a bridge for crossing, we were accompanied with the use of a small boat. At Barricata, it is possible to see the Po flowing into the sea and to discover the fascinating tangle of lands, canals, lagoons and sandbars. This environment is home to numerous resident and migratory bird species that are easy to encounter during excursions; red and grey herons, marsh harriers, black-winged stilts, pink flamingos.



Figure 7 Barricata beach seen from multiple angles.

Boccasette, however, can be reached by a narrow paved road from Boccasette in Porto Tolle (about 30 km. from the junction on the Romea state road), between fishing valleys and embankments, at the end of which there is a small parking lot. From the parking lot you cross a wooden walkway on the outer channel of the fishing

valleys. Several kilometers long, it is one of the few remaining 'free' beaches, mostly left completely in its natural state, even with some 'staking' and occasional cleaning (Figure 8). The abandonment to the natural state, to the force of the wind, to the violence of the sea storms, and to the imperceptible but relentless work of transporting materials from the river, is evident in the imposing mass of waste materials, including trees and various materials, especially garbage.

This last observation depicts the entire coastal area specifically for this case Boccasette and Barricata.



Figure 8 Boccasette beach seen from multiple angles.

### **3 Techniques and methodologies for the survey**

### **3.1 The approach to the study of the coastal area**

This experimentation is aimed at defining a methodology for identifying the coastline, which allows for a number of advantages in terms of accuracy, time and cost of the survey phase.

It is evident that the current period of climate change causes a considerable impact on beaches, considering also the insufficient transport of debris to the sea related to anthropogenic damming phenomena on catchment areas.

It should also be considered that the areas in question are subject to the phenomenon of subsidence, an aspect of considerable importance that complicates the dynamics of the study. The survey process was carried out on two different days, one for the coastal stretch of Boccasette on January 27, 2022, and the next on February 25, 2022 in the Barricata belt, both located in the PRD. The objective of this survey campaign aims at evaluating the three different methodologies used (classical topography with Total Station, GNSS, and drone Photogrammetry), in order to highlight pros and cons in the use of the same for the study of deformation aspects along the coastline.

The instrumental accuracies of the methods used differ from each other, but considering the context in which we find ourselves, we can say that the instrumental precision is far superior to the identification of the phenomenon we are studying, considering the wave motion that even if greatly reduced at low tide, is still present, we will therefore go to evaluate through the mean and standard deviation the difference between the various methods to assess the errors that can be obtained in identifying the coastline.

The choice of the most appropriate methodology will therefore be the product of a combination of advantages, including the time to perform the survey, an aspect of considerable importance considering that the low tide has a relatively short stability time, secondly but not least, depending on the chosen methodology it will be possible to extract more or less information of the study area.

The processed data, in addition to the evaluation of the current state for the coastline, allows to obtain a multi-time analysis in the evolution of the coastline variation at zero level, thanks to the comparison between photogrammetry performed in the survey campaigns covered by this thesis, and the LiDAR data of the year 2018.



The following instrumentation was used for the survey phase:

- Leica TCR1201 Total Station;
- GNSS TOPCON Hiper HR;
- Photogrammetry with Parrot Anafi Drone.

It was decided as we can see to operate by developing an "integrated" surveying experience that intertwined several surveying technologies, from the most modern to the most traditional ones, thus managing to achieve a comparable result based on the results obtained.

### **3.2 Survey methods**

Traditionally, the following operational methodologies are distinguished in topographic surveying: topographic (or indirect) instrumental surveying, in that measurements are not taken directly from the object, but through instruments with medium to high technological content, which allow their acquisition, and finally, photogrammetric surveying, developed mainly for land surveying, and aims to rigorously reconstruct the geometric correspondence between image and object at the time of acquisition, so in our case it allowed us to acquire metric data for the study of the coastline. This technique has become one of the fastest and most effective methodologies. The three different and autonomous methodologies were used by making them interact with each other in order to identify the most suitable for the study of the phenomenon. In our case we define instrumental (or indirect) surveying as that carried out with topographic instruments (classic topography, GNSS). For this type of surveying, as a rule, the measuring instrument is not placed directly on the object to be surveyed. Instrumental surveying is used for high-precision surveys, to determine the measurement of large objects, to survey inaccessible points, and to connect an object to the national trigonometric network. On the other hand, photogrammetric surveying is defined as surveying carried out with photographic imaging and restitution instruments (metric cameras, restitutors). Photogrammetric surveying is employed when a large amount of information is to be determined with respect to the elevations of interest (static instabilities, deterioration) or when a natural or man-made structure, the roofs of a building, an urban center, or a portion

of land is to be surveyed (aero photogrammetric surveying) as in the present case. As a rule, a survey is carried out through a series of distinct and concatenated operations, which for convenience are grouped into two phases: the first is the information retrieval phase, and the second is the information processing and return phase. The first phase of the survey involves:

- specification of the purpose of the survey
- field reconnaissance (site survey)
- retrieval of archival data
- survey design
- taking of measurements

The second phase of the survey involves:

- organization of the data
- graphic restitution

The methodology of the survey should be evaluated according to the type of information to be obtained, the time available, which as we shall see in the case under consideration is limited due to natural causes related to tidal times, the budget and the accessibility of the places to be surveyed, which is not particularly problematic for the research in question. In most cases, a combination of methods is inevitable, "integrated" surveying in order to obtain a result with high reliability.

### 3.2.1 Classical instrumentation (Total Station)

The instrumentation used was classical topographic with the use of a first-class Total Station of Leica brand (Figure 9), which allows the measurement of angles and distances necessary for monitoring the coastal variations under consideration. The use of the Total Station is made using a tripod, consisting of three extendable legs that are hinged to a plate, called a support plate or plinth. Seen from above (Figure 10) the plate has a triangular shape with rounded corners and a central hole.



Figure 9 Total Station for measuring angles and distances (source: faradsrl.it).

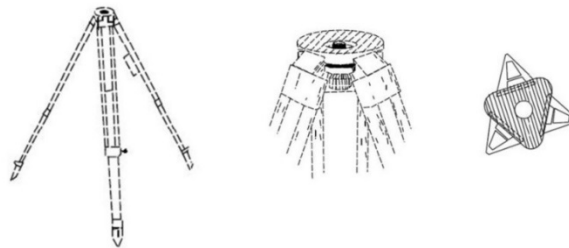


Figure 10 From left to right we have first the tripod, second case we can clearly see the plate with the screw in the middle, in the third case view from above (source: slide for GIS course by M. Fabris).

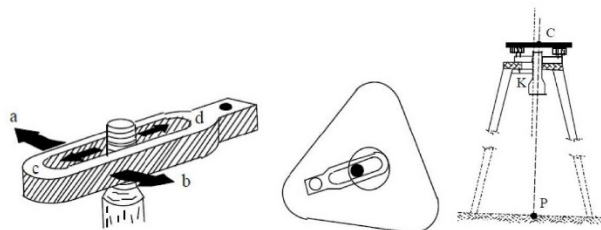


Figure 11 Details previous image.

When one wants to make a measurement, the first operation to be done is to put the tripod in station on the point, that is, to position the tripod so that the center of the hole of the support plate is approximately on the vertical passing through the point materialized on the ground and the plate is approximately horizontal. This operation is far from simple if you are in the countryside or in mountainous areas where you often work in uneven terrain with the presence of vegetation or rocky boulders, which requires that the legs of the tripod are of different lengths and uncomfortable positions. To achieve the purpose, one must consider and take advantage of the fact that the tripod legs are of variable length and independent of each other. Next verify that the position of the support plate is fairly centered on the point one can use a plumb line, or simply a small gravel dropped vertically from the center of the plate while a common mason's level can be used to put the support plate approximately horizontal. Once the instrument is fixed to the tripod and the point on the ground is centered, care must be taken that the levels are centered, that is, the spherical one present in the base plate and the toric one present in the fork of the optical telescope of the instrument. So, when the bubble is inscribed in the circle engraved on the spherical cap, in this condition the plane of the base is perfectly orrizontal, while in the toric to arrange the central tangent horizontally it is necessary to position the level itself so that the bubble is arranged with the ends equidistant from the central point of the graduation (as in the right part in Figure 13).

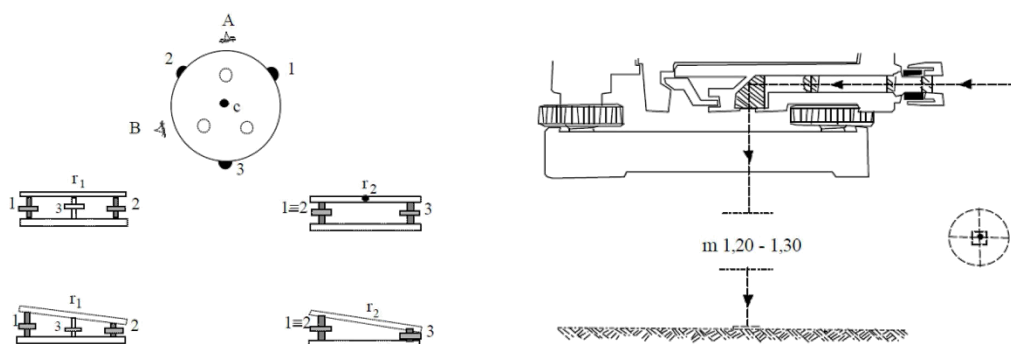


Figure 12 On the left we have the image related to the base screws for centering the bubbles of the spherical and toric levels, on the right the optical (or digital) lead for centering the point in the ground (source: slide for GIS course by M. Fabris).

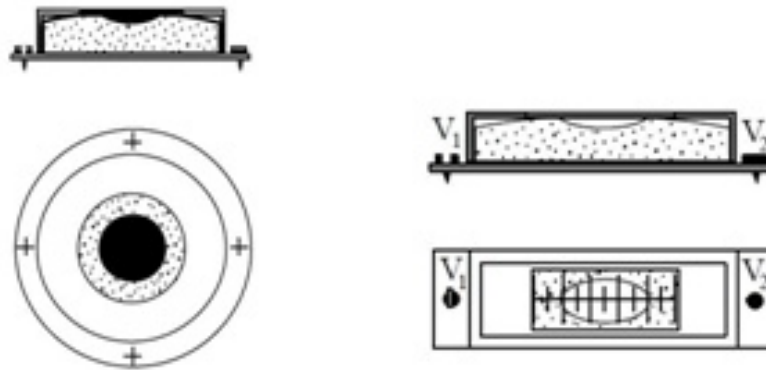
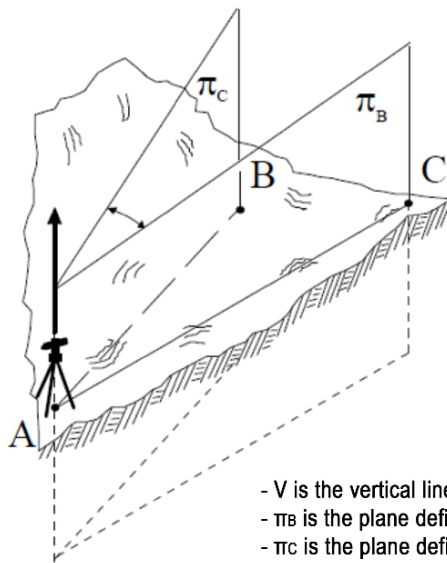


Figure 13 Spherical level on the left and toric on the right (source: slide for GIS course by M. Fabris).

As for the instrument, it consists of an electronic distance meter for measuring distances between the instrument and the point being framed, and two electronic protractors useful for the instrument to read horizontal called azimuth angle (Figure 14) and vertical called zenith angle (Figure 15) through a graduated circle.

#### Azimuth angle

We consider three points in the terrain A, B and C



- V is the vertical line passing through A;
- $\pi_B$  is the plane defined by the vertical V and the conjunct AB;
- $\pi_C$  is the plane defined by the vertical V and the conjunct AC;
- we call the azimuth angle the dihedral angle defined by the planes  $\pi_B$  and  $\pi_C$  and having the vertical V as its edge.

Figure 14 Azimuth angle (source: slide for GIS course by M. Fabris).

### Zenith angle ( $\xi$ )

Given a point A and a point B, the zenith angle  $\xi$  is the angle formed by the vertical for point A and the conjunction of points A and B

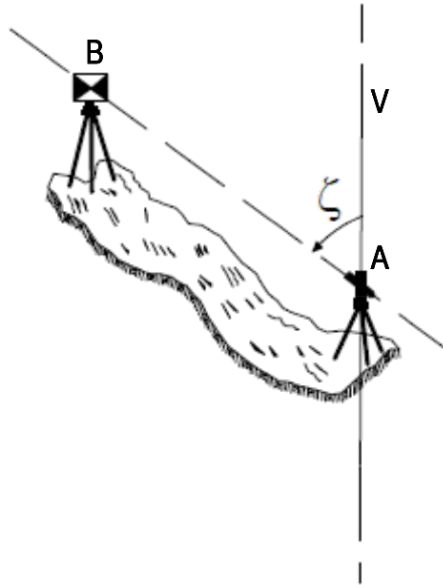


Figure 15 Zenith angles (source: slide for GIS course by M. Fabris).

All data measured in the field during the survey phase are stored in a card that can be pulled out of the instrument so that computer processing can be done later. The Total Station then allows us once we have determined angles and distances for a series of points, to determine the exact spatial location relative to a predefined coordinate system.

For maximum accuracy in distance and angular measurements, it is necessary once the instrument is put on station to collimate each point with the telescope until it is displayed exactly on the intersection of lines corresponding to the optical center of the target (Figure 16).

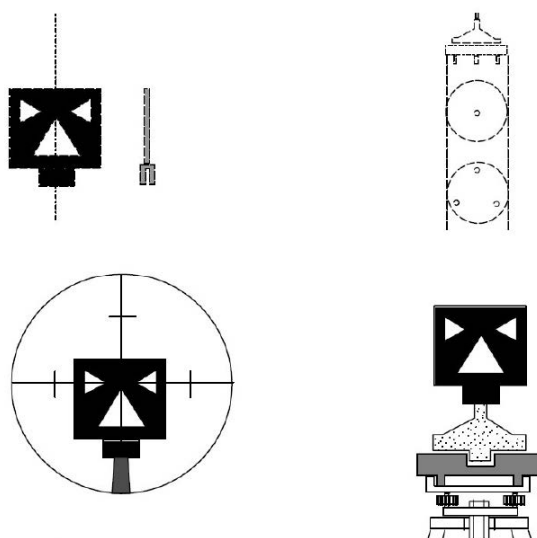


Figure 16 Characteristics of signals for the precise collimation of the points  
(source: slide for GIS course by M. Fabris).

For distance measurement, the Electronic Distance Measurement (EDM) technology built into the Total Station is used, which detects the time taken by the ray to travel to and from the point struck to the telescope, after which the instrument stores the data, and in the display of the instrument, polar coordinates can be read. The Total Station measurement operation can be carried out in two different ways:

- Infrared beam: the measurement of points is done through the use of a prism, this is a special reflecting mirror that allows the distance between it and the Total Station to be measured.
- Laser beam: used to detect points that are difficult for the operator to access, since no reflective system needs to be placed, well identifiable points, such as stainless steel doilies, are sufficient.

The model used for the Boccasette and Barricata campaigns is the TCR1201, this instrument allows us to reach an angular precision of 1.0", as you can see the angular precision is very high, just to give an example we know that  $1^\circ=60'$  and if we want to convert it to seconds we have 3600" therefore the precision of the instrument is 1/3600 of a degree or  $0.0002778^\circ$ . For distances the precision is less accurate but still very high in the topographic field, it is composed of 2 components (1mm+1.5ppm),

we have the first component, that is the fixed part, while the second is the relative (distance dependent component), the fixed part is always present, so it cannot be eliminated or in any case reduced and it is 1 mm, while the relative part is related to the measured distance, and it is equal to 1.5 ppm (1.5mm/1km).

Let us now pose an example to understand the component related to precision, if we find ourselves measuring a distance of 500 m in this case, we have the fixed error of 1 mm to which must be added the relative equal to  $1.5 \cdot (0.5\text{km}/1\text{km}) = 0.75$  mm, therefore the final precision will be:  $1 \text{ mm} + 0.75 \text{ mm} = 1.75 \text{ mm}$ .

The details just discussed about precision are valid at the time of collimating with the prism, in case of collimation without a prism the precision is reduced and will be:  $2\text{mm} + 2\text{ppm}$ .

### ***3.2.2 GNSS (Global navigation satellite system)***

The GNSS surveying part was performed through the use of the TOPCON Hiper HR instrument (Figure 17), available in the Laboratory of Surveying and Geomatics at the University of Padua, is a compact and powerful receiver, built with the most advanced technology in the field and suitable to withstand the harshest environmental conditions. The instrument made it possible to detect a large number of points for coastline identification in a short time.



Figure 17 TOPCON GNSS Receiver (source: geoshack.com).

So GNSS instrumentation is a precision sensing system that provides us with the continuous, real-time position of an observer on the ground anywhere on the globe,



all made possible by the reception on the ground of radio signals emitted by satellites placed on nearly circular orbits with a radius of about 26.500 km (from the center of mass or barycenter of the earth). Thanks to the GNSS system, we can improve the accuracy of positioning.

The GNSS system consists of several constellations including:

- GPS (Global Positioning System, America), consisting of 30 satellites, arranged in 6 orbital planes, tilted about  $55^\circ$  from the equator;
- BEDOU 3 (China), consisting of 28 satellites;
- GALILEO (Europe), consisting of 26 satellites, designed to eventually contain 30 satellites in orbit;
- GLONASS (Global Navigation Satellite System, Russia), consisting of 24 satellites, located in 3 orbital planes with an inclination of  $64.8^\circ$ ;
- then we have RNSS (India) and QZSS (Japan), which have considerably fewer satellites than the above systems, with 7 for RNSS and 4 for the QZSS system.

This linking of constellations allows us to always receive a large number of signals, an element of considerable importance, because if, for example, we wanted to rely on the GLONASS system the small number of satellites does not allow us to work independently, which is why more constellations are needed to increase the accuracy of the data to an acceptable level for the topographic field.

The reference system used in this GNSS survey is WGS 84 (Figure 18), a reference ellipsoid adopted worldwide to mathematically approximate the shape of the Earth's surface.

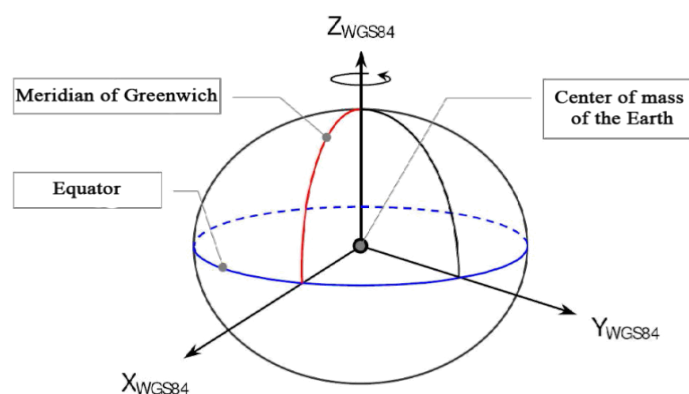


Figure 18 WGS84 system diagram (source: author).

Is named WGS84 (World Geodetic System 1984): the origin of the coordinates is coincident with the Earth's center mass; the Z axis is chosen in the direction of the Conventional Terrestrial North Pole (CTP – Conventional Terrestrial Pole) defined by the BIH (Bureau International de l'Heure) in 1984; the X axis passes for the intersection between the Meridian reference plane defined by the BIH in 1984 (passing for Greenwich) with the equatorial plane connected to the CTP; the Y axis complete the orthogonal system and belong to the equatorial plane, 90° East of the X axis; the cartesian system is fixed to the Earth. The origin and the axes of coordinates are also the center and axes of the Ellipsoid connected to the system, with Z axis of symmetry of the Ellipsoid.

So, this is the reference system for the representation of the earth surface.

To clarify now how the process between ground point and satellite works, let us consider the GPS system, remembering that the operating procedure is done in the same way for the other constellations used in the GNSS system.

With the GPS system developed by the U.S. Department of Defense we go to measure the time required for the exchange of information between satellite and receiver.

Some of the features of the instrument include the following:

- Real-time 3D positioning system over the globe, based on a constellation of artificial satellites;
- The satellites are positioned on approximately circular orbits with radius of about 26500 km from the earth's center;
- It provides the three-dimensional position of a point on the Earth's surface with a maximum accuracy on the order of 1 cm, but not in real time, in this case the final accuracy is on the order of meters from 1 to 10 m, for maximum accuracy you have to process the data;

To better understand let us briefly describe the 3 segments of GPS, namely:

- Space;
- Control;
- Users.

The spatial configuration is made up of about 30 Satellites, placed on 6 orbital planes, spaced in Longitude of  $60^\circ$  and inclined of  $55^\circ$  with reference to the equatorial plane, the distance from the Earth's surface is about 20200 km (Figure 19-20), the period of rotation is 11 hours and 58 minutes and with this geometry can be observed, at any time, from anywhere on the Globe and simultaneously, a number of 4÷12 Satellites with an elevation of at least  $15^\circ$  above the horizon, but remember the minimum number of satellites for positioning is 4, more is much better.

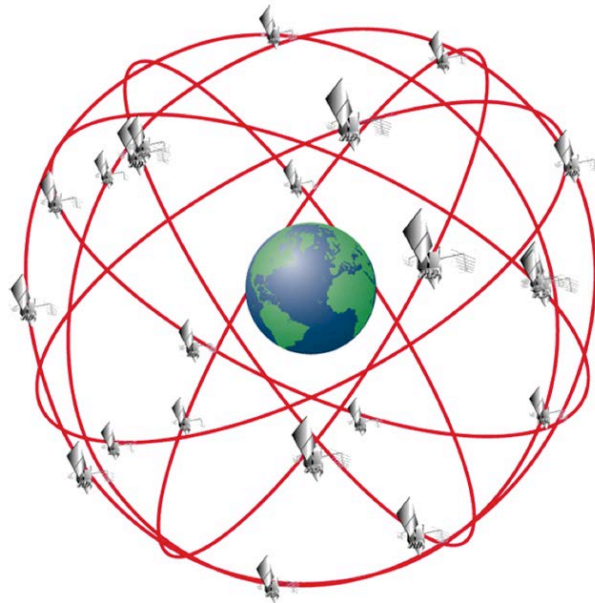


Figure 19 GPS Constellation (source: code7700.com).

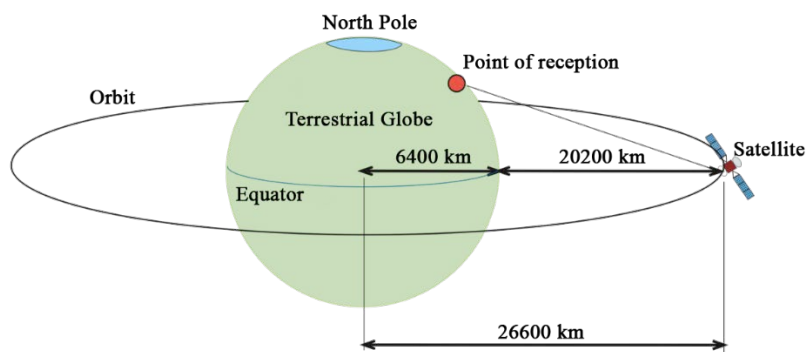


Figure 20 Position of the satellite relative to the Earth and its center. (source: author).

The reason why the minimum number is 4 is as follows, if we think of the problem in space, with GPS we measure the distance from the center of the satellite to the point on the earth's surface, so knowing the coordinates of the satellite we can determine the distance from the satellite to the point on the ground, let us now see the reasons for the minimum number of satellites:

- With one the receiver could be at any point on that sphere (Figure 21);

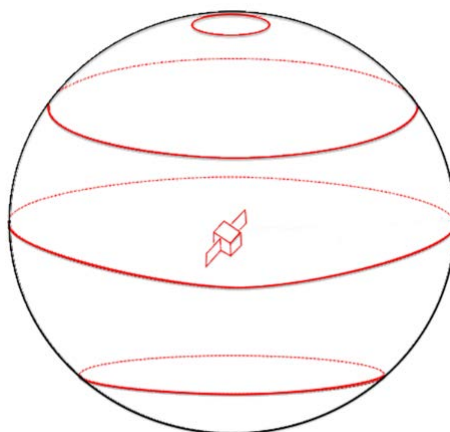


Figure 21 One satellite (source: code7700.com).

- With two satellites you have an intersection of two spheres and the receiver could be in any position along those intersecting spheres (Figure 22).

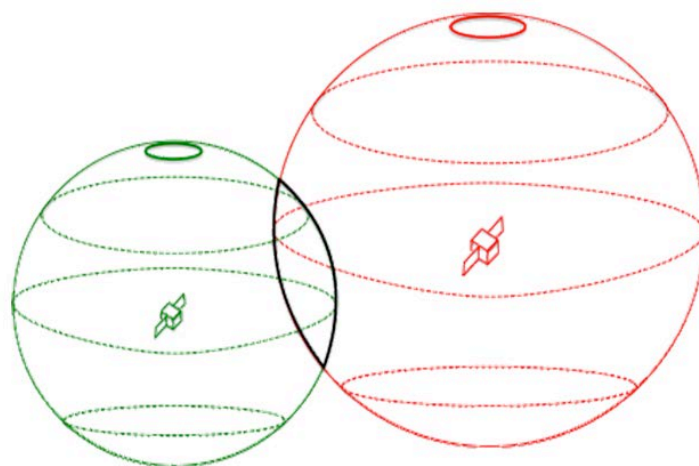


Figure 22 Two satellite (source: code7700.com).

- With three satellites you narrow the possible location down to one of three points (the three black and white points), (Figure 23).

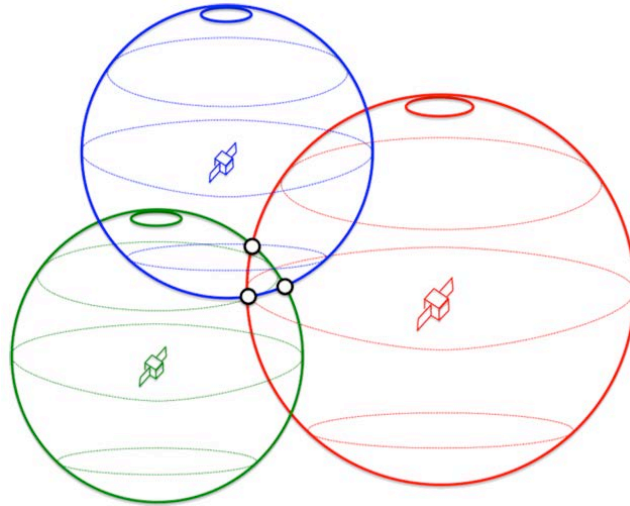


Figure 23 Three satellite (source: code7700.com).

- With one more satellite, you have narrowed the universe of possible intersections to just one (the single black and white point), and each Satellite transmits encoded signals to the Users (with Receiver), (Figure 24).

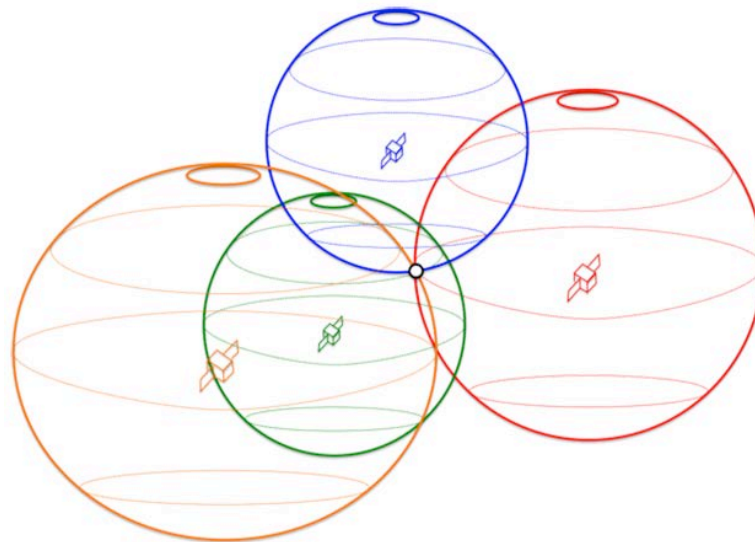


Figure 24 Four satellite (source: code7700.com).

As for the second segment which is about control, we have 5 control stations (Figure 25) along the Earth's equatorial line (Hawaii, Colorado Springs, Ascension, Diego Garcia, Kwajalein), which follow the satellites and process data for orbit correction of the satellites, checking ephemerides<sup>9</sup> and predict the next orbit (for a limited time).



Figure 25 GPS system control stations (source: slide for GIS course by M. Fabris).

Colorado Springs is the Master Station: collects the data from the other stations and, processing these data, estimates the ephemerides of the Satellites (as well as other parameters of the Space segment).

The other Stations transmit the data processed by the Master's one to the Satellites (ephemerides update, correction of orbital parameters, information on the effects of the atmosphere on the waves propagation, etc.).

The procedure for calculation is as follows:

- Data collected by the Control Stations in the last week are processed, in this case, is compute a first estimation of the trajectory that the Satellites will follow in the subsequent week;
- These trajectories are named "reference ephemerides" and are characterized by an accuracy in the order of 50 m;
- Subsequently, data collected in the last 12-24 hours are compared with the reference ephemerides;

---

<sup>9</sup> Satellite coordinates along their orbits.

- The reference ephemerides are re-computed, adapting them to a newer configuration that allows the determination of the Predicted ephemerides (Broadcast Ephemerides);
- Predicted ephemerides are sent to the Satellites that, subsequently, they will send to the Users by means of the low frequency signal;
- A User with a GPS Receiver, collects simultaneously and at any time, signals on two carriers  $L_1$  and  $L_2$ , and the ephemerides of each “visible” Satellite;
- This information allows to carry out a positioning (with low accuracy) in real time.

Errors associated to the Predicted ephemerides:

- About 1-4 m for the radial component (Satellite-Receiver direction);
- About 7-12 m for the tangential component;
- About 3-6 m for the orthogonal component.

Higher accuracies are obtained with the processing of the GPS data on the basis of the real trajectory followed by the Satellites. These data are available with a delay of 10-15 days from the time of acquisition of the GPS signals (Precise ephemerides can be downloaded from several web sites, for example from NASA).

In this case, the positioning will be postponed.

Regarding the third and last segment we have the users, that is, the technicians equipped with a GPS receiver, it can be low-cost with a precision on the order of the meter, such as the one found in cell phones and simple handling or geodetic systems with a maximum precision on the order of the centimeter, for precision positioning.

At this point the operation of the system should be clarified, it now remains to understand what happens between the satellite and the receiver on the ground, i.e., the data flow between the two, in this case we have several components that are generated by the fundamental frequency ( $f_0=10.23$  MHz), the signal can take on different frequencies. For the purpose of this thesis, I will not go into specifics, we just need to know that the components of the signal are as follows:

- carriers  $L_1$  and  $L_2$ : are the two waves with frequency of 154 and 120 times  $f_0$  respectively, and wavelengths resulting of 19.05 cm and 24.45 cm;

Then we have the C/A, P and W codes called square waves; these are pseudorandom codes, that is, sequences of +1 and -1, which repeat after an interval of time. Specifically:

- C/A code (Coarse/Acquisition or Clear/Access) the sequence is emitted at a frequency of  $0.1 f_0$  and is repeated every millisecond ( $10^{-3}$ s), and a C/A code (for identification) is assigned for each satellite;
- P code (Precision or Protected) is repeated every week and is a more precise signal, and there is the possibility of encrypting the P code with a W code known only to authorized Users and emitted at a frequency of  $0.2 f_0$ . This encryption operation is referred to as A-S (AntiSpoofing).

The C/A code is modulated only on the  $L_1$  carrier, while the P code is modulated on both the  $L_1$  and  $L_2$  carriers. Instruments receiving the P code are characterized by high accuracy.

Then we have message D: with this message the User is informed about the operating status of the Satellite, about the clock, and, especially, about the orbit through its ephemerides.

The different components of the signal thus enable us to acquire an accurate position.

Therefore, if we want to determine with sufficient accuracy the distance between a point and a satellite we need to determine the time elapsed between the transmission of a signal emitted by the satellite and the reception at the point of measurement, and for this to happen each satellite sends a signal represented by a simple binary sequence, at first glance it may seem to us to be a random sequence but specifically it is well known, and it is repeated with a long periodicity (pseudo\_random). To better understand the concept we can see it as the recording of a series of tones in an audio track that are emitted by the satellite starting at a very precise instant, a listener in this case the receiver, hearing the sequence of tones and since these are practically non-repeatable, could figure out at what instant of the track the playback arrived.

This sequence is absolutely characteristic of each satellite so that, after a given observation period, which is used by the detector to determine at what point in the sequence the satellite arrived with the transmission, one is able to stable the time at which the satellite would have emitted it, and comparing it with the detector clock



one is able to determine by difference the time  $\Delta t$  elapsed between transmission and reception (Figure 26).

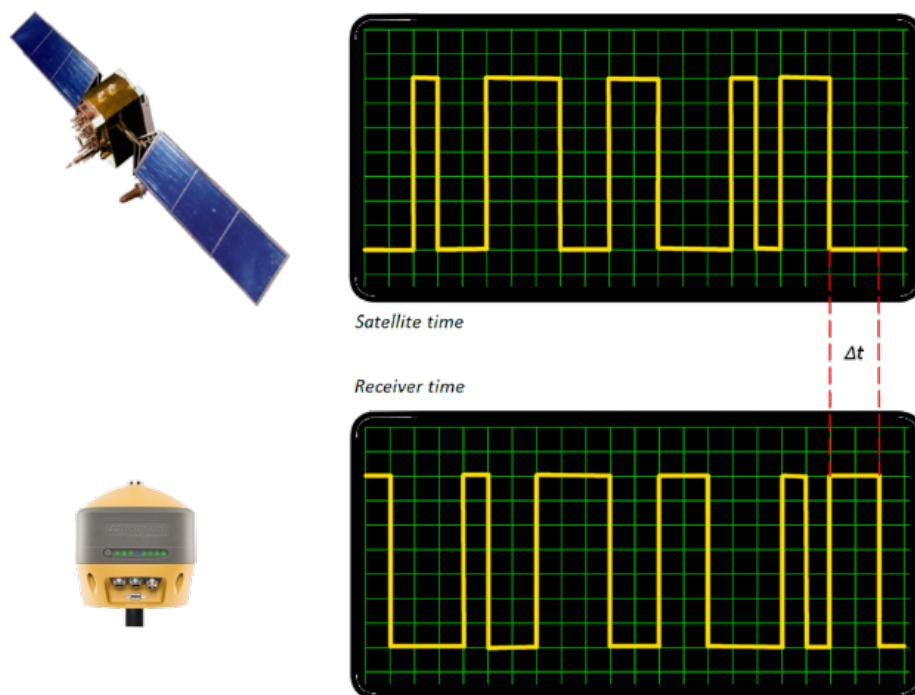


Figure 26 Signals emitted by satellite and receiver, respectively (source: author).

The difference in time that is going to be recorded is related to the precision of the on-board clocks in the respective components, in fact, in the satellite we find a high-precision (atomic<sup>10</sup>) clock with an accuracy of  $10^{-14}$ (s) while in the receiver also due to an economic condition of cost, we find quartz<sup>11</sup> clocks with a precision of  $10^{-6}$ (s). So, the time that will be of fundamental interest is the synchronization error between the two clocks, which we can call  $(\pm \delta t_{ij})$ . The symbol  $(\pm)$  is inserted because we do not know a priori whether the receiver clock starts before or after the satellite clock. If we now return to our objective what we want to find are the coordinates in the terrain of a given point  $(x_i, y_i, z_i)$  and they are 3 unknowns, to which we add the

---

<sup>10</sup> Clock in which the time base is determined by the resonance frequency of an atom.

<sup>11</sup> The passage of time is determined by the oscillations of a quartz crystal.

synchronization error ( $\delta t_{ij}$ ), the equation for the satellite and receiver distance is then given by the following relation:

$$\rho_{is} = \Delta t_s * c = \sqrt{[(x_s - x_i)^2 + (y_s - y_i)^2 + (z_s - z_i)^2]} \pm \delta t_{ij} * c$$

In the equation we thus find:

- $\Delta t_s$  = time taken by the signal to reach the center of the instrument;
- $c$  = velocity that the signal has in vacuum, which can be assumed 300000 km/s;

in the second part we have:

- The coordinates of the point on the ground ( $x_i, y_i, z_i$ );
- The coordinates of the satellite ( $x_s, y_s, z_s$ );
- And finally the parameters already described.

At this point it is evident that with only one equation we have 4 unknowns ( $x_i, y_i, z_i, \delta t_{ij}$ ) and the problem is not solvable, but knowing that the unknown coordinates of the point we are looking for are the same if we consider 4 satellites, thus 4 equations and the same goes for the synchronization error, the problem becomes 4 unknowns and 4 equations and thus solvable.

It is now well known why the minimum number of satellites is 4, obviously a higher number leads to increasing the accuracy of the method. The GPS allows us 3 different types of positioning as can be seen from the tables below (Figure 27).

POSITIONING	N. OF RECIVER	PROCESING	EPHEMERIDES	PRECISION	APPLICATIONS
ABSOLUTE	1	REAL TIME	PREDICTED	~ 1-20 m	NAVIGATORS
DIFFERENTIAL	1 - 2	REAL TIME	PREDICTED	~ 3-30 cm	ROAD SURVEY TERREIN SURVEY CARTOGRAPHY
RELATIVE	1 - 2	POST PONED	PRECISE	~ 1 cm	PRECISION SURVEYING

Figure 27 Types of positioning (source: author).

We can use the following methods in the table for measurement (Figure 28).

<b>METHODS</b>	<b>TIME AT THE POINT</b>	<b>POSITIONING</b>	<b>PRECISION</b>
<b>STATIC</b>	<b>~ 20 - 60 min</b>	<b>RELATIVE</b>	<b>~ 1 cm</b>
<b>RAPID STATIC</b>	<b>~ 5 - 10 min</b>	<b>RELATIVE DIFFERENTIAL</b>	<b>~ 3-30 cm</b>
<b>KINEMATIC</b>	<b>/</b>	<b>ABSOLUTE DIFFERENTIAL RELATIVE</b>	<b>~ 10 cm - 20 m</b>

Figure 28 Types of measurement (source: author).

One of the last aspects we are going to look at in GPS, but no less important, concerns errors in positioning. GPS requires a great deal of care in order to maintain a high range of accuracy, otherwise it risks invalidating the measurements made.

In the GPS surveys the position of the point on the Earth's surface is computed performing measurements of the Satellite-Receiver distance (knowing the position of the Satellite on the basis of its ephemerides), and the accuracy of positioning will be influenced by several errors that always affect the Absolute positioning, but are drastically reduced in the Relative and the Differential positioning.

The main types of errors are:

- Errors of the Satellites orbit: for the positioning in real time the Predicted ephemerides are used (transmitted by the Satellite in real time and characterized by a precision in the order of 10-20 m);
- Errors of non synchronization clocks: are due mainly by the Receiver clock that, to reduce the costs, is characterized by a lower precision;
- Errors due to the signal propagation, because we have assumed that the signal crosses space but it is not really so, because it must cross the atmosphere, composed of the troposphere (0 - 50 km) and ionosphere (50-1100 km).

A dispersion that is difficult to control is present in the ionosphere (Figure 29), where the disturbance can be more or less pronounced depending on the position of the satellite relative to the surface as shown in Figure 30, we clearly see that D2 is higher than D1, consequently, the disturbance will be greater.

High resolution geomatics techniques for coastline detection and monitoring:  
Bocasette and Barricata case studies (Po River Delta, Rovigo, Italy).

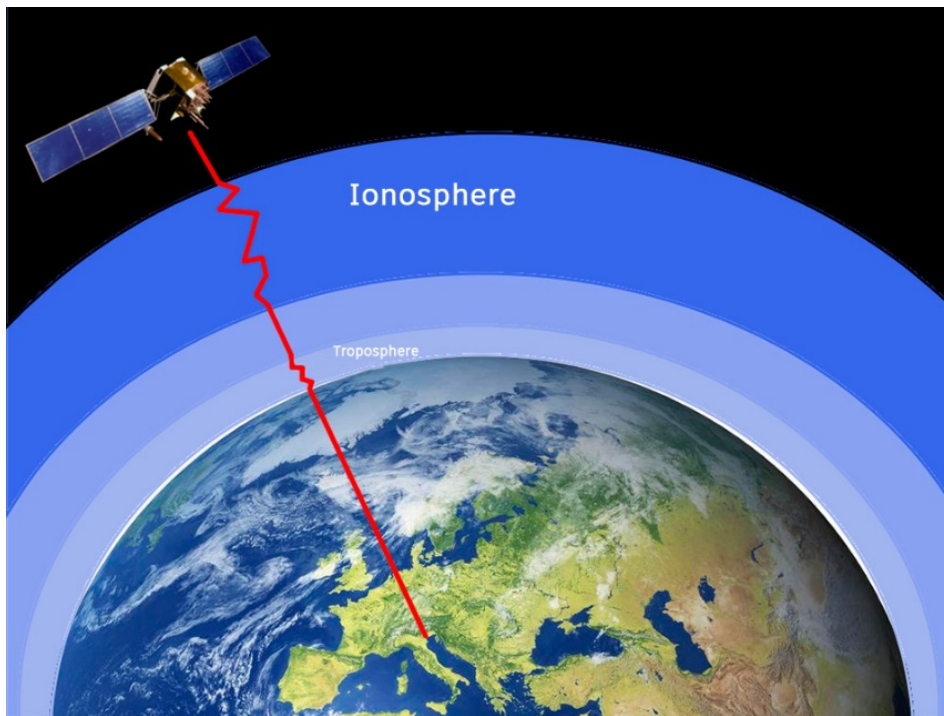


Figure 29 Disruption Ionosphere and Troposphere.

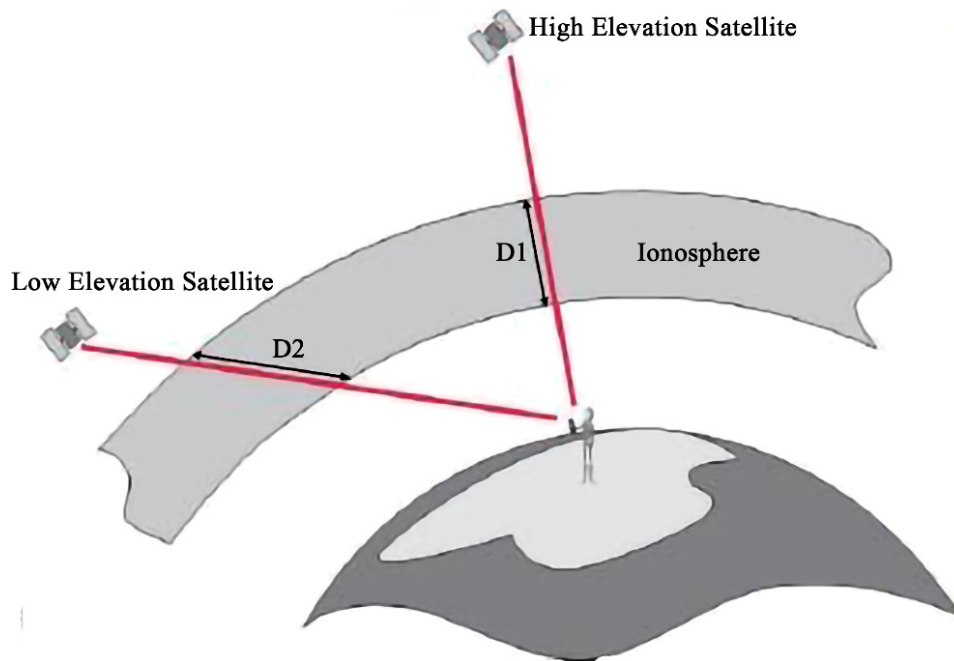


Figure 30 Difference in the disturbance according to receiver and satellite position (source: electroyou.it).

To reduce the following error, an angle called Cut off is used, and only satellites within the cone should be considered as we see in Figure 31. The angle to the horizontal is usually 13-15°.

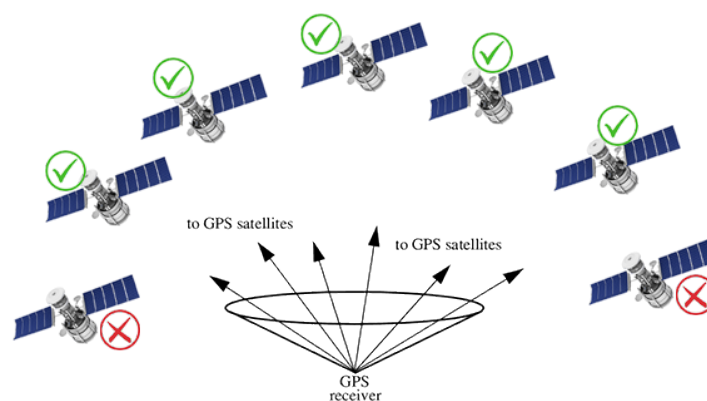


Figure 31 Cut off angle (source: author).

Problems in signal propagation as we see in Figure 29 are also found in the troposphere. Several studies have been carried out to overcome these difficulties, but the problem is still open, although thanks to some mathematical models we are able to reduce the influence of the disturbance by going to include environmental parameters, but it should be remembered that it cannot be eliminated at present. Other errors in GPS measurements can be:

- Errors due to multiple reflections (multipath), in addition to the signal coming directly from the Satellite, other signals may arrive at the GPS Antenna of the Receiver after reflection on reflective surfaces (longer paths), then these signals, introducing noise in the data, complicate the reception and the procedures of analysis of the correct signal by the Receiver, are very problematic reflections that occur near the Receiver Antenna due to the walls of buildings, rock walls, expanses of water, etc... ;
- Cycle Slip temporary interruption of the Satellite visibility; this effect creates big problems, especially in the kinematic surveys: particular attentions must be pay to any obstacles;
- Errors due to receiving Station: derive from the Receiver electronics, the instability of the oscillator which generate the standard frequency and then the signal replications, the instability of the Antenna phase center (i.e. the point inside to the Antenna where the signal is effectively received, that is the instrumental center);

- Errors due to the operator: stationing, measure of Antenna height, etc...

For the elevation part, the GPS measures elevations relative to the ellipsoid, so it will be necessary later to go and convert this data to obtain orthometric elevations<sup>12</sup> (Figure 32).

Ellipsoidal and orthometric elevations are connected by the relation:

$$h = H + N$$

- h: ellipsoidal elevation provided by the GPS;
- H: geoidic or orthometric elevation measured with the leveling;
- N: Geoid ondulation.

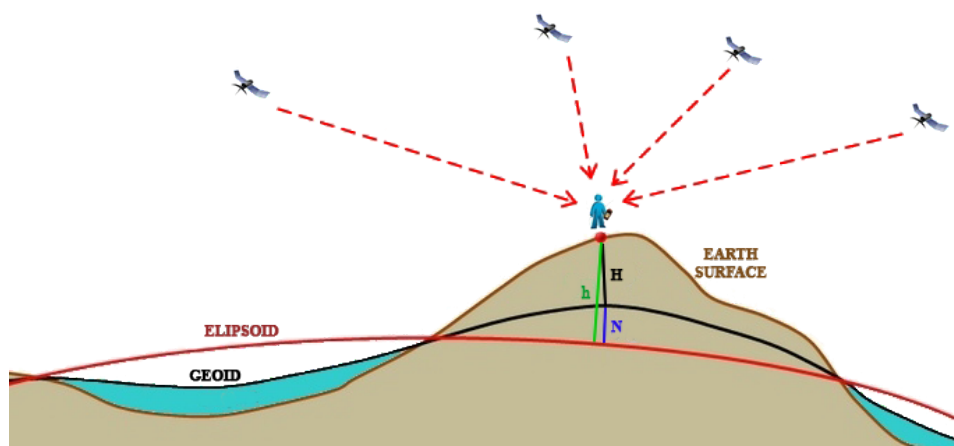


Figure 32 GPS-based altitude measurement (source: mondogeo.it).

The GNSS systems indicate altitude as the third position parameter (latitude, longitude and altitude). This is an ellipsoid altitude, that is, referred to the ellipsoid of the geodetic datum used by the GNSS system.

The altitudes shown on the maps are those referred to the geoid surface and are called Orthometric. Orthometric altitude is referenced to the equigravitational surface<sup>13</sup> of the geoid and is the one that tells us whether sponsting in the environment "we are moving flat, uphill or downhill" and that is what we are interested in. Ellipsoidal altitude refers to the mathematical surface of the ellipsoid. This has no direct relation

---

<sup>12</sup> It represents the elevation of the measured point relative to the surface of the mean sea level (geoid).

<sup>13</sup> Surface on which the potential of a conservative field has a constant value.

to equigravitational surfaces and so is not useful for moving in the environment. The value of the Geoid ondulation can be measured by means of gravimetric surveys (precision in the order of centimeters).

In Italy ITALGEO: Geoid model obtained with gravimetric measurements with 3'x3' grid (about 5.5x5.5 km) with declared precision of 4 cm.

For the two surveys discussed in the thesis, the coastline measurements were taken in kinematic mode with differential positioning. Let us now look at two approaches of this methodology, in the first case it will be explained how the correction takes place thanks to a master, in the second case we see the correction process in the network, which was also used in the measurements in question of Boccasette and Barricata.

### CASE 1

Differential GNSS (DGNSS) is based on the consideration that two ground-based GPS detectors that are fairly close together (on the order of a few kilometers) will have the same satellites visible on the sky, and therefore the influence derived from the passage of signals for the ionosphere and troposphere is felt on both equally.

If the position of one of the two detectors is exactly known a priori, the same difference in reading between the detected position and the known position must also apply to the other detector. In this way the second detector can, by applying this correction, determine the point with greater accuracy, this time dependent almost exclusively on the goodness of the GPS detector. To realize this system there is a need for the GPS detector to be able to receive correction data (RTCM) from a fixed station via a dedicated channel for data transmission (Figure 33).

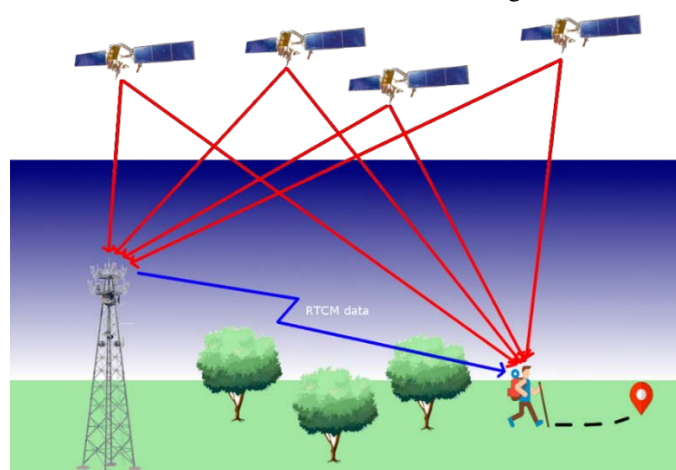


Figure 33 Differential GNSS.

## CASE 2

There are publicly accessible implementations via the Internet that provide GNSS corrections data (Figure 34). For example, the Veneto region, through an online service by registering on the dedicated site, in collaboration with the University of Padova, provides a free service that allows obtaining data in NTRIP (Networked Transport of RTCM via Internet Protocol) format from 30 stations located throughout the region. Similarly, all other regions do the same in a more or less similar way. In this case, the accuracy is on the order of 10 cm, because unlike the master, in this case we have the 30 stations collecting data and creating a more precise mapping on location, plus the coastal area does not have any particular disturbing elements and therefore a large number of satellites can be picked up.

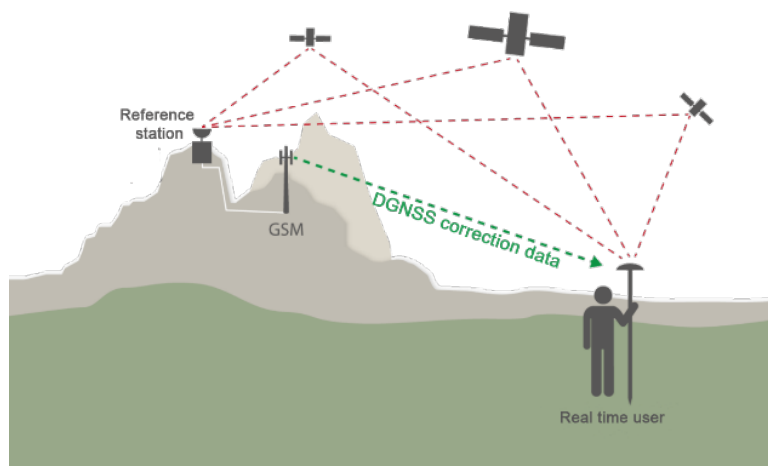


Figure 34 Networked Transport of RTCM via Internet Protocol (source: [www.swisstopo.admin.ch](http://www.swisstopo.admin.ch)).



### 3.2.3 Photogrammetry (Drone)

Aerial photogrammetry carried out using a drone (also referred to by the abbreviation SAPR - Remotely Piloted Aircraft System) is part of the most advanced technological innovations of recent years. For the photogrammetric survey of the coastline, a lightweight drone, model ParrotAnafi (Figure 35), was used. The drone has a 21 MP 1 / 2.4" Sony CMOS sensor (diagonal size: 7.834 mm; unit cell size: 1.2 x 1.12 m) and was acquired in JPEG" rectilinear format "(4608x3456 pixels, 4: 3 format, 75.5° HFOV) with a focal length of 4 mm corresponding to 23 mm (35 mm format equivalent).



Figure 35 Drone used for surveying (source: parrot.com).

It allows the cartographic production of medium to large expanses of the territory, the taking is done with sophisticated cameras, equipped with automatisms, positioned on the SAPR system so that the axis remains as vertical as possible, and facing downwards, for the taking of the territory (nadiral taking).

Thus, it involves surveying remotely, directly on images of the object, without physical contact with it. It allows us a simultaneous survey of many points, from which we obtain a large amount of information. The basic principle is similar to that governing human view, our ability to perceive the third dimension (depth) derives from the fact that, for each object in the field of view, we "perform" two photographs from two different viewpoints, from this information it is immediately obvious that one image is not enough, but it takes two images (minimum number) acquired from different viewpoints, thus the principle of photogrammetry in order to obtain the frame map requires that each generic point A on the ground be taken from at least two consecutive frames. The two images A' and A", homologous to A, whose

coordinates in the image plane are  $\xi'$ ,  $\eta'$  on the first frame and  $\xi''$ ,  $\eta''$  in the second frame, which will be measured during restitution and allow the subsequent positioning of A. In Figure 36 we see the aerial photogrammetry scheme, the drone in our case, follows a straight trajectory at constant speed, at a certain height H above the ground, at the instant  $t_1$  the camera's grip center is at  $O_1$  and takes back the first frame, and at the instant  $t_2$  (after traveling a certain space that constitutes the grip base B) it will be at the position  $O_2$  where it will take back the second frame.

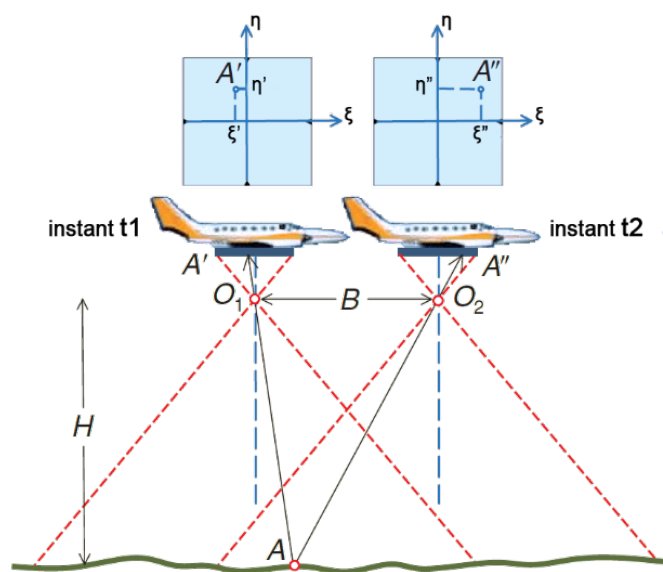


Figure 36 Grip pattern between two frames (source: Zanichelli).

At this point we can then introduce the concept of "photogrammetric model" defined as the part in common between two images, more precisely the overlapping part between two images in which photogrammetric principles can be applied, which allows "stereoscopic vision" with appropriate devices (looking at the two images at the same time, with the left eye we "see" only the left image, the right eye only the right, while in our brain the "fusion" of the two images and thus the perception of the third dimension is generated). To compose the survey, the drone flies over the terrain, according to a scheme worked out before the survey campaign in the laboratory, as we see in Figure 37, the drone performs the takes in a sequence of straight paths side by side along parallel directions.

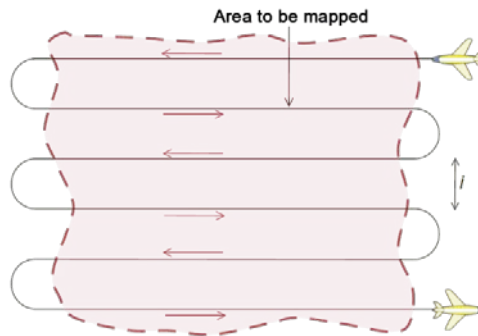


Figure 37 Land-covering scheme with a photogrammetric flight organized into straight, parallel trajectories during which a certain number of frames called a swipe is taken (source: Zanichelli).

Frames taken along the same straight path constitute a swipe. The set of several swipes is called a swipe block. As we can see in Figure 38 in addition to the longitudinal overlap ( $\mu$ ), which is generally 60% we have an overlap between two adjacent swipes termed overside ( $\epsilon$ ), with value between 10-20% of the L embrace of the frame, these rules allow optimal overlap so as to avoid holes in the ground cover. Photographic captures of the terrain must take place in such a way that the entire area to be surveyed remains decomposed into stereoscopic patterns such that each point on the terrain appears, as mentioned, on at least two frames. We know that this requirement is ensured by the longitudinal overlay of the L embrace of the frame.

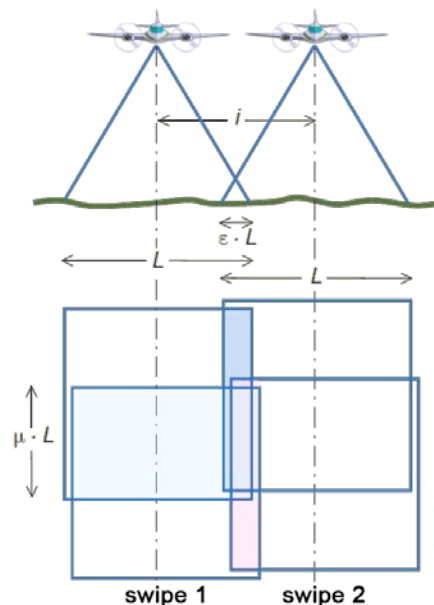


Figure 38 Overlap between different frames and swipes (source: Zanichelli).

Regarding the geometric principles of photogrammetry, without going into specifics we have our visible photogrammetric camera in Figure 39, consisting of:

- ⇒ The image plane;
- ⇒ The center of acquisition (O);
- ⇒ Total length (c).

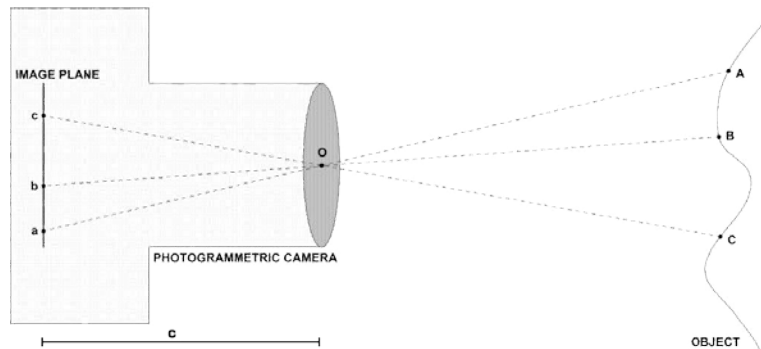


Figure 39 Schematic example photogrammetric camera (source: slide for GIS course by M. Fabris).

Each point on the ground is projected into the image plane, which is present inside the camera and outside it, the inner one visible in Figure 39 is the negative plane, while the outer one not shown but exactly the same, is considered positive, we can call it an imaginary plane, which has a reference system with origin at the center of the plane and coordinates  $(\xi ; \eta)$ .

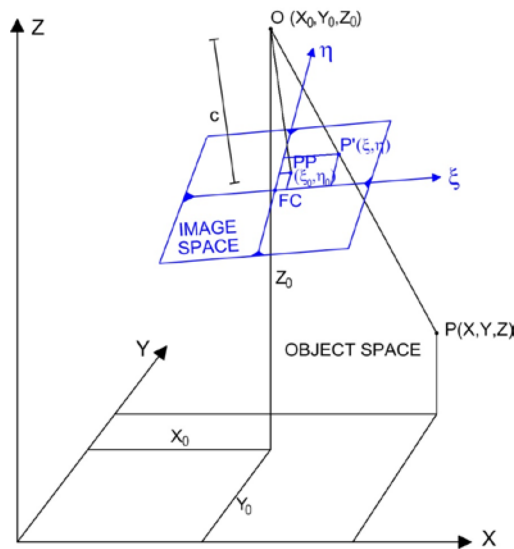


Figure 40 Image plane diagram and acquisition center (source: slide for GIS course by M. Fabris).

In Figure 40 we have:

- $(X_0, Y_0, Z_0)$ : Center of acquisition;
- PP  $(\xi_0, \eta_0)$ : Principal Point (projection of O on Image Plane);
- FC  $(0,0)$  Fiducial Center (Origin);
- $c$ : Focal length;
- $\xi, \eta$ : Image system;
- $X, Y, Z$ : Object system.

Let us now try to understand why we have all these parameters. If the camera were perfect, the projection of point 0 in the image plane could be coincident with the fiducial center (FC), but the camera is not perfect, which is why the principal point (PP) is defined, which is the projection of 0 along the perpendicular to the image plane with coordinates  $(\xi_0, \eta_0)$ . The maximum distance between PP and FC is less than 20  $\mu\text{m}$ , but it is important to consider it because with the projection into the ground it can be on the order of a few meters.

At this point starting from the coordinates  $(\xi, \eta)$  we go to see the mathematical relationship that allows us to determine the coordinates of the points on the ground  $(X; Y; Z)$ , and these equations are the collinear equations<sup>14</sup>, which connect the coordinates from the image plane to the object system with an image.

$$X = X_0 + (Z - Z_0) \cdot \frac{r_{11} \cdot (\xi - \xi_0) + r_{12} \cdot (\eta - \eta_0) - r_{13} \cdot c}{r_{31} \cdot (\xi - \xi_0) + r_{32} \cdot (\eta - \eta_0) - r_{33} \cdot c}$$

$$Y = Y_0 + (Z - Z_0) \cdot \frac{r_{21} \cdot (\xi - \xi_0) + r_{22} \cdot (\eta - \eta_0) - r_{23} \cdot c}{r_{31} \cdot (\xi - \xi_0) + r_{32} \cdot (\eta - \eta_0) - r_{33} \cdot c}$$

In the equations we have:

- Parameters of Internal Orientation:  $c, \xi_0, \eta_0$  (Certificate of calibration of metric camera)
- Parameters of External Orientation:  $X_0, Y_0, Z_0, \omega, \varphi, \kappa (r_{ij})$  (Ground Control Points).

If all the parameters are known we have a system of 2 equations and 3 unknowns ( $X; Y; Z$ ) and with are 1 image we cannot solve the problem, but with are 2 images of the

---

<sup>14</sup> The collinearity equations are two expressions that indicate the relationship between the coordinates from a point in a three-dimensional coordinate system and the coordinates of its central pixel projection on an image plane, as with a camera.

same point we get 4 equations for 3 unknowns and here is also mathematically explained why we need overlap.

An important parameter in an aerophotogrammetric survey is spatial resolution, defined by the G.S.D (ground sampling distance), which is the distance measured on the ground between two neighboring pixels in the image, or rather the pixel size in the field. Going to zoom the digital (raster) image at some point we will begin to see all the squares (pixels) that make up the image. The lower the GSD, the greater the detail of the photograph. This parameter (GSD) depends on the resolution of the camera mounted on the drone, the focal length and the flight height. Through these parameters it will then be possible to determine the accuracy of the photogrammetric survey. As an example if the pixel size is 2 cm, this does not mean that the accuracy is 2 cm it will then be related to how accurate the photo restitution phase will be, we could be wrong by one two pixels so the accuracy will be about 4-6 cm. The size of the pixels then will have to be decided according to the final quality that is to be achieved, more pixels also means larger size in processing and in the final product.

As for land cover patterns, swipes and photogrammetric blocks, they will be covered in Chapter 4, in the flight planning phase.

In order to obtain good restitution, thus excellent out-puts to work on, photogrammetric flights must be carried out under perfect meteorological conditions (no clouds, but also no haze), and during the middle hours of the day, to take advantage of the maximum available illumination and to minimize the influence of ground shadows. It follows that there are very few (an average of 20-40) days in a year that are adequate to carry out this activity.

Summarizing the figures shown in the photogrammetry, the symbols used have the following meanings:

- H: average height above the ground maintained by the drone during the swipes;
- L: embrace, i.e., side of the ground frame contained in a frame;
- B: grasp base, distance between two consecutive  $O_1$  and  $O_2$  grasp centers;
- l: effective useful side of the frame (close to 230 mm);
- p: main distance of the camera, believed to be equal to the focal distance of the lens;
- $\mu$ : longitudinal overlay, overlap of two consecutive frames; generally 60% of L;
- $\varepsilon$ : lateral overlay, overlapping of two adjacent strips; in general 20% of L;

- $i$ : swipe spacing, i.e., distance between the axes of two adjacent swipes.

Photogrammetry can be divided into:

- Aerial photogrammetry;
- Terrestrial photogrammetry.

In aerial photogrammetry a camera is inside an airplane, or as in the present case placed in a drone. In terrestrial one, a camera is placed on a tripod, as if it were a real classical topographic instrument, with the camera lens toward the object to be surveyed. In the field of digital photogrammetry, both aerial and terrestrial, digital surface models (DEM - Digital Elevation Model, DTM - Digital Terrain Model, DSM - Digital Surface Model) can be obtained as a product. Photogrammetry turns out to have characteristics of:

- rapidity: the actual surveying is done after the fact, directly on the images;
- cost-effectiveness: as we have a lower cost in producing for example cartography, compared to using traditional methods;
- uniformity of accuracy: all points on the images have the same accuracy, regardless of whether they are in the center or in the edges of the image.

It is therefore a true technique of digital photography, in this case with a drone, which can then be processed with special professional software. The software uses the aerial footage of the drone to detect points in common (called homologues) between all the inserted images, on which the point cloud is built, that is, a group of points with the characteristic of being positioned by coordinates with precise values associated with them, the image thus obtained with the point cloud, the final digital products can be processed.

To obtain the photogrammetric survey, first of all it is necessary to acquire the frames, then when the frames are aligned mesh and textured-model processing is carried out, so as to obtain the vectorized elevations.

There are differences among different SAPRs that make them suitable or unsuitable for certain operations; one of the distinctions is based on the type of wing with which it is equipped:

- Multirotors;

- Fixed wing;
- Hybrid drones.

In the case under consideration we limit ourselves to briefly describing multirotor SAPRs, corresponding to the type used for the survey in question, they are the most common, this is related to a variety of characteristics including cost size and possibility of use. Such aircraft consist of arms, generally distributed in a radial pattern, on which the rotors are mounted. An important detail, which we can identify as a strong point on multirotors is the fact that they can be stationed on a given point at altitude (hovering), simultaneously varying in case of need the shooting angle, or perform rotations on the same axis. In contrast, we can point out the rather low flight autonomy (10-30 minutes), mainly related to weight, resulting in limited areal coverage.

For multi-rotor drones the frame is generally made of carbon fiber which ensures good strength and at the same time lightness, the structure must be designed in such a way as to ensure a perfect balance of the aircraft, so as to ensure stability and maneuverability. The arms that support the engines are often foldable for ease of transport. The flight controller represents the heart of the SAPR, a device containing a concentration of microelectronics that manages through the inertial measurement unit IMU, every flight parameter. The IMU is composed of several sensors including, gyroscope, accelerometer, digital barometer, magnetometer, and GPS.

The operations that the flight controller allows us are many, namely:

- ✓ Perform automatically programmed flights;
- ✓ Check the quality of the radio signal between drone and radio controller;
- ✓ Check the status of the batteries; check the quality of the GPS signal;
- ✓ Use telemetry, which in turn allows real-time transfer to the ground station;
- ✓ The attitude data;
- ✓ The GPS position;
- ✓ The HDOP (related to the number of satellites connected to the GPS antenna instant by instant, the lower the better the geometry of the satellites);
- ✓ The cruising speed;
- ✓ The wind speed (if the drone is equipped with a special pitot tube);
- ✓ The flight height;
- ✓ The distance from the home (take-off point),etc....



In addition, it should not be overlooked that the controller has the function of ensuring that the drone performs flights safely, the flight parameters (LOG) also are recorded in a manner quite similar to the black box of conventional aircraft.

The radio system for controlling a drone consists of two-way radio devices, which can provide various information, commands given by the pilot to the aircraft, battery status, driving mode, radio signal quality. Multi-channel radio controls also provide the ability to control other systems in addition to the drone, such as the camera. Generally, radio controls for professional use operate in the 2.4 GHz band and ensure a reliable signal within a distance of 2 km.

### **3.3 Software used**

The software used made it possible to study coastline variations, performing a comparison on the efficiency of the methodologies used in terms of speed, time and cost. As we will see later, the various methodologies offer quite different characteristics in this context, which is why careful processing is of fundamental importance. The choice of such software was made out of personal preference in approaching the case, but the phenomenon can be analyzed with different methodologies.

So the programs used are:

- Agisoft metasheape: for processing images acquired by drone and creating the orthophoto and DTM;
- AutoCAD: for a check on the restitution of data, this as we will see allowed us to calculate the useful data with a step by step approach, to learn if the calculation performed by QGIS software gave the same result.
- QGIS: this software that allows to visualize, organize, analyze and represent spatial data, allowed the calculation of the mean and standard deviation on the comparisons of the returns between different methods. It is a very interesting software because, as we will see, it simplifies and greatly reduces processing time compared to other software, such as AutoCAD (not really suitable for these studies).

### ***3.3.1 Agisoft Metashape***

Agisoft Metashape is a stand-alone software that performs photogrammetric processing of digital images and generates 3D spatial data. It can be used for GIS applications, documentation of cultural heritage, production of visual effects, as well as indirect measurements of objects of various scales. Digital photogrammetry techniques, implemented and applied with computer vision methods, result in an automatic and intelligent processing system that, on the one hand, can be handled by beginners in the field of photogrammetry, but, on the other hand, can offer much to the professional who can model the workflow to different types of jobs and different types of data. During the different case studies Agisoft Metashape has proven to produce accurate and quality results, ensuring a simple and integrated workflow for drones and for Remotely Piloted Systems. The software generates dense point clouds, textured polygonal models, georeferenced precision orthomosaics and DSM / DTM from images taken during APR flights.

It is used following the photographic campaign, and for each surveyed area it allows post-processing, taking advantage of the Structure from Motion (SfM) strategy, which allows to automatically orient a group of images and generate a point cloud, accompanied by meshes and textures for the visual rendering of the final model, through some consequential steps. So, we can in a simplified way summarize what was introduced with the following steps:

- Build: Generate 3D models, point clouds, DSMs of digital photos;
- Measure: Collect spatial data: distances, areas, volumes;
- View: Textures in HDR quality for excellent detailed presentation of results.

As can be guessed, it is a very helpful support as in the present case in the field of cartography and topography, it ensures a simple and integrated workflow.

The software is the ideal complement and offers absolute accuracies up to 2-5 cm (depending on the GSD, as we have already said a parameter that relates to the pixels of a digital image, the pixel representing the smallest identifiable unit within the image). Of course, the precision must be related to the case study, just to give a simple example, if we have to study a phenomenon with a precision on the order of a meter, using high-detail pixels only increases the time needed for processing and the

weight of the output file. Therefore, it is good to analyze and process the data according to the features of interest that we intend to study.

### **3.3.2 AutoCAD**

The following software as already mentioned has proven to be useful for performing verifications on calculations, but let's take a moment to understand what it is all about, although its use in this thesis is not decisive.

Autocad is the main software intended for the production of 2D and 3D digital drawings, developed by the well-known company 'Autodesk' for the design of infrastructure, civil and industrial construction. It is a CAD system, which stands for Computer-Aided Design. It is part of that field of information technology that uses software and computer graphics technologies to support the activity of designing both virtual and real artifacts. Autocad involves the use of both basic and advanced practical technical skills. The interface is the common one of a main window with a toolbar and related functionality. The purpose is to provide all the tools and options needed to create geometric elements. The native format of the generated file is dwg., but it is also possible to generate files in formats compatible with other CAD systems to facilitate the exchange of information and elements between different software.

### **3.3.3 QGIS**

QGIS is an Open Source Geographic Information System, released under the GNU (General Public License). QGIS is an official project of the Open Source Geospatial Foundation (OSGeo). The program supports numerous vector, raster, database and feature formats. It is, therefore, a computerized geographic information system that processes information derived from geographic data and allows:

- Acquisition;
- Recording;
- Visualization;
- Sharing;
- Presentation.

It is possible in this way to realize the analysis and representation of a given area and everything that occurs in it.

Let us now look at the capabilities of this particular software capable of handling geo-referenced information.

The data collected in a GIS system are usually represented through cartograms (graphical representation of statistical data related to a phenomenon for the purpose of study) or tables relating to more or less extensive areas, but unlike other computer systems, there are many possibilities of use.

GIS technology, in fact, integrates 2 systems into itself:

- The computer-aided drafting system or CAD;
- The relational database DBMS or Data Base Management System, a software system designed to enable the efficient creation, manipulation and querying of databases, hence also called the "database manager or engine".

It thus enables the analysis and search operations proper to Databases, with the geographical analysis and representation typical of CAD, allowing a greater yield by being able to analyze a geographic area at 360° through the simultaneous analysis of:

- Geometric data  
(shape, size, geographical position of objects);
- Topological data  
(connection, adjacency and mutual relationships between objects);
- Informational data  
(numerical or textual data related to objects).

Thus we are able to analyze a geographic entity in several aspects simultaneously, in a more interactive, effective and immediate way, thus saving time in the execution of procedures, as we will see in the next chapter in the data processing phase.

So just as we use a text editor to write documents and manage text with a computer, we can use a GIS application to manage spatial information.

#### **3.3.3.1 Reference Systems**

One aspect of considerable importance in QGIS is the reference systems, which if set up in the wrong way we may encounter problems in visualizing and positioning data or in performing certain functions.

Therefore, we will now briefly see what they are by trying to clarify the topic.

The map has always been an imperfect representation of the earth's surface, which has a roughly spherical shape, and to report that surface on a plane is impossible without deforming it, and this is true whether we do it in analog form on paper or in digital form on a computer screen. The earth's surface is not mathematically representable, which is why theoretical reference surfaces have been defined that best approximate its shape. We have the geoid, which coincides with the sea level also reported in the landmass part and is used to define the elevation of points.

However, even the geoid is not a mathematically defined shape because variations in gravity and density of the various areas of the earth result in a spheroid that is not regular, so it is not reliable for planimetric measurements. We then have a second reference surface that corresponds to a geometrically well-defined solid, the rotation ellipsoid, a spheroid flattened at the poles, with a surface approximating the geoid that allows formulation and mathematical projection onto a plane. In Figure 41 we can see the comparisons.

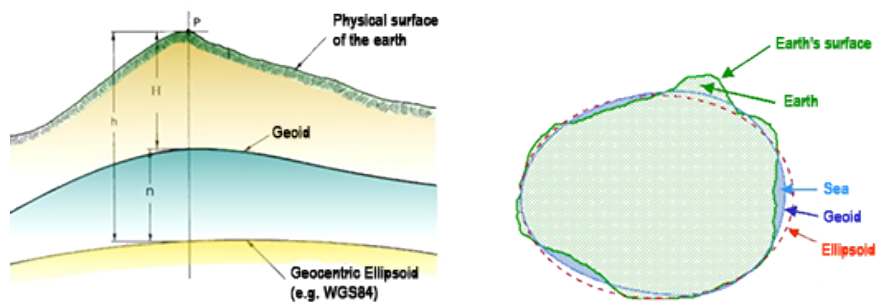


Figure 41 On the left geoid and ellipsoid representation, on the right earth surface and reference surfaces (source: openoikos.com).

Various ellipsoids have been defined over time, and the choice depends on the best degree of approximation to the surface one wants to represent.

This is often done by moving the ellipsoid in such a way as to minimize differences with the geoid in a given geographical area. The choice of the reference ellipsoid and its preferred orientation relative to the geoid constitutes what is called the datum, which can be of two types (Figure 42):

- Local datum, where the ellipsoid has been translocated with respect to the Earth's center of mass and oriented in favor of a particular region (e.g., ED 1950 or Rome 1940 datums);

- Geocentric or global datum when the center corresponds to that of the earth (e.g. WGS 84, which is the datum on which GPS surveying rests).

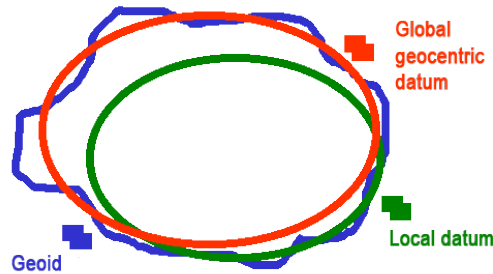


Figure 42 Local and global datum comparison with geoid (source: 3dmetrica.it)

Once the surface of the reference solid and its position relative to the Earth have been defined, the cartographic representation on a plane is obtained by projection (Figure 43). This is a process that has a mathematical formulation through algorithms but can also be "seen" geometrically. This involves projecting the ellipsoid onto a plane tangent to the area you want to better represent, or even better, in order to reduce deformations, projecting it onto curved unrolling surfaces such as those of a cylinder or cone.

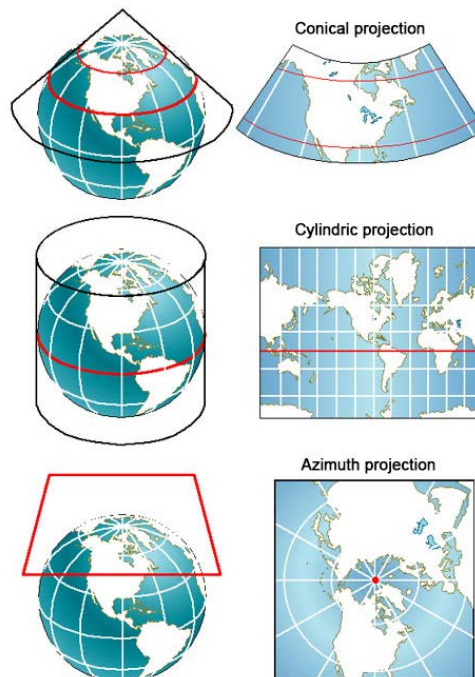


Figure 43 Conical, cylindrical and tangent plane projection (source: openoikos.com).

In any case, distortion of the cartographic result is inevitable because transferring a spheroidal surface onto a plane always leads to deformations that are greater the larger the area to be represented. To limit this phenomenon, conventions are often introduced, such as the most adopted one of projecting the ellipsoid by making it into segments, thus obtaining projected zones (Figure 44). The most widespread conventional projection is the Gauss conformal, and is the one on which much cartography produced in Italy is based in the UTM or Gauss Boaga systems.

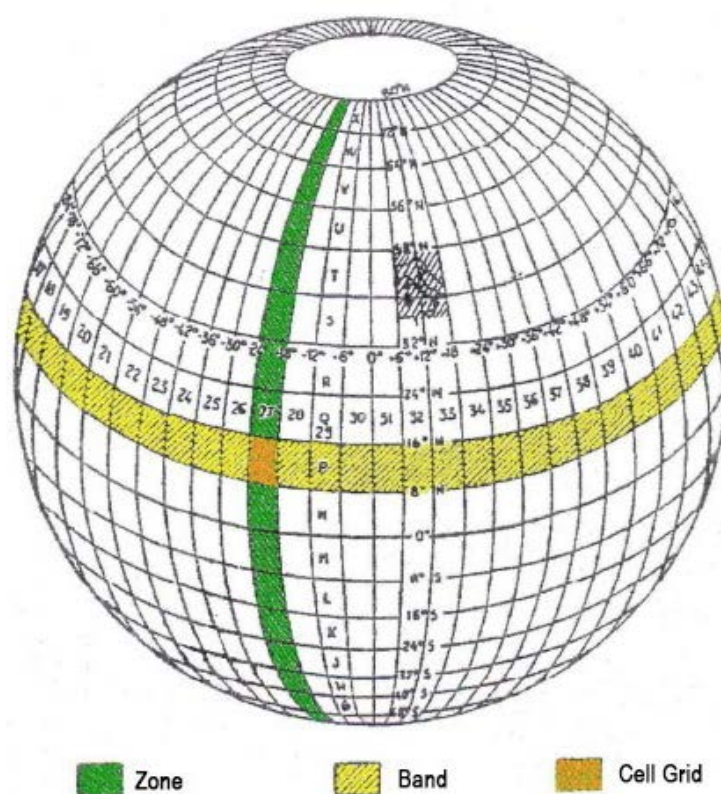


Figure 44 Zones and bands in the UTM system (source: openoikos.com).

Projecting by zones (in the UTM system each of these represents 6° of longitude) it can be seen that the deformation increases as you move away from the central meridian. Therefore, the cylinder is rotated so that the ellipsoid is reprojected from the central meridian of the area to be mapped.

Once the map is represented, it is then a matter of assigning a coordinate system that defines the geographical positioning of the objects.

In GIS these reference systems are called CRS (Coordinate Reference System) or SRS (Spatial Reference System) or more simply SR, which can be classified into two basic categories:

- Geographic (or non-projected) SRs, in which each point on the earth's surface is located based on the angular values of latitude and longitude;
- Projected SRs, in which the location of each point on the earth's surface is the result of a projection resulting in a two-dimensional Cartesian system in which each point has an X,Y (E,N) coordinate pair.

For the GPS survey system, it became necessary to use a datum that is no longer local but global, namely the WGS84 (World Geodetic System 1984) datum. The WGS84 UTM system is based on the datum just seen in geocentric configuration but associating with it the UTM projection system. The WGS84 UTM system is not to be confused with the geographic WGS84 system, which is not a projected system but is based on latitude and longitude values in angular degrees, for the representation of planimetric coordinates. However, a Reference System is the result of several factors, which is why that there are many of them, depending on local needs but also on the diversity of datums, projections, conventions, coordinate systems, temporal evolutions, etc. A new GIS user may have difficulty, even distinguishing one from another on the basis of names, which is why there is the European Petroleum Survey Group (EPSG) registry, managed by an international organization that assigns a unique code to each archived system (Figure 45). To avoid confusion, it is recommended to refer to this registry in the QGIS Reference System database.

DATUM	PROIEZIONE	CODICE EPSG	ALIAS
Roma40	Gauss-Boaga	3003 (fuso Ovest)	Monte Mario / Italy zone 1 (fuso O)
		3004 (fuso Est)	Monte Mario / Italy zone 2 (fuso E)
ED50	UTM	23032 (zona 32 N)	ED50 / UTM zone (32)N
		23033 (zona 33 N)	ED50 / UTM zone (33)N
		23034 (zona 34 N)	ED50 / UTM zone (34)N
WGS84	UTM	32632 (zona 32 N)	WGS84 / UTM zone (32)N
		32633 (zona 33 N)	WGS84 / UTM zone (33)N
		32634 (zona 34 N)	WGS84 / UTM zone (34)N
ETRS89	UTM	25832 (zona 32 N)	ETRS89 / UTM zone (32)N
		25833 (zona 33 N)	ETRS89 / UTM zone (33)N
		25834 (zona 34 N)	ETRS89 / UTM zone (34)N
RDN2008	UTM	6707 (zona 32 N)	RDN2008 / UTM zone (32)N
		6708 (zona 33 N)	RDN2008 / UTM zone (33)N
		6709 (zona 34 N)	RDN2008 / UTM zone (34)N

Figure 45 Main projected SRs used in Italy and their EPSG codes (source: openoikos.com).



In the table above as shown, are the main SRs but not all of them, in fact the processing of coastline change data were performed with the EPSG 6876 RDN2008 / Zone 12 (N-E) reference system. The "Zone 12" system refers to a cartographic system, called "Zone 12," introduced in 2013 to overcome the discontinuity problems encountered in processing data for areas straddling the meridian 12° East from Greenwich, and thus falling within both traditional spindles: 32 and 33. Reprojection from one reference system to another is termed:

- Conversion when it occurs within the same datum;
- Transformation when it occurs between different datums.

Conversion occurs automatically without error while transformation is generally a more approximate operation. One reference system is an ellipsoid (with its mathematical equation), where the surface is made to coincide at a "convenient" point on the earth's surface, which is then turned, constraining it at this very point, to find an even more convenient orientation. On this ellipsoid, all other points on the earth's surface are located by coordinates.

Switching between coordinate systems is not something that can be done rigorously because one does not know the analytical relationships between the reference systems. To understand better consider that Rome 40 and ED50 use the same ellipsoid (oriented differently) and this is good for coordinate transformation, although the accuracy hardly falls below one meter, while to switch between WGS84 and Rome 40 or ED50 things get even more complicated because the ellipsoids are different, we have distortions and contractions.

When we import a file to QGIS, with a different reference system than the project reference system, the program performs what is called "on-the-fly reprojection," that is, it automatically reprojects (provided this is properly georeferenced) a shapefile (or other entities) to the project reference system, but it is a simple visualization operation, which does not convert or transform the object that is inserted into the map. To convert or transform an entity from one reference system to another there is either special software (e.g., CartLab, Verto, Transpunto) or it is a feature that many GIS platforms have (including QGIS) but good results are not always obtained. For example, in QGIS it is necessary to export the projected file indicating the new reference system.

High resolution geomatics techniques for coastline detection and monitoring:  
Boccasette and Barricata case studies (Po River Delta, Rovigo, Italy).

To achieve greater accuracy requires the use of the grids produced by the IGM, which are available in various formats but are not free.

In this thesis, we relied on the potential of QGIS in the input of LiDAR data belonging to a different datum than the project datum in order to compare the zero-line obtained with SfM technique (EPSG 6876 system) and that with LiDAR (EPSG 32632 system).

## **4 Acquisition processing and data return**

## 4.1 The objectives

The approach used in this study aims to compare 3 different methodologies for coastline identification in order to interrogate the various data and obtain a reliable result. On comparing the methodologies, the statistical analysis described below first considers the distances between the measured segments and then the areas.

This procedure allows a more accurate control, because as we will see for some points the complexity of the geometries that came to be created made it difficult to have a correct distance relationship in the evaluation, approximating the calculations, a problem not encountered instead with the use of areas. Once the accuracy of the various methodologies has been analyzed, the interest will be to establish the pros and cons of them based on the following points:

- Accuracy;
- Execution time of the survey phase;
- Amount of data that can be collected by the method;
- Costs.

The Objective of the processing in question as mentioned allows us a comparison between the different methodologies used, using as a study parameter the standard deviation or mean square deviation between the measurements, thus allowing us to have a summary index of the differences of the values of each observation from the mean of the variable, because each observation has a deviation from the mean. To simplify the concept, we can say that the term standard refers to the fact that the calculated deviation represents an average distance, that is, a "typical" distance of each individual observation from the mean

If the observations are exactly the same as the mean, the deviation is equal to zero. If the observed value is less than the mean, the deviation will be negative. Conversely, if the observed value is greater than the mean, the deviation will be positive.

For the calculation it will be necessary to calculate:

$$\diamond \text{ The average } \bar{x} = \sum_{n=1}^n \frac{x_i}{n}$$

❖ The standard deviation  $\sigma = \sqrt{\frac{(\bar{x} - x_i)^2}{n-1}}$

As can be seen from the formula to calculate the standard deviation we use the squares of the deviations, by squaring a deviation  $(\bar{x} - x_i)^2$  we get a positive number, whether the deviation is positive or negative. So, the square allows negative deviations to be added to positive ones without the signs affecting the result by making it zero. The sum of all the variances of the mean squared is called deviance.

On the other hand, the mean of the squared deviations, expressed as the square of the unit used for the variable, is called variance.

For example, in our case the unit of measurement of the variable is meters for distances, the variance will turn out to be expressed in square meters, a quantity that is in fact not very interpretable from a practical point of view for distances.

Since interpreting the value of a unit of measure squared is not easy, we prefer to use the square root, which has the same unit of measure as the variable and the mean. The square root with positive sign of the variance is called the standard deviation or mean square deviation. As for the result, the more variability there is among the observations, the larger the deviations from the mean, the larger the sum of squares, and the higher the value from the variance and consequently also the mean square deviation, so to understand better the standard deviation is equal to zero only if there is no dispersion (all statistical units have the same value), in all other cases it is always greater than zero, and the farther the value is from the mean, the larger the standard deviation. Before starting the discussion on processing it is good to clarify the concept on data conversion. By exporting the survey data to the laboratory the coordinates of the points are obtained, at this point the coordinates must be converted to the desired reference system, in the case under consideration as we have seen the reference system is EPSG 6876 RDN2008 / Zone 12 (N-E) a cartographic, projected reference system. To obtain the following system for all coordinates we used the ConVE program, provided by the Veneto Region, which allows coordinate transformations between different geodetic and cartographic reference systems.

## 4.2 In situ data acquisition

The acquisition phase took place on two different dates, the first at Boccasette on January 27, 2022, and the next at Barricata on February 25, 2022.

For data acquisition, exactly the same approach was used for both case studies, using the time frame of one hour, specifically half an hour before the tidal minimum and half an hour later.

For the use of classical topography, first of all, the ground station points were materialized, point 1000 for the execution of all measurements (Figure 46) and point 2000, to carry out the zeroing operation, or configure the zero angle on a reference (another point). In this case, since there are no redundant measures, no compensation has been made, they are directly obtained. During the days in the available time interval of low tide 278 points were recorded for Boccasette and 230 for Barricata, following the coastline as seen in Figure 47 with an average distance between points of 2.40 meters.

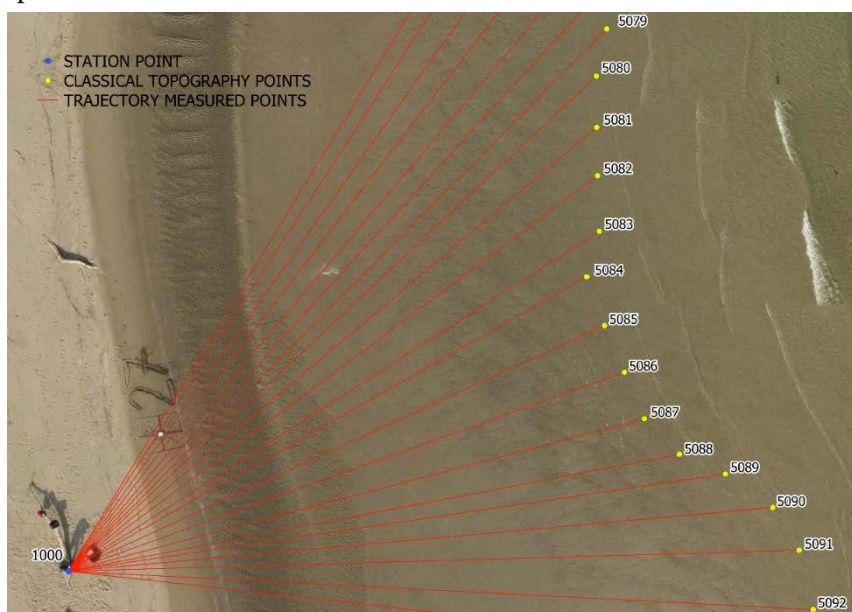


Figure 46 Measurement scheme carried out with Total Station (source: software QGIS).



Figure 47 Measurement acquisition with Total Station in Boccasette.

The use of the GNSS system results as we shall see simpler and faster, the potential of this methodology will be clarified later. For both Boccasette and Barricata, the survey was carried out in kinematic mode and with differential positioning, with a sampling rate of 1 second (Figure 48); thus, each step corresponds approximately to the acquisition of a new point, surveying 4109 points for Boccasette, and 3007 points for Barricata with an average distance between one point and the next of 1.3 m in both surveys.

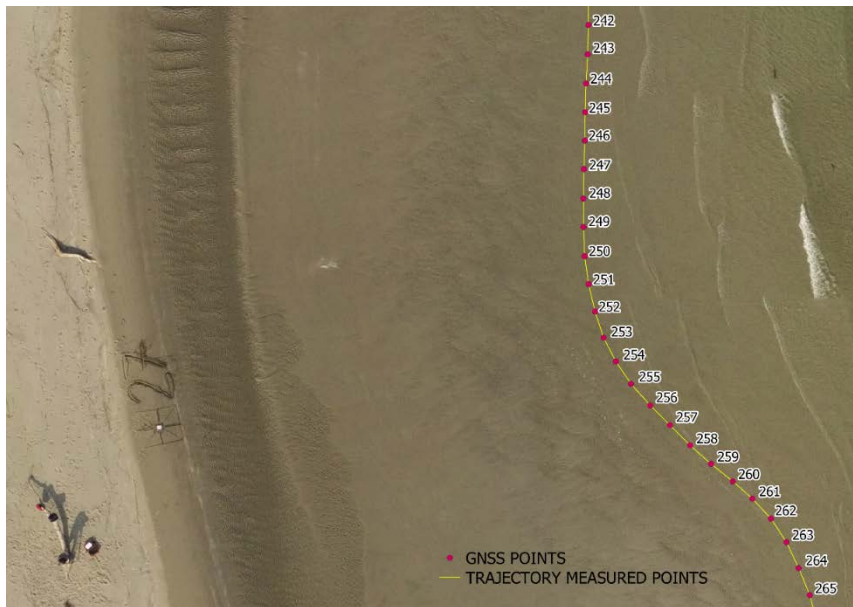


Figure 48 Measurement scheme carried out with GNSS (source: software QGIS).



Figure 49 Measurement acquisition with GNSS in Boccasette.

GNSS was then used to detect the coordinates of station points of classical topography and for the drone survey support points (for external orientation of photogrammetric images), again with differential positioning but in this case rapid static mode.

The support network for the drone on Boccasette consists of 31 points, for which yellow and black targets of 25x35 cm were used (Figure 50), the same for Barricata with 30 points. In both cases, the following aspects were taken into consideration for target placement:

- Visibility in drone photos;
- Good spatial distribution.



Figure 50 Target for the Drone.



The photogrammetric taking phase performed by drone was divided into 4 flights of 15-20 minutes each, in order to be able to cover the area of interest. In surveying the coastline for flight planning, the "Free Flight 6" application was used by programming the following main parameters (visible in Figure 51):

- Flights with 5/6 swipes;
- Length of crawls 420 m;
- Distance between the swipes 30 m;
- Flight altitude 60 m.
- 4 blocks with overlap 50 m.

Flight conditions do not necessarily remain constant throughout the duration of the survey, which is why the cameras are equipped with control devices and maneuvering apparatus that allow in-flight modification of the parameters that condition the flight itself. It is therefore clear that the above parameters are essential to set up the flight correctly to ensure a good survey, but they should be considered as a rough programming of the flight itself. This is because it is not possible to predict the exact course of events during the flight time, either because of the peculiarities of the terrain, which could cause the magnitude of the flight to vary, or because of small but unavoidable variations in the drone's speed, or because of the movements imparted to the drone by the winds. In the present case, a large overlap, > 60%, was made, as we shall see; in this way, most of the points on the ground are acquired from at least 9 images, which allows for increased accuracy. For this survey methodology, the different climatic conditions encountered at Boccasette compared to Barricata greatly affected the final orthophotos, highlighting limitations and difficulties.

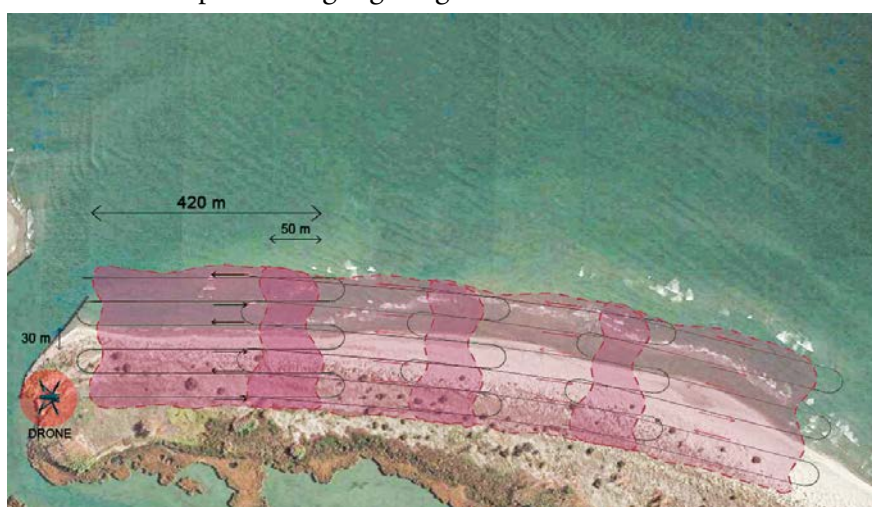


Figure 51 Photogrammetric acquisition scheme in Barricata.

High resolution geomatics techniques for coastline detection and monitoring:  
Boccasette and Barricata case studies (Po River Delta, Rovigo, Italy).

In image 52 we see an example of the principle of image acquisition, in drone during the flight takes a whole series of images, leading to the result visible in Figure 53.



Figure 52 Measurement acquisition with Drone in Barricata.

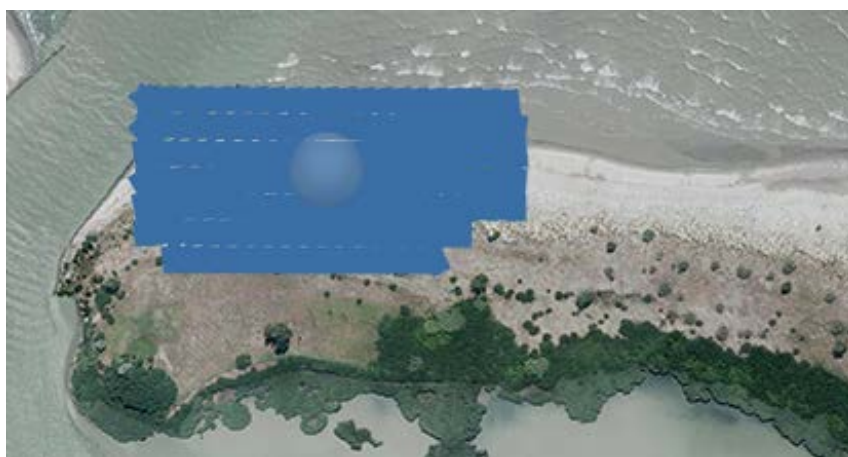


Figure 53 Image block after photogrammetric survey.

### 4.3 Image processing with SfM technique

Once the data has been set to perform the survey and the survey has been carried out, we move on to the post-processing phase of the drone images, and Agisoft Metashape software was used to do this.

The mentioned software automatically recognizes the homologous characteristic points in the various photos, thanks to computer algorithms of computer vision. We have inverse perspective construction algorithms that align the photos with each other producing a scattered point cloud, and then proceed to align the entire set and distribute the error thus allowing the production of a dense cloud through classical stereophotogrammetry formulas. Through interpolation of the dense cloud, it produces a three-dimensional surface (mesh), on which it projects the photographs, thus generating the complete texture. A three-dimensional model of the area in this case is thus created. Images concerning a terrestrial acquisition or a photogrammetric flight can thus be inserted within the program.

The workflow in the software can be divided into the following stages:

- Photo insertion;
- Image alignment: where the software automatically goes to identify homologous points, detects the position of each image and refines the calibration parameters, returning a sparse point cloud;
- Construction of the dense point cloud;
- Alignment and merging of chunks;
- Construction of the 3D polygon mesh;
- Texturing operations in the 3D model, creation of orthophotos and Digital Terrain Model (DTM);
- Orientation and scaling of the model.

Once the photographic set is complete, individual photographs can be acted on in postproduction to sharpen them using noise filters, balance whites, or correct their color palette and apply color profiles. Agisoft also offers the possibility of using masks to remove noise that is not necessary for the restitution of the object, such as persons. The process for loading photos into the software is as follows: *Workflow > Add photos*, once the images are uploaded, the screen appears as in Figure 54.

High resolution geomatics techniques for coastline detection and monitoring:  
Boccasette and Barricata case studies (Po River Delta, Rovigo, Italy).

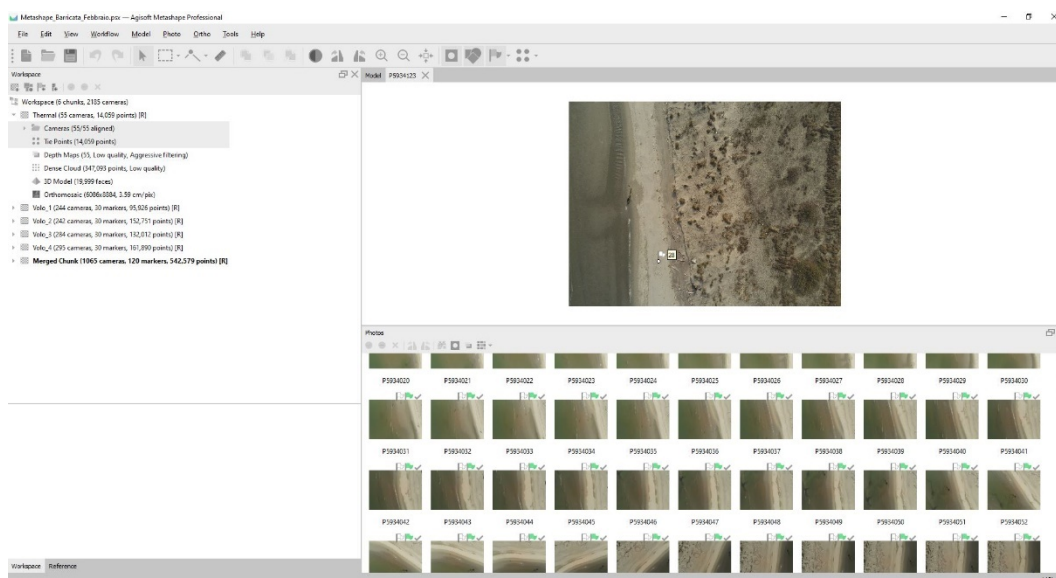


Figure 54 Loading images within the Agisoft Metashape software.

We now proceed to the observation of the loaded images, in particular to their quality, a poor dataset could negatively affect the results of the alignment, the program to facilitate the process allows a function of automatic estimation of image quality, through the command "estimate image quality", the process analyzes all the images in the dataset giving a judgment, based on the stability, sharpness, accuracy and illumination condition of the images, in the quality column we see values between 0 and 1, in this case 0 worst quality 1 highest, images with quality at 0.5 units are recommended to disable them and then exclude them from photogrammetric processing, provided that the rest of the photos fully cover the scene. Next, I import the list of targets with their coordinates (georeferenced), I then go on to manually identify on the images the target centers by assigning the relevant target from the list of imported ones.

Now we move on to setting the reference systems, indicating to the software, the general design one (UTM zone 12), the one of the drone-supplied grab positions (WGS 84), and the reference system of the targets' coordinates (UTM zone 12), after which the software proceeds with a seven-parameter transformation to unify everything in UTM zone 12.

The next step involves aligning the images, through the *Workflow > Align photos* command, and in the screen, we can decide the quality of the alignment (Figure 55).

The targets do not intervene in the orientation of the individual images but in the rototranslation and scaling (and thus georeferencing) of the 3D model (sparse cloud consisting of the tie points, produced with the "Alignment" phase of the images. In the image alignment phase I already obtain errors on the targets that give us the accuracy of the produced model through the root mean square deviation (RMS), so I know the mean error, calculated on the model targets, which in our case for Barricata results in 3.6 cm using 30 targets and for Boccasette in 4.2 cm using 31 targets.

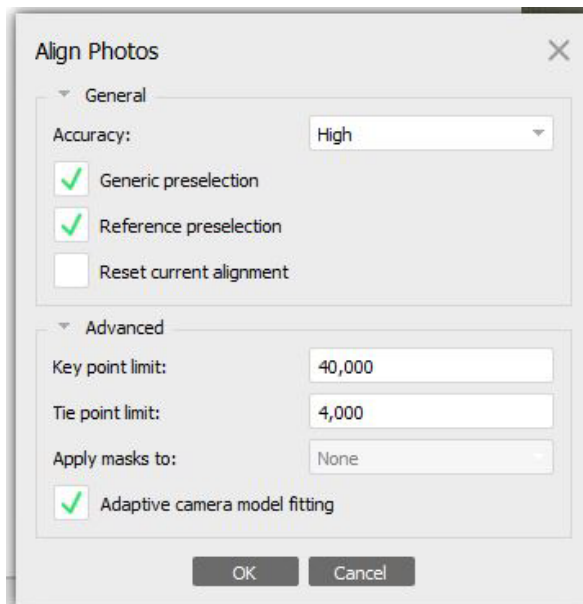


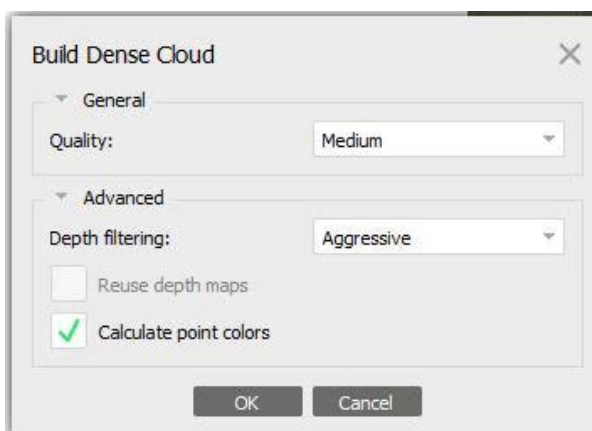
Figure 55 Screenshot of Metashape with photo alignment setting.

At this point the next step is the cleaning of the sparse cloud to remove all the parts that do not concern the area of interest, to lighten the file for the next steps.



Figure 56 Sparse cloud.

Now let's see how to switch from the sparse cloud (Figure 56) to the dense cloud (Figure 58) , to do this we follow the following *Workflow > Build Dense Cloud* commands (Figure 57). If we set higher quality settings we get more detailed geometry, but on the other hand we have heavier



processing that takes more time. The interpretation of quality parameters at

Figure 57 Screenshot of Metashape with the dense cloud setting.

this stage is similar to those given in image alignment. The only difference is that in the case of *Ultra High* setting the images are processed in the original format, while each subsequent quality implies a reduction in scale. *Depth filtering* indicates the depth of the Metashape calculation map, or rather the methodology for dealing with anomaly points, referred to as *outliers*. In the project under consideration, the Aggressive filtering algorithm was used to eliminate most of the *outliers*, this is because the beach has a fairly flat surface. I could not have done so in the case of complex surfaces where moderation of filtering is recommended. Sparse points present as a result of processing can be removed manually if not considered necessary.



Figure 58 Dense cloud.

So after aligning the photos and creating the dense point clouds, we now need to merge them with the command: *Workflow > Merge chunks*, which performs the merge of the different chunks based on the georeferencing information, which was previously performed on the individual chunks, thanks to the georeferenced targets. In the study design we have 4 chunks for Boccasette and 4 for Barricata, corresponding to the 4 flights performed for each area. After the creation of the dense cloud we move on to the creation of the mesh, to do this always in the usual panel we execute the command *Workflow > Build Mesh* (Figure 59).

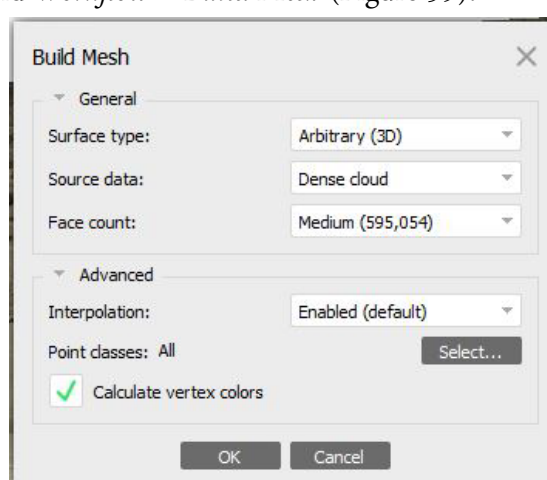


Figure 59 Screenshot of Metashape with the mesh setting.

In this case a number of faces must be set for our mesh, depending on the number of faces the file will have a different weight and resolution, and the time for computation will be directly proportional to the choices made. At this point the software allows us to color the mesh seemingly very good (Figure 60), but if we go to zoom in I notice that it loses quality and detail, and in our case the detail in the identification of the coastline is crucial to establish the precision of the method, it is therefore necessary to apply the texture derived directly from the images, since the one produced through the color of the individual points of the dense cloud is not sufficiently resolved.



Figure 60 Mesh of Barricata.

The mesh can in fact be colored according to the point cloud, but as mentioned, to obtain an excellent and detailed orthophoto, the next step requires texturing using images. Texturing gives us a different order of perception than the previous steps, due to the photorealistic 3D representation with high quality and detail, thus achieving better graphic content. The command is executed as in the previous cases from the *Workflow > Build Texture* (Figure 61) panel in this case if I have not generated the mesh I cannot generate the texture, and the texture is closely related to the mesh on which it lays, if I change the detail of the mesh, I have to redo the texture.

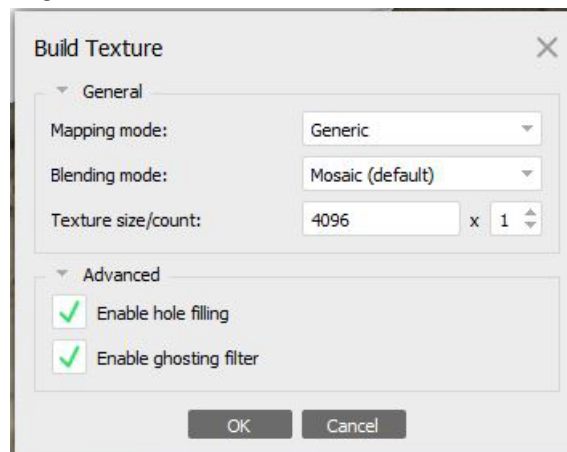


Figure 61 Screenshot of Metashape with the texture setting.



As you can see, we can say that the photogrammetric process generally proceeds in cascade. The resulting product, termed, global orthophoto is a purely two-dimensional product, a high-definition raster (image) constructed by taking all the images in the dataset that make up the photogrammetric project (or those that I am interested in) to create the final product.

The photos are corrected in distortion, are projected onto a surface that can be for example the DEM or Mesh, and a product is generated that is very useful for topography but also for the purpose of planning. The classic zenith orthophoto has the characteristic of being a georeferenced image, so it includes all the georeferencing information derived from the project, from the support points, and verified on the control points, with coordinates within a particular reference system. It is orthorectified, that is, each point is viewed as if it were projected orthogonally, distortions related to photographic optics are eliminated, it is scaled correctly, and it is oriented with respect to north. I thus obtain a product that allows me to work within a GIS or CAD, and because of the fact that it is georeferenced and scaled data, the measurements I take on an orthophoto, between two points, is effectively (minus the accuracy of my survey) the same planimetric measurement that I would take going into the field with the topographic instrument.

Following image 62 and 63 we see the orthophotos obtained respectively for Boccasette and for Barricata.

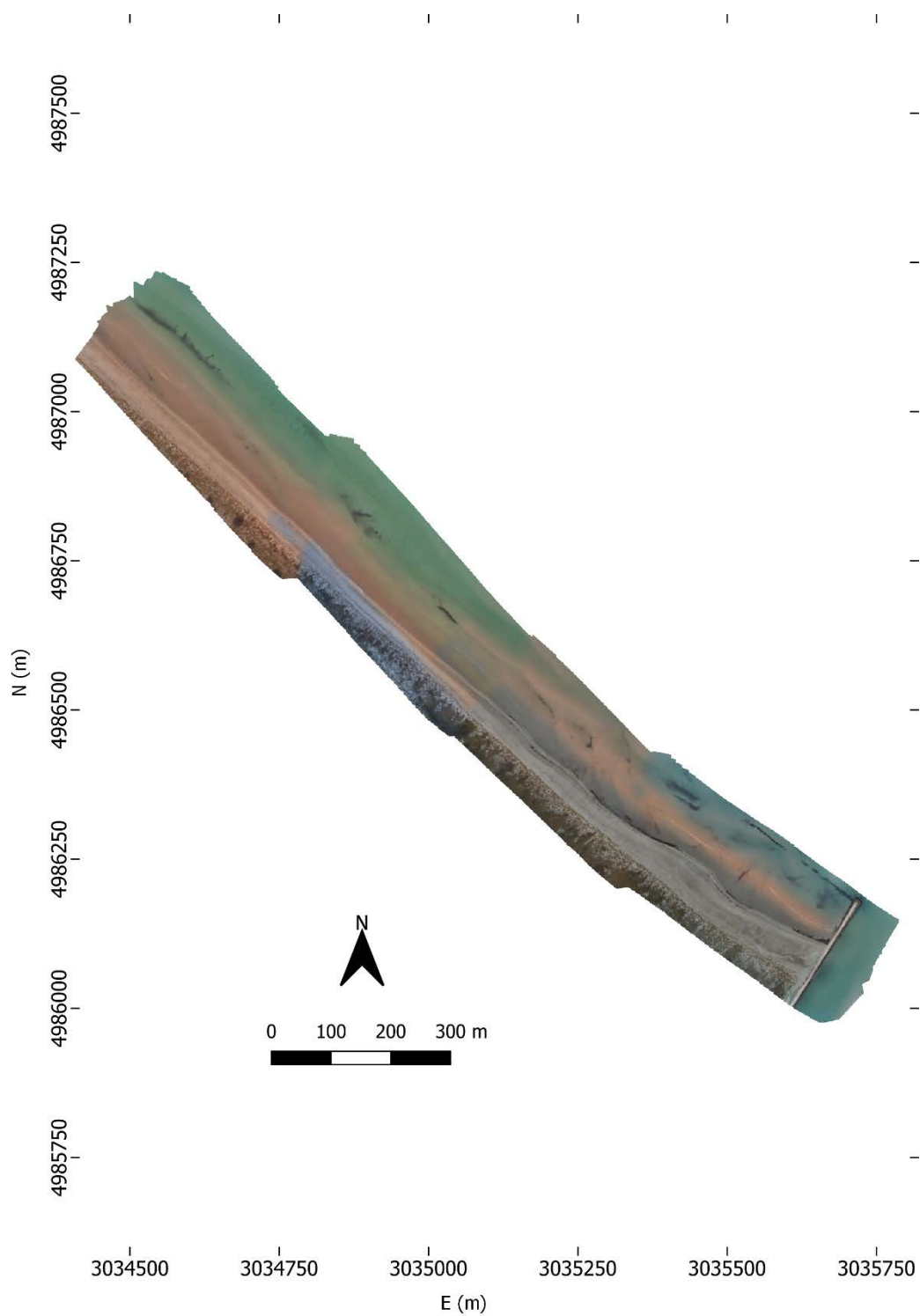


Figure 62 Final product following texture mesh dressing for Boccasette.



Figure 63 Final product following texture mesh dressing for Barricata.

As we have said the orthophoto is a two-dimensional product, so from it we can derive planimetric measurements, to obtain elevation references, with lower resolutions, generally compared to the point cloud, we have to go to the creation of a DEM (Digital Elevation Model), to create it we go to *Workflow > Build DEM* (Figure 64).

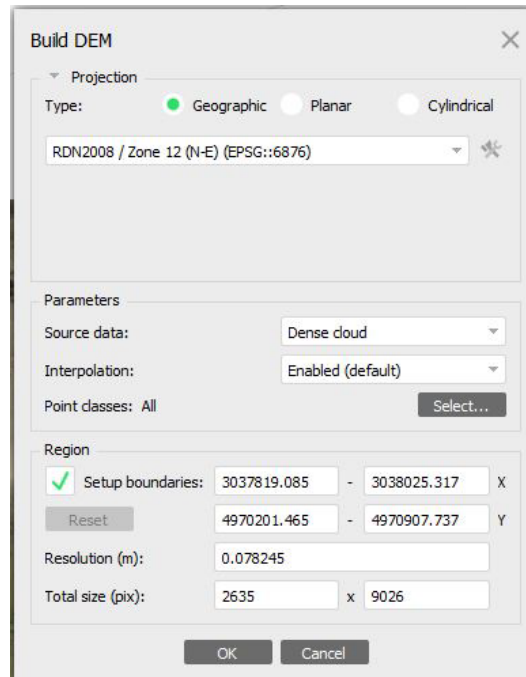


Figure 64 Screenshot of Metashape with the DEM setting.

For the creation of the DEM the basic data is the point cloud, which in this case is dense, the final product is composed of pixels with a size of 0.078 m in the present case. So as can be learned the raster is composed of a large number of pixels to retain higher accuracy (richer in information). We can see the DEM in image 65.

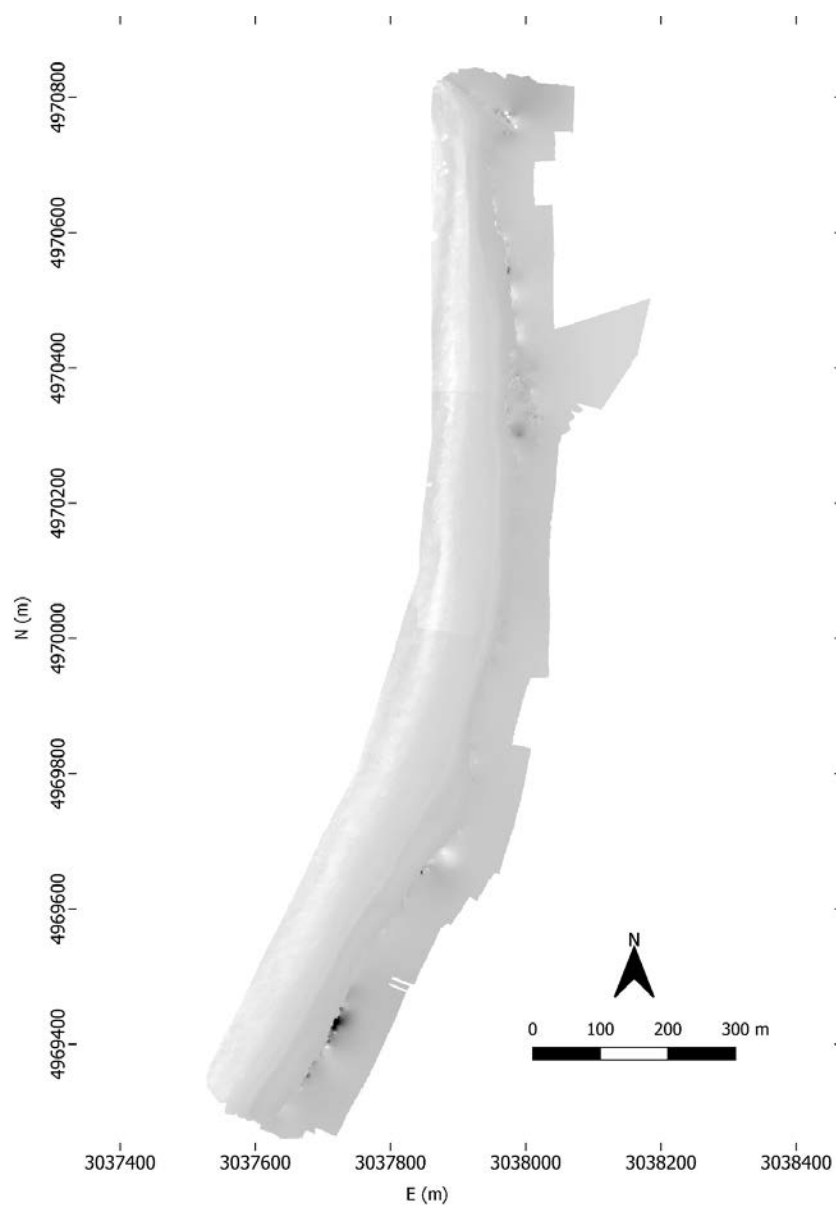


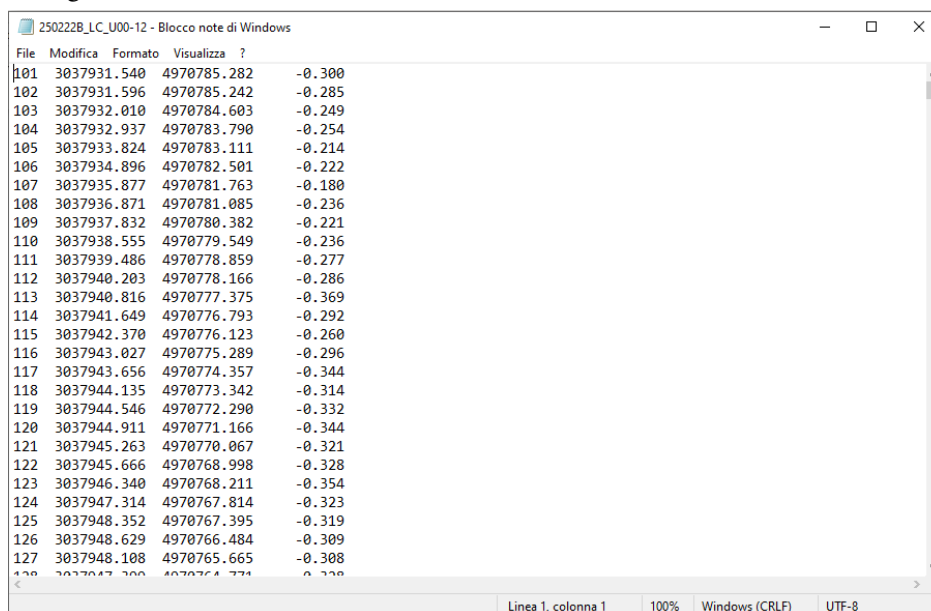
Figure 65 Product processing DEM for Barricata.

Having arrived at this point we can consider the post-processing on Metashape as finished, we now have the possibility to export the data in different formats and then, use the result with other software, deriving all the information we wanted to get from the photomodeling. The procedure seen was followed similarly for both Boccasette and Barricata beaches.

#### 4.4 Geomatic data processing for coastline definition with AutoCAD

AutoCAD software devised by Autodesk, allowed us a step-by-step study in coastline identification. AutoCAD was created for 2D and 3D drawing as we have seen, modeling the elements at will according to our needs. I chose the following software and did not go directly to GIS to verify that the calculations performed automatically by the GIS software, were in line with what was to be achieved, that is, the calculation of the mean and standard deviation. As we will see later, I did not analyze both zones and all cases with AutoCAD, but only one, this was because then the process was repeated and once the correspondence was verified in the GIS software the work was greatly speeded up and simplified. In fact, GIS as we will see in the next section offers several plug-ins that allow to speed up the steps and shorten the processing time. Let us now look at the procedure for processing data with AutoCAD in order to create a clear and defined overview of the choices made.

Once you have set up the data on the desired system as we have seen you can start processing with the software. The data are presented in text format, on a file as can be seen in Figure 66.



File	Modifica	Formato	Visualizza	?
101	3037931.540	4970785.282		-0.300
102	3037931.596	4970785.242		-0.285
103	3037932.010	4970784.603		-0.249
104	3037932.937	4970783.790		-0.254
105	3037933.824	4970783.111		-0.214
106	3037934.896	4970782.501		-0.222
107	3037935.877	4970781.763		-0.180
108	3037936.871	4970781.085		-0.236
109	3037937.832	4970780.382		-0.221
110	3037938.555	4970779.549		-0.236
111	3037939.486	4970778.859		-0.277
112	3037940.203	4970778.166		-0.286
113	3037940.816	4970777.375		-0.369
114	3037941.649	4970776.793		-0.292
115	3037942.370	4970776.123		-0.260
116	3037943.027	4970775.289		-0.296
117	3037943.656	4970774.357		-0.344
118	3037944.135	4970773.342		-0.314
119	3037944.546	4970772.290		-0.332
120	3037944.911	4970771.166		-0.344
121	3037945.263	4970770.067		-0.321
122	3037945.666	4970768.998		-0.328
123	3037946.340	4970768.211		-0.354
124	3037947.314	4970767.814		-0.323
125	3037948.352	4970767.395		-0.319
126	3037948.629	4970766.484		-0.309
127	3037948.108	4970765.665		-0.308
128	3037947.300	4970764.731		-0.300

Figure 66 Geomatic data in text format.

In Figure 66 we have, in the first column ID of the point, in the second the EAST coordinate, in the third the NORTH coordinate, and in the last the elevation. The elevation as noted is expressed in orthometric (geoid) coordinates, although the GNSS detects ellipsoid elevations, this conversion is always done with the conVE software.

At this point once we have clarified the data, we are left with the import within Autocad software, to do this we use the DxfF\_Coo plug-in (Figure 67) provided by the Survey and Geomatics Laboratory of the University of Padova.

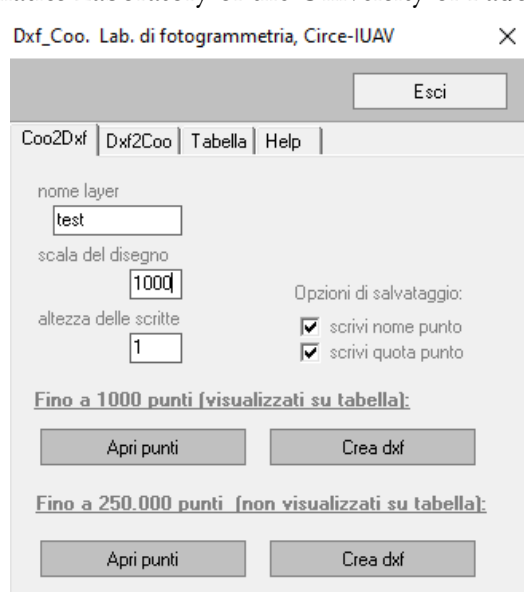


Figure 67 Plug-in DxfF\_Coo setting.

You go to set the parameters, and proceed with open, at this point once you have done the procedure you will come up with a dxf. file that can be read by the CAD software. Within AutoCAD you just head to insert, then insert again, on the screen that opens enter the dxf. file. At this point the data is entered as a point file, I perform the procedure for both those measured with GNSS and with classical topography (Total Station).

Being point data we need to run a polyline between the various points in order to draw the line connecting the GNSS points and topographic points, and then draw the distance between them and calculate the areas of the polygons between the two lines. In our case, the GNSS data being a fairly large number, we made use of software for automatic polyline creation, thus saving time in creating the paths.

The software in question is Grasshopper for Rhino 7, one of the most powerful algorithmic modeling software for creating and controlling simple and complex shapes in architecture, engineering, and design.

Grasshopper requires no programming or scripting knowledge; the computational process is done by defining a node diagram (algorithm) that can describe the mathematical and geometric relationships present. In Figure 68 we can see the algorithm that allowed us to construct the polyline.

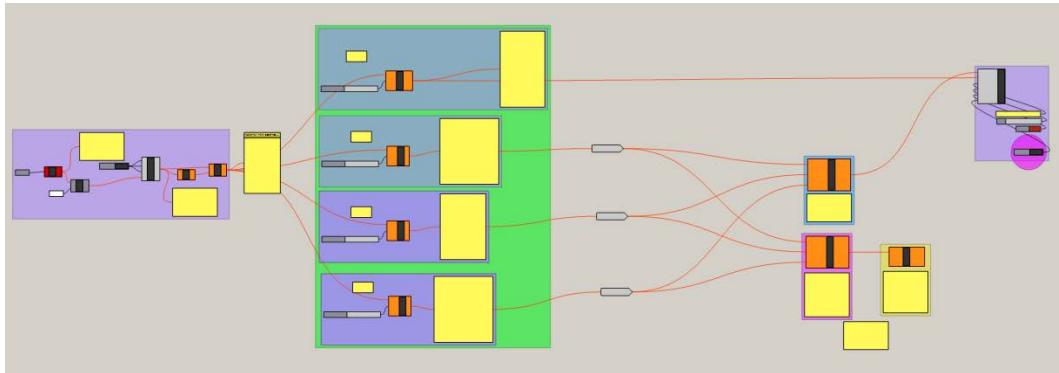


Figure 68 Algorithm created on Grasshopper for Rhino 7.

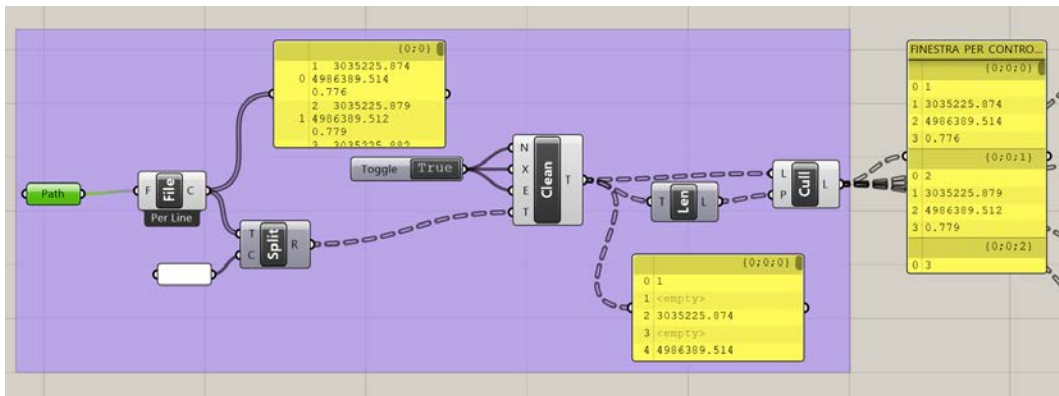


Figure 69 Algorithm details first box at left image 68.

Models developed with Grasshopper are dynamic systems that can be modified in real time by varying the parameters defined during diagram construction, with immediate advantages in shape control and rationalization. Once the file is created simply save it in dwg. format. Without divulging too much about Rhino we now return to the project in CAD, having loaded the polylines we can now move on to the study of the coastline, for the determination of the distances it was decided to



project the points surveyed with classical instrumentation on the GNSS point line, while for the areas we created screens, for both areas and distances we considered positive the values to the northeast of the GNSS line and negative the values to the southwest of it. We see in Figure 70 the extraction of part of the processing with relative legend.

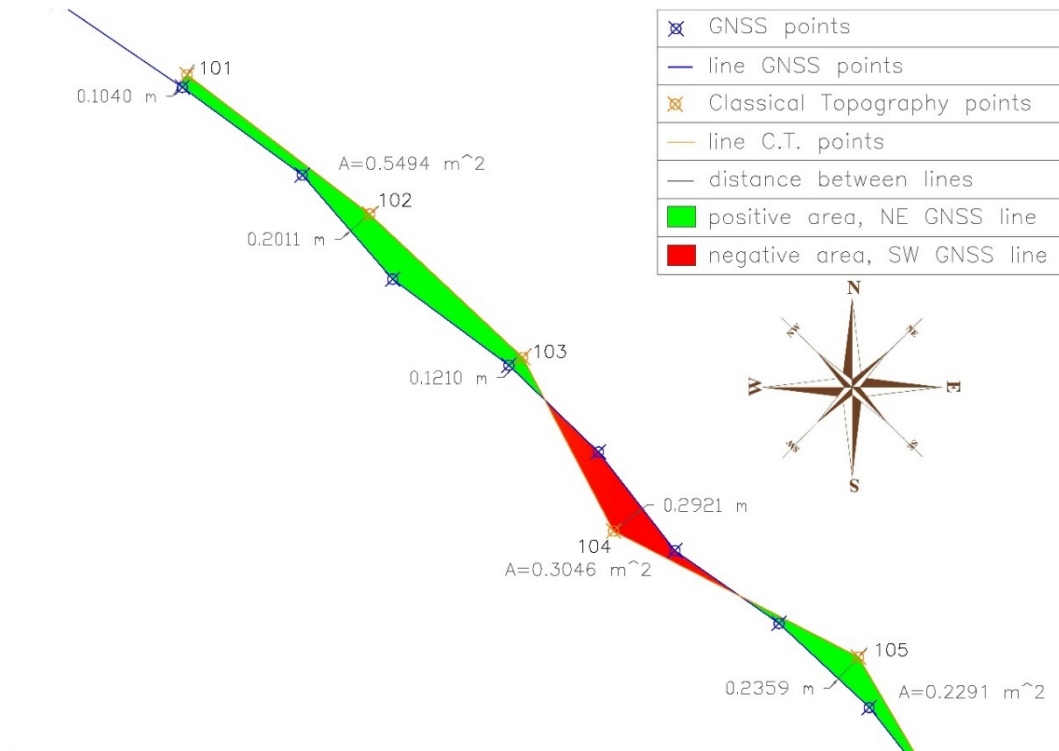


Figure 70 Result with AutoCAD software for distances and areas.

Once the design was executed and the various aspects necessary for the study determined, the values were reported in an Excel spreadsheet for the calculation of mean and standard deviation, to assess the dispersion of the data when comparing the two methodologies. As it can be guessed from this brief discussion following such a procedure for the study we are dealing with turns out to be a long and laborious procedure, in my case it was useful to verify the equality obtained between the calculation performed on Excel of which I know the steps and the one elaborated by the GIS software, once I verified everything I switched to GIS which is much more practical and fast for these types of analyses.

With this does not mean that AutoCAD is not a good software, but it is inferred that it is more suitable for the production of digital drawings, in our case the main objective is not drawing but the study of geographic data.

#### **4.5 Geomatic data processing for coastline definition with QGIS**

In this section we are going to look at the basic steps to compare the various methodologies, thus going into detail about the survey in post-processing.

When starting the software, the first step is to open the orthophoto available from the Veneto Region as a base of support, so the position of the points in the context once imported will be immediately known. In the GIS environment, setting the correct reference system is of fundamental importance as different systems could result in points being inserted in completely different areas.

To insert the orthophoto we go to the Veneto Region geoportal, and we go to copy the link that shows the orthophoto entry, which is present among the OGC services made available. From QGIS we go to open the orthophoto via, *Browser > WMS/WMTS > new connection*, we enter a name, and in the URL field we enter the link, at this point by clicking the *WMS/WMTS* entry the new option will be visible, we select the orthophoto of interest and give the correct reference system.

Continuing, for data entry within the GIS software there are no particular problems, as the data are available in text format (notepad), once the delimited format (.csv) is created it is possible to bring them within the program. The data exported from the tools look like we saw in the previous paragraph image 66, to convert them to csv. format once they are organized it will be enough to set to *"Save as > All Files"* and in the file name enter the suffix *".csv"*. An important note on this step concerns the organization of the data, it is recommended to set in the first line the identifier of the coordinates (*ID, E, N, Z*) so that the software manages to place each point in its place and using the replace command we go to set the subdivision of the data by setting the desired separator, thus avoiding trivial errors.

At this point we move inside QGIS, on the menu bar we head to *Layer > Add Layer > Add Delimited Text Layer*, once we select the file and set the parameters, we can check the preview and if everything looks correct, we click Add.

QGIS returns us a point file and each point has its own coordinates.

In the process of saving files it is good to be ordered by creating separate folders for each block of steps, this organization is very useful to us if we want to delete layers that we no longer need. We proceed in a similar way for the various data surveyed with classical topography (Total Station) and GNSS in the survey areas.

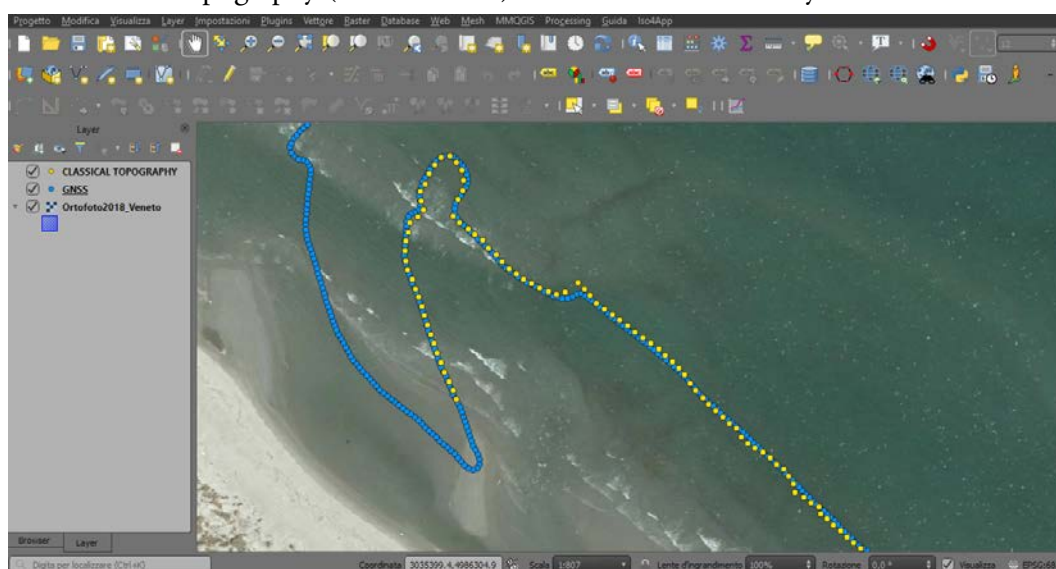


Figure 71 Points exported to QGIS from csv. format Excel files related to Total Station and GNSS.

As you can see from Figure 71 the points appear to be distant from the shore, this is not an error because both surveys were done at low tide, so the moment we go to insert the orthophoto created at low tide the points will appear to be in place, at the moment we use this orthophoto as a general verification base.

At this point it is necessary to save the imported files within QGIS, to do this we go to the layer right button *Export> Save elements as...* in the screen that opens we can select the desired format, in this case in *shapefile*. The procedure just seen has to be repeated for each layer. In the destination folder created earlier to respect the order in data management five files will be created for each layer, it is good not to delete any of them as they contain useful information for reading the shapefile (*shp*). Just to clarify the concept among the 5 files we have (*.prj* and *.qpf*) this means that the reference system (SR) is defined, in fact opening with notepad these files I see the reference system (Figure 72), if instead they are not present it means that the SR is not defined. The remaining files (*.dbf*, *.shp*, *.shx*) are critical, if I delete even one of them by mistake the file will be corrupted and no longer functional.

High resolution geomatics techniques for coastline detection and monitoring:  
Bocasette and Barricata case studies (Po River Delta, Rovigo, Italy).

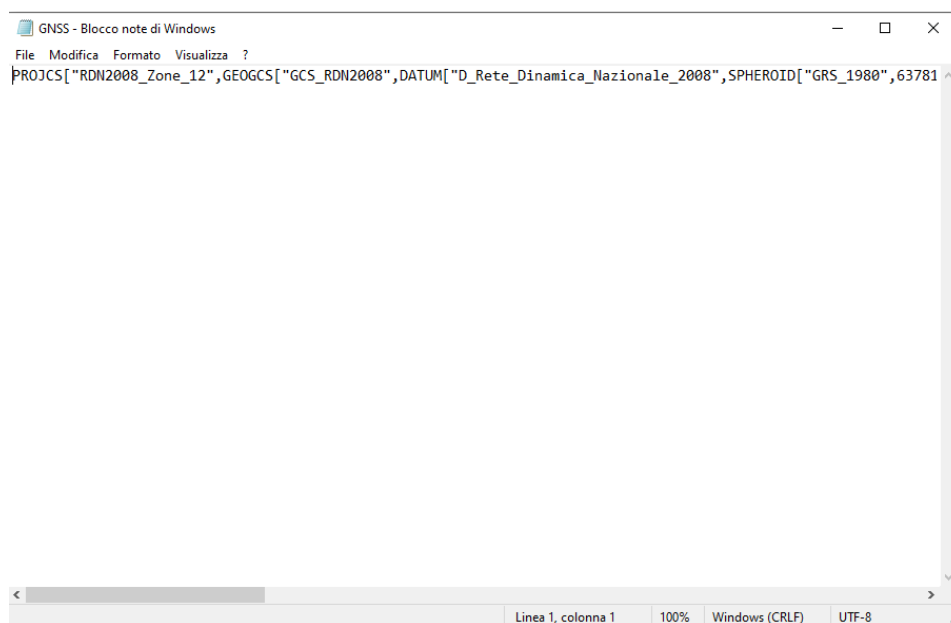


Figure 72 Reference system display from notepad.

Having arrived at this point, we have all the data we need to carry out the coastline identification and variation study.

#### ***4.5.1 Methodology for comparing classical topography (Total Station) and GNSS***

Once the data have been imported, the comparison phase can be started to evaluate as we said the mean and standard deviation. The first comparison is made between classical topography and the survey with GNSS, first analyzing the distance ratio, between the points measured with classical topography and the perpendicular with the line constructed on the GNSS points. A second check, on the other hand, concerns the polygons that are formed between the segments joining the points of the same methodologies. For all cases, the comparison involves distances and areas, due to the problems outlined in the discussion of the objectives. These two approaches thus allow us to identify how far apart the two surveys, made with two methodologies that are both accurate but used by two different operators, are, thus including the sensitivity of the operator in identifying the coastline. An important note to make concerns the precision of the instruments, in this case both instrumental accuracies are well above the margin of error, related to the fact that the coastline between land

and water is not uniquely definable due to the wave motion of the sea, which despite being greatly reduced at low tide is still present.

Another important note to consider before starting the discussion concerns the division of distances and areas, we consider positive value if in the direction of the open sea relative to the GNSS line, negative in the opposite case (beach direction).

#### 4.5.1.1 Calculation with distances

To perform the following step, within the QGIS software, we are going to join the GNSS points with a continuous line. To do this from the menu bar; *Processing* > *Tools* > *Vector Analysis* > *Points to Line*, as input vector GNSS points, sort ID and then run. We are ready to go and calculate the perpendicular distance between the points of the classical topography and the GNSS line we just created. On the classical topography points we open the field calculator, once the screen opens, we set as in Figure 73.

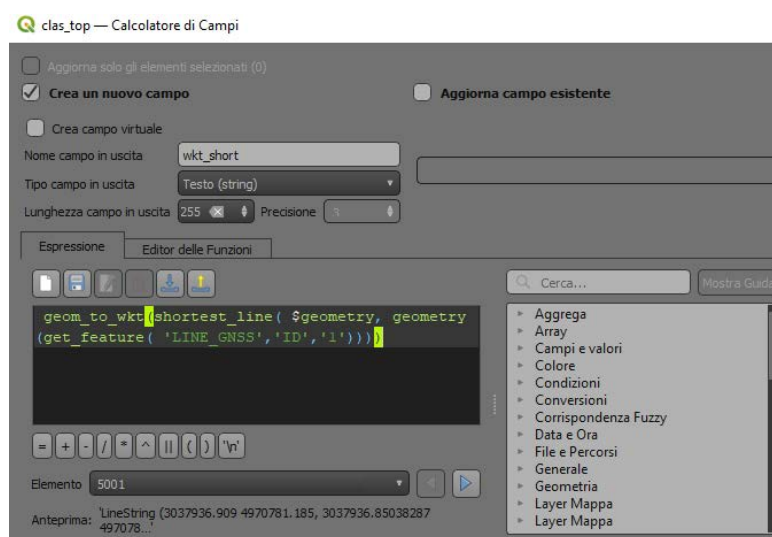


Figure 73 QGIS field calculator setting for line point distance.

At this point from attribute table, we can see the whole string for each point reporting the line of minimum distance, or rather the geometry, but we are interested in its distance value, to do this, from attribute table we open the field calculator and create a new field set as in Figure 74.

High resolution geomatics techniques for coastline detection and monitoring:  
Boccasette and Barricata case studies (Po River Delta, Rovigo, Italy).

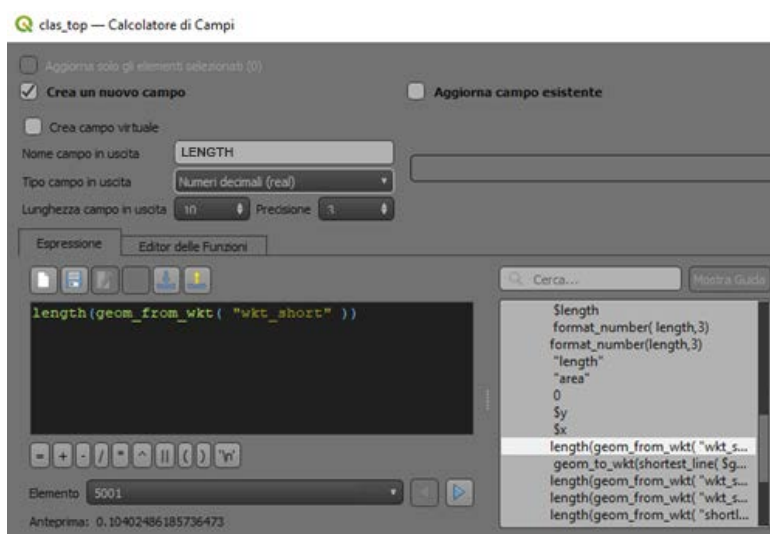


Figure 74 Setting the QGIS field calculator to obtain the distance value.

We have thus calculated all the perpendicular distances. If we want to view them to understand how the software worked, we export the point file and save it in delimited text format (.csv) by going to the right-click layer and clicking on export. If we go to now import that file into the project the distances in meters appear. To see the value on the screen double click on the layer and activate simple label.



Figure 75 Result processing with distances in meters.

Once we get the distance, the values are all positive, but as we had mentioned earlier, we want the positive sign for the points toward the sea and negative for those toward the beach. To do this we duplicate the GNSS line and modify it with the vertex tool command creating a closed boundary on the points towards the sea, we select the created boundary and go to *Processing > Tools > Vector Geometry > Line to Polygon*, or *Processing > Vector Geometry > Polygonize*, the next step aims to cut the points that fall into the created polygon (points towards the sea), so we go to *Vector > Geoprocessing Tools > Cut*, set up the two layers and the program returns an output with only the points falling in the chosen boundary, we do the same procedure for the points toward the beach and thus get its layer of points. Now we want the values towards the beach to be negative, so from the attribute table I open the field calculator and create a field where I enter the name and, in the function, the negative sign in front then recalling the field with positive value, in this way it turns out negative (Figure 76), or if we don't want to create a new field I use an expression as in the Figure 77.

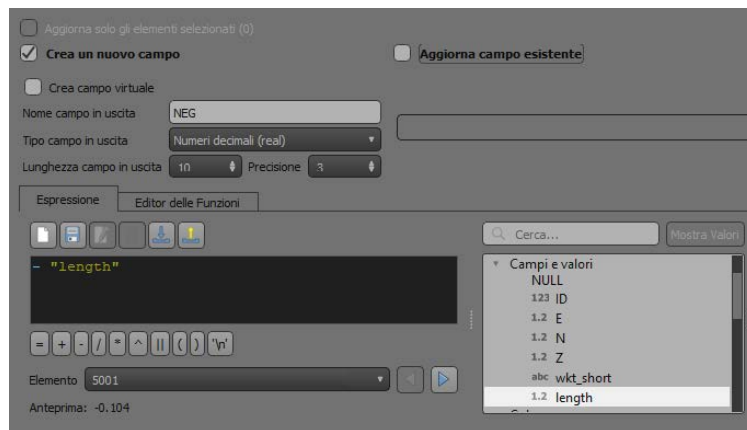


Figure 76 With field calculator.

	ID	E	N	Z	wkt_short	sum_len
1	5001	3037936,908999...	4970781,184999...	-0,31	LineString (303...	0,104
2	5002	3037938,370000...	4970780,069000...	-0,302	LineString (303...	0,2011
3	5003	3037939,595999...	4970778,921000...	-0,407	LineString (303...	0,121
4	5004	3037940,324000...	4970777,532999...	-0,414	LineString (303...	-0,2921
5	5005	3037942,285000...	4970776,524000...	-0,38	LineString (303...	0,2359

Figure 77 With expression.

All that remains is to merge the two layers to get the final product that will allow us by querying it to find the dispersion of the measurements, to do this from the *MMQGIS* > *Combine* > *Merge Layers toolbar*, the final product will be a single layer with two fields inside one with the positive values and the other with the negative values, even those we use the field calculator to merge them, and as seen just now for the negative value, I call up the fields and put a sum sign between the two in this way in output I get only one field with the desired values. In Figure 78 we have the result.

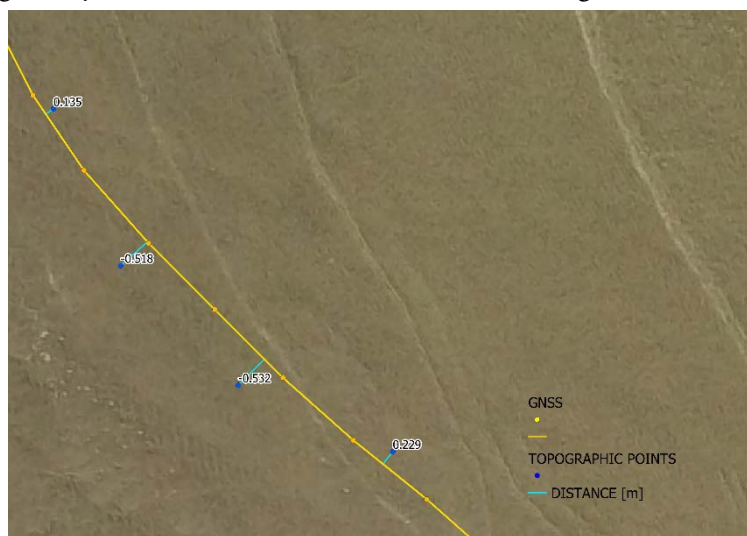


Figure 78 Layer union with positive and negative distances for calculating mean and standard deviation.

For the mean and standard deviation, we now just go to *View* > *Summary Statistics*, set the layer created and the last field created with the summed lengths, and the software automatically returns the values searched.

#### 4.5.1.2 Calculation with areas

Let us now consider the areas for calculation, to do this we use the segments joining the points measured with classical topography and GNSS, respectively. Before creating the lines in a similar way for what we have seen in the calculation with distances, it is essential in this case to bring the elevations of the points to zero and consider only their planimetric position, in order to be able to create the areas between the points of intersection of the lines, otherwise if we leave the value of the elevation the lines will never intersect and the calculation of areas is not possible. To do this, from the attributes table we update the dimension (z) field with the value to



zero. We create the lines again with the points at zero elevation and then move on to merge the two lines to create the polygons inside, to do this we go to *Processing* > *Tools* > *Vector Overlay* > *Merge*. Still in the processing menu we now go to *Tools* > *Vector Geometry* > *Polygonize*. The output layer is the various areas between the two lines divided by the intersection points (Figure 79).

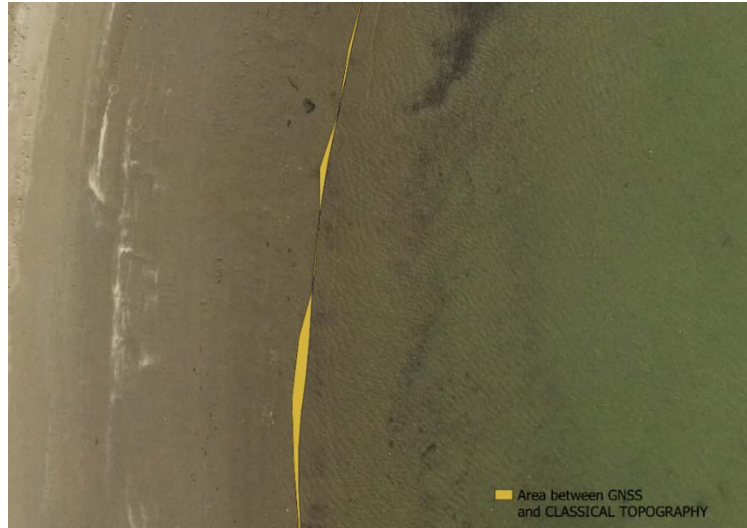


Figure 79 Area created between the two lines as a result of the polygonize command.

Now as with the distances we want to subdivide the positive areas towards the sea from the negative areas towards the beach, with respect to the GNSS line. So, let's go and create as before a copy of the GNSS line and create a closed line that takes in all the positive areas. At this point in a similar way to the previous case we use the command from *lines to polygons*, thus we obtain the polygons. By heading to the menu bar *Vector* > *Geoprocessing Tools* > *Cut*, we can extract the areas of interest by difference (Figure 80).

The same procedure should be followed for the negative areas. Having arrived at this

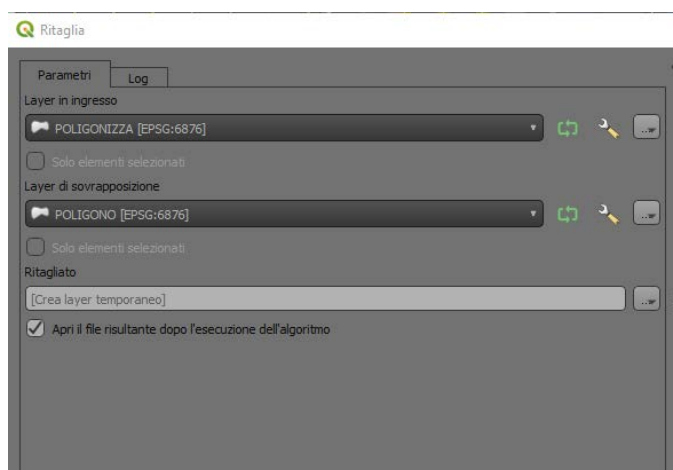


Figure 80 Setting to cut polygons.

point we have two layers one with negative areas and one with positive areas, it is now necessary to head to the attribute table, calculate the areas using the field calculator, heading to the geometry item and I give the command  $\$area$ . Another step is to delete the fields with zero area and assign the negative areas the negative value. Similarly, to the distance points with the Merge Layers command, we merge the two shapes and thus obtain the product (Figure 81) to query via *Summary Statistics* to obtain mean and standard deviation.



Figure 81 Layer union with positive and negative areas for calculating mean and standard deviation.

#### 4.5.2 Methodology for comparing photogrammetry and GNSS

At this stage, the objective still remains the comparison between survey methods, for the identification of the coastline, but the approach changes. In the previous case the measurements were directly provided by the instrumentation, in this case for the photogrammetric part the restitution of the coastline took place directly on the orthophoto produced with Agisoft Metashape treated previously. As can be guessed, the final result is closely related to the quality of the orthophoto produced and the accuracy of the operator in identifying and drawing the "land-water" boundary directly from the photo. As far as the study parameters are concerned, the considerations of distances and areas remain the same as in the previous case, we also keep here the GNSS line as the reference line. To make the comparison we then go to construct the line, heading to *Layer > Create Vector > New Layer Shapefile*, and on

the geometry type we set line. We now select the *add element* command to begin drawing the line as shown in Figure 82.



Figure 82 Plotting the coastline from the orthophoto.

#### 4.5.2.1 Calculation with distances

Proceeding similarly as seen in the previous comparison, we go on to perform the second analysis, the only difference being in the initial step. Once the line is drawn, our interest is the distance between point (on photogrammetry) and GNSS line. So, we need to introduce points along the linear vector on the photogrammetric survey, to do this QGIS allows us to introduce points at intervals of interest. The chosen interval is 0.5 m between one point and the next, so we have a good sampling. To run the command, *Processing > Tools > Vector Geometry > Points Along Geometry*. Once the points are created, the distance between the point and GNSS line is calculated, and we get the result in Figure 83.

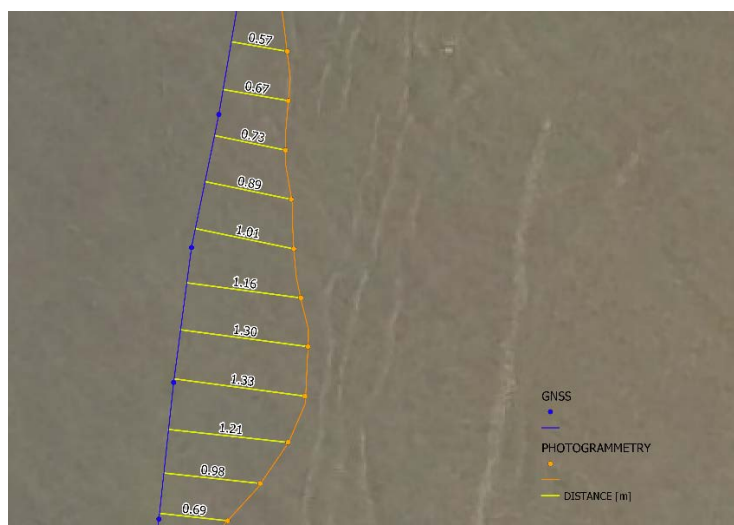


Figure 83 Result processing with distances in meters.

In this case, the difficulty in identifying the coastline has given problems that make the calculation with distances unreliable due to "complex" geometries as we can see below in Figure 84, and so the study with areas is essential.

#### 4.5.2.2 Calculation with areas

We proceed similarly to the comparison between the line of classical topography and the GNSS line, using the coastline plotted on the orthophoto and the GNSS line. We will see later in the discussion of the results that this comparison is preferable, as certain geometries are formed that do not allow the calculation with distances to be fully exploited (Figure 84), leading to approximations. These unintentional errors are due to the difficulty of interpreting Drone images. It is clearly evident in Figure 83 where the division between emerged and submerged areas was not clear due to the clarity of the water. These characteristics also related to other factors including the low light in the Boccasette survey and the discontinuity of the coastline, make this type of error very easy to make. Therefore, it results in the need for an approach that evaluates areas in order to obtain valid data.



Figure 84 Line photogrammetry and GNSS on Boccasette.

Performing the same procedures here as in the previous comparison (result Figure 79), one can immediately see in Figure 85 the differences in complexity and size.

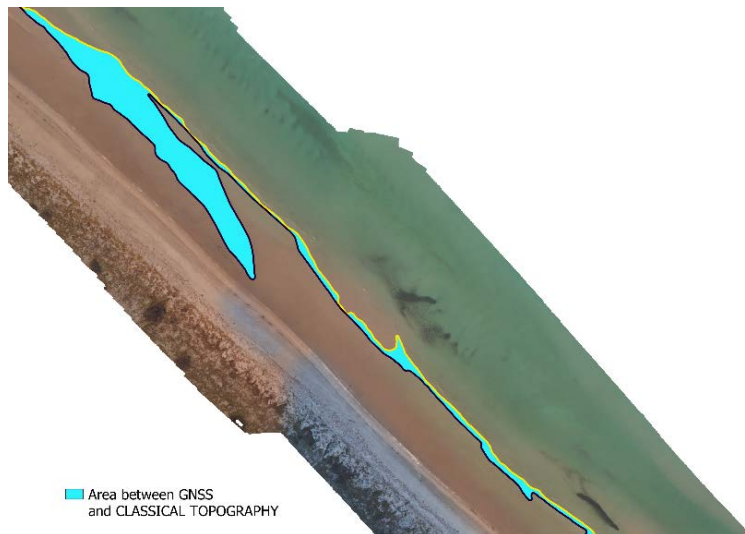


Figure 85 Area created between the two lines as a result of the polygonize command.

## **4.6 Multi-temporal study for the estimation of coastline changes in GIS.**

The survey obtained through photogrammetry or rather SfM technique, allowed us to perform a multi temporal analysis. In the previous case orthophotos were used to draw the coastline directly from the photos, in this case we are going to use an additional product of photogrammetry, the DEM obtained again thanks to Metashape. Processing is made possible through the construction of contour lines, which allow identification of the line at zero elevation. The analysis then takes place between the zero-line extracted with SfM technique (2022) and a LiDAR flight performed in 2018, of which the zero line was already available in dwg. format, georeferenced. We therefore do not go into the specifics of the LiDAR methodology since for this part of the thesis, the interest is in estimating the coastal behavior under consideration.

### ***4.6.1 Methodology for comparing Photogrammetry and LiDAR***

Unlike the cases seen so far, in which we were interested in the identification of the coastline, we are now instead focused on determining beach erosion or deposition with respect to the zero line in terms of areas, "easily" identified by the DEM model due to low tide. For this phase only the area approach will be used, to derive from it the square meters, and thus provide by difference an index on the behavior of the coastline. It must be said that since the subject treated is quite detailed, the area that will now be studied is certainly a limited area to be able to express a certain data on the behavior of the coast, but it helps us to understand the potential of the methods used to study these fragile and always rapidly changing areas.

As mentioned earlier the zero line of the LiDAR flight was already available in dwg. format, so it was necessary to clean up the file by obtaining the section of interest, and then upload it into QGIS as a vector file. An important note concerns the reference systems, we are working in EPSG:6876 RDN2008/Zone 12 (N-E), and the LiDAR data are in EPSG: 32632 WGS 84/UTM Zone 32N, to standardize everything once loaded in the GIS environment it will be transformed and projected on the fly by the software, to save it in the project system we go to export it

indicating the system EPSG:6876, in this way we avoid problems in the execution of the commands. Instead, let us now see how to derive it from the new data for the year 2022. We move to QGIS we import the DEM produced with Metashape, now very simply we head to *Raster > Extraction > Contourlines..*, the parameters have to be set and we give execute. The result produced needs correction by the operator in order to identify a zero-level coastline that can be used for comparison. In Figure 86, we see in light blue the software result and in yellow the processed data edited by operator.

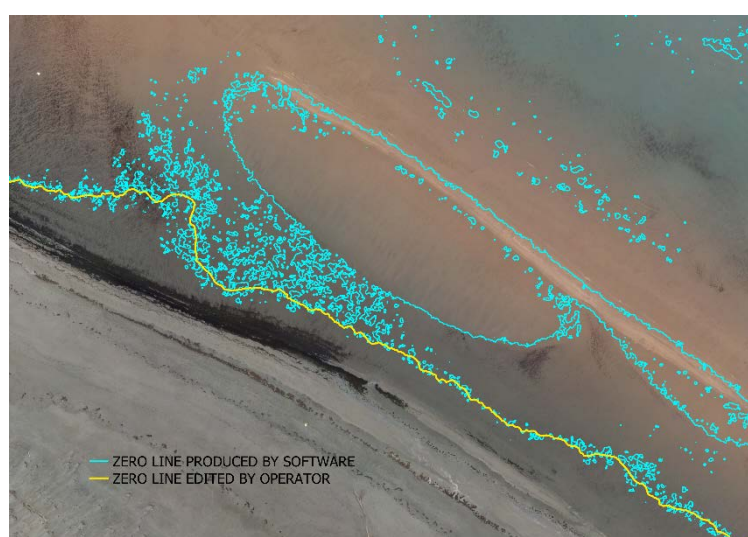


Figure 86 Zero-line cleaning produced by QGIS.

#### 4.6.1.1 Multi-temporal comparison with area analysis

We now use the layers useful for multitemporal comparison, covering 2018 for LiDAR and 2022 for photogrammetry. Once loaded into a QGIS file we immediately notice the differences in terms of areas, and in this case unlike previous cases our interest falls no longer on the mean and standard deviation but on the size of the areas in square meters, and thus their difference.

Positive areas are considered when exposed in the direction of the open sea with respect to the line drawn with LiDAR of the year 2018, thus expansion of the coast, negative in the direction of the beach, with erosion phenomenon (Figure 87).

Proceeding as seen for the extraction of areas in the previous comparisons, the results searched can be obtained, which will be analyzed and commented on in the following chapter.



Figure 87 Local expansion and erosion, zero line in the Boccasette multitemporal comparison.



## **5 Monitoring results and discussion**

## **5.1 General background on the results**

The Boccasette and Barricata coastlines were identified using a rigorous approach, which provided reliable calculated surfaces.

In this chapter we go into the specifics of the discussion, exposing the critical aspects of the methods through a case-by-case evaluation, bringing back all the main graphical elaborations produced in the process. If until now the exposition of the procedures within the GIS software has not clearly separated what is the Boccasette beach from Barricata, it is simply related to the fact that data processing is done in a similar way and a repetition would have burdened the discussion. It follows that this approach can be applied, also, to other coastal realities similar to those under consideration, or to the extension, always detailed of a greater coastal strip under consideration. In this section the focus will be on the efficiency of the methods applied, their capabilities in terms of accuracy, time, and coverage.

The comparison thus allows us to bring to light the differences between the various methodologies, focusing in conclusion on the most productive for this purpose. We can say for certain that there is no right and wrong methodology, but as can be seen two of the methodologies (GNSS and Total Station) allow a much higher detail for our purpose, but at the same time one of them offers limited overlay.

The limitations of the chosen approach in identifying the coastline by photogrammetry will also be noted, including the influence of the meteorological factor that negatively affected the quality of the photogrammetric product in the Boccasette coastline.

## **5.2 Comparison of results between different methodologies**

As already mentioned several times in the following thesis work, the goal is the comparison of various methodologies in order to identify the most suitable to the identification of the coastline. We will go in order, starting first with Boccasette, being chronologically the first survey carried out, in the same the processing data will be compared and discussed, and then moving on to Barricata.

To better deepen the methodological comparisons, they will be explained starting from that considered less accurate for the study, up to that more practical and

precise. As already mentioned, this comparison does not classify instruments in general terms, but according to their effectiveness in the field of study. We are talking about topographic instrumentation with a very high precision, and each of which is more suitable for some types of surveying than others. In fact, the methodology of photogrammetry (SfM) allowed us not only to plot the coastline at low tide, but to go and extract the zero line directly from the DEM. We start our comparison precisely from this methodology because among those chosen for the study it showed a greater complexity in the plotting phase from the orthophotos, and an almost double error compared to the comparison with classical topography (Total Station) and GNSS.

It is known from the previous chapters the procedure followed, now through the export of the various graphic works we are going to comment and expose all the study details.



Figure 88 Po delta area as seen from satellite (Kosmosnimki.ru).

### 5.2.1 *Boccasette results*

#### 5.2.1.1 GNSS and PHOTOGRAMMETRIC RESTITUTION (distances)

Let us start the comparisons from the orthophoto, this product that we can see in Chapter 4 image 62, served us to draw the coastline. It is clearly visible from the digital image that the land-sea distinction is not well defined in terms of coloration, thus making it difficult to process in some stretches, especially for those areas that have an recess towards the beach, where the clear water presents a flat pattern compared to the shores where even if slight there is wave motion, detectable from the photos. It should be specified that the weather conditions in the Boccasette survey (Figure 89), adversely affected the quality of the photogrammetric product, and it is very clear in the comparison with Barricata where the more favourable light conditions offered a much better restitution. Let us now see through the exposition of the tables the complexities encountered.



Figure 89 Boccasette weather conditions January 27, 2022.

We can easily see the differences in restitution in the Figure 90, we see in blue the points surveyed by GNSS directly in the field, and in green the photogrammetric restitution. We can state from the outset that the following approximations are not negligible for a detailed survey, due to the poor visibility from the photos for the reasons previously explained.

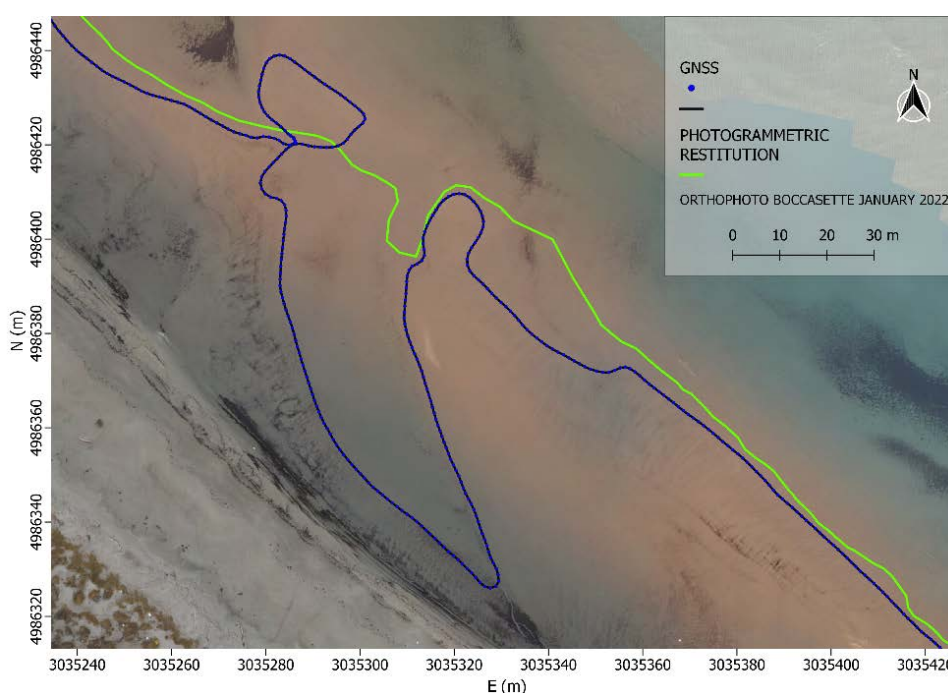


Figure 90 Difficulty in drawing the line (green) directly from Orthophoto for Boccasette.

Another important difference concerns the amount of data that can be obtained. While with GNSS methodology it was possible to cover almost the entire length of the Boccasette coastline, getting to trace the coastline for a length of 5290.29 m, built from the 4009 surveyed points, with photogrammetry the amount of coastline traceable from the orthophotos is much less with 1874.52 m for a total of 3750 points inserted through QGIS with 0.50 m interval for studying distances. This difference is mainly due to two reasons, the most obvious one concerns the amount of area covered for the same amount of time, in fact it can be seen from the image 91 that the orthophoto covers a little less than half of the area surveyed with GNSS, even if one wanted it is therefore impossible to proceed with the tracking of more coastline without the orthophoto below, the second point concerns the difficulties encountered in the recesses not visible from the orthophoto that led to approximate several areas making it difficult to compare with the distances and increasing the approximation of the results (Figure 92). For illustrative convenience in the figure to follow, the GNSS points will not always be shown but only the line connecting them, making it easier to see them graphically.

High resolution geomatics techniques for coastline detection and monitoring:  
Boccasette and Barricata case studies (Po River Delta, Rovigo, Italy).

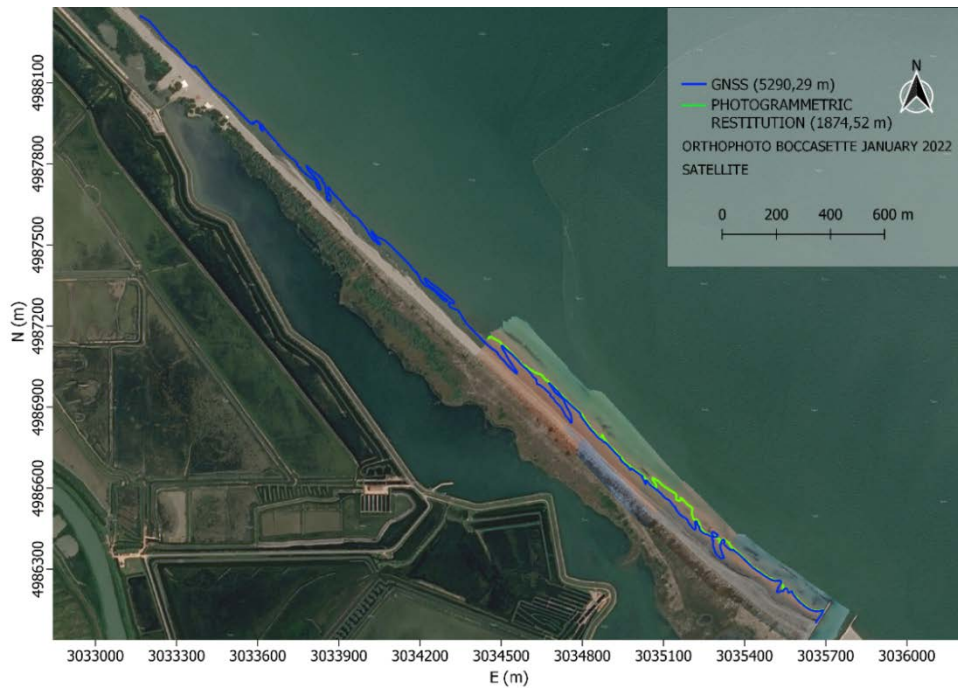


Figure 91 Total GNSS and photogrammetry comparison.

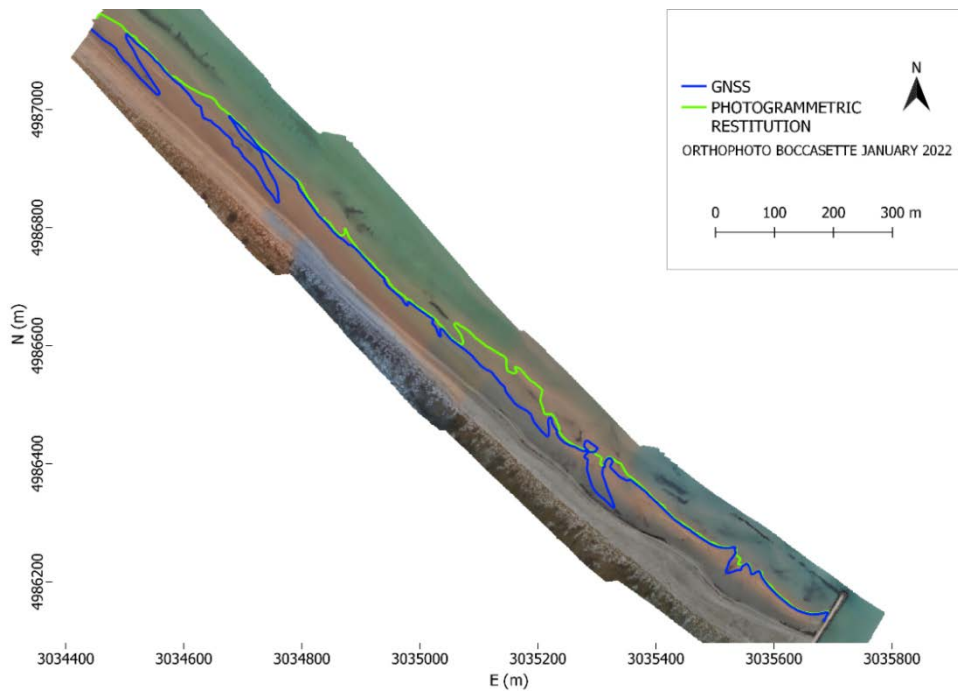


Figure 92 Variation between GNSS and photogrammetry in the area covered by the orthophoto.

The next step is to study the mean and standard deviation, to evaluate, compared with the more accurate and precise GNSS line, the reliability in post-relief processing directly on the photos. Given the problems encountered so far, we do not expect optimal results for the scale of study, but it might be of interest in cases where less detail is required, in which context a higher margin of error could be tolerated.

From Figure 93 we can immediately see the difficulties encountered in identifying the line from the photos, which has led as can be seen to a considerable increase in distance for some points even in the less complex areas, where the coastline is identifiable only through wave interpretation.

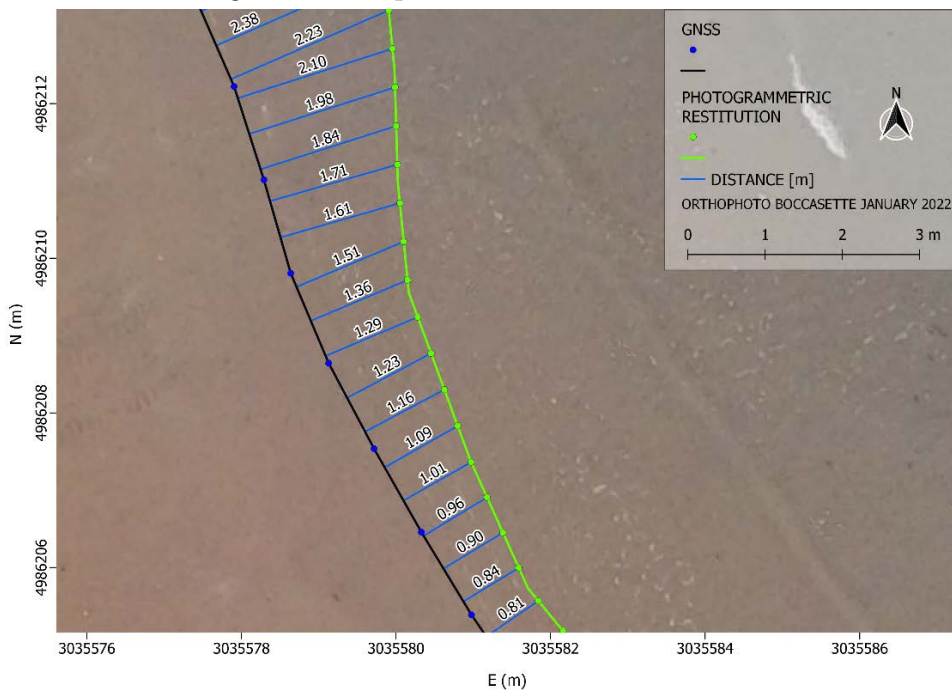


Figure 93 Comparison of GNSS and photogrammetry in unproblematic areas.

In the following image (Figure 94) we see the negative influence of the difficult interpretation, which led to considerable deviations with geometries not easily calculated through distances. Reiterating the fact that our comparison aims at a restitution of details, distances such as these reaching up to 40 m are certainly not acceptable.

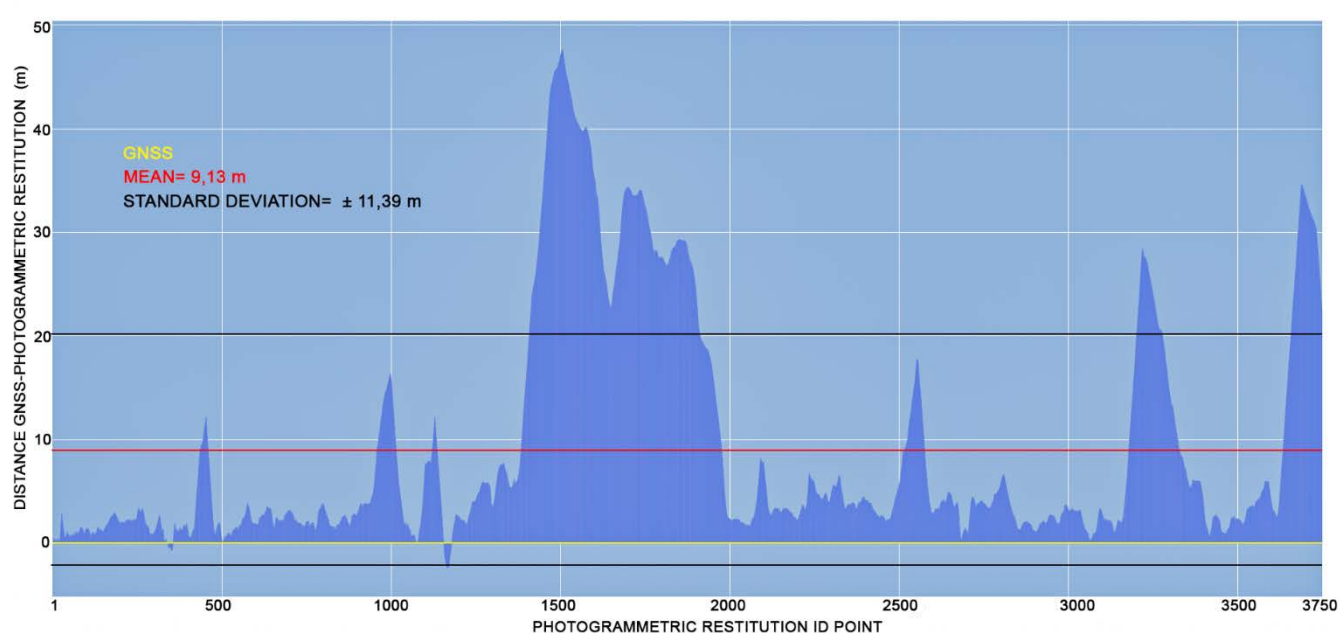


Figure 94 Very low correspondence between GNSS and photogrammetry.

Closing this first comparison, we can report the results obtained, the points show an average distance of  $9.13 \text{ m} \pm 11.39 \text{ m}$  standard deviation, with individual distance values touching  $47.63 \text{ m}$ . Having considered the distance value to be positive in the open sea direction and negative in the beach direction, a positive average indicates that the photogrammetric return tended to be plotted in the open sea direction, relative to the GNSS line. On the following page, the graph (1) shown helps us to better understand the result obtained, highlighting the deviation of each individual point from the GNSS line considered as a reference for comparison. Through an analysis carried out within QGIS on the 3750 points obtained along the photogrammetric restitution line at an interval of  $0.50 \text{ m}$  it turns out that only 253 points have a distance from the GNSS line  $\leq$  to 1 meter (6.74 % of the points), raising the tolerance to 3 meters it turns out that 1536 (40.96%) values are  $\leq$  to 3 meters that is less than half. If we now do a reverse search and look for the largest values, for example, at 10 meters it follows that 965 points out of the total have distances  $\geq$  10 meters. We can then conclude this first comparison by stating that, even considering a wave variability of 2 meters we certainly cannot obtain a detailed survey. We can certainly state that the greatest error is found in the areas of



indentation as can be seen from the Figure 94 and graph 1, where the values increase considerably. Considering also the difficulties of the software and thus the approximations in plotting the distance, at points where the geometry became complex, the actual results are even worse. It follows that an analysis with area study is able to provide a more accurate figure on the accuracy achievable with these two methodologies compared.



Graph 1 Comparison between GNSS and photogrammetric restitution (Boccasette).

#### 5.2.1.2 GNSS and PHOTOGRAMMETRIC RESTITUTION (areas)

Taking now into consideration the two approaches we are going to expose the results with the areas (Figure 95), as already mentioned this does not lead to the improvement of the result, because as we have seen beyond the approximations made by the software the measurements deviate a lot from acceptable values, but the use of the areas helps us to have an accurate estimate on the error obtained in drawing the line from the orthophoto.

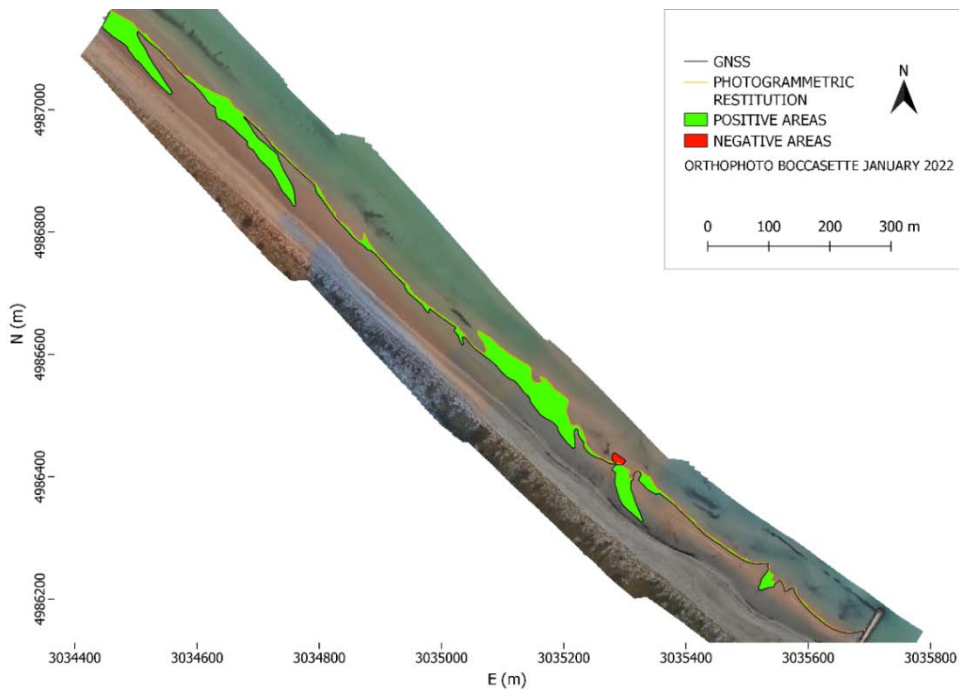


Figure 95 Positive and negative areas between GNSS line and photogrammetric restitution.

Once again, we can clearly see from the general framing the limitations of the methodology, only for a few sections do the GNSS line and photogrammetric line return relatively small areas, but for the most part we have significant deviations, with a marked trend of tracking in the offshore direction. In image 96 we can see that in the indentation areas from the photos, the beach/sea area is not distinguishable, without the support of the GNSS line.

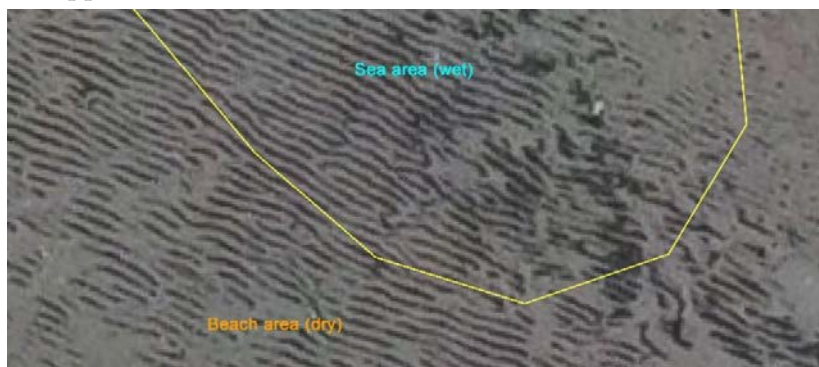


Figure 96 GNSS beach/sea boundary line.

We now illustrate specific areas (Figure 97) on the method under consideration and then present the results obtained in terms of mean and standard deviation.

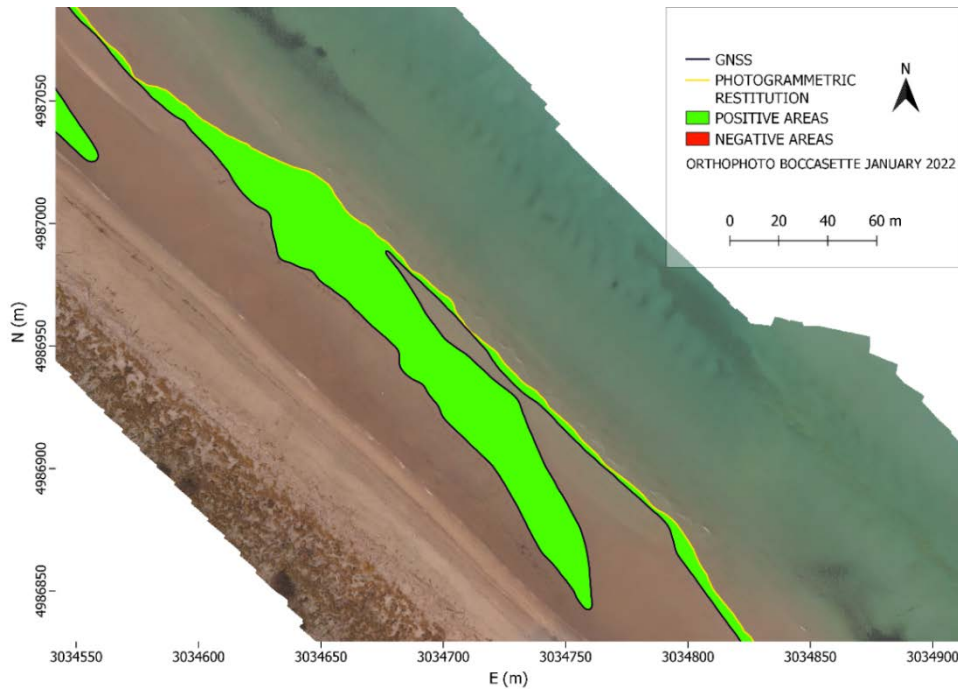


Figure 97 Considerable variations between the two lines.

The tables emphasize as already mentioned the weakness of the method with regard to coastline interpretation in the points already explained. Indeed, we see that in those areas the coastline trend could not be interpreted because of the clarity and stability of the water.

We can therefore conclude this first comparison by reporting the results obtained with the areas. The overall areas show an average of  $3234.62 \text{ m}^2 \pm 6542.61 \text{ m}^2$  standard deviation, with individual area values reaching  $19060 \text{ m}^2$ .

### 5.2.1.3 GNSS and CLASSICAL TOPOGRAPHY (distances)

In this section we see two methodologies applied directly in the field, namely GNSS also used in the previous comparison and classical topography (Total Station), two precise methodologies but unlike photogrammetry that allowed post survey data acquisition in this case for both the data is taken in situ by positioning on the point to be surveyed. What we expect in this case certainly is a marked improvement in the

results since the acquisition is not constrained by the quality of the orthophoto but by the accuracy of the operator, in identifying the coastline with consistent rigor. In this case as we mentioned earlier the instrumental accuracy is well above the margin of error. So, the differences to be encountered are related to the sensitivity and accuracy of the operator in identifying the land-water boundary, considering wave disturbance on the order of one meter. This last note obviously covered the previous case as well, but from what we could see there the relevant problems were quite different. Let's start by studying the "first" image (Figure 98), we immediately notice the differences, as the difference between the two lines connecting the surveyed points (278 classical topography, 520 GNSS related to the length considered for comparison) is almost imperceptible, if we think about the previous case (Figure 92) the situation was already quite different. On the other hand, it is immediately apparent by looking at the length of the traces the amount of detectable area for the same amount of time, in fact with classical topography the amount of area that can be covered is severely limited compared to the other methods used as we can see below in Figure 99.

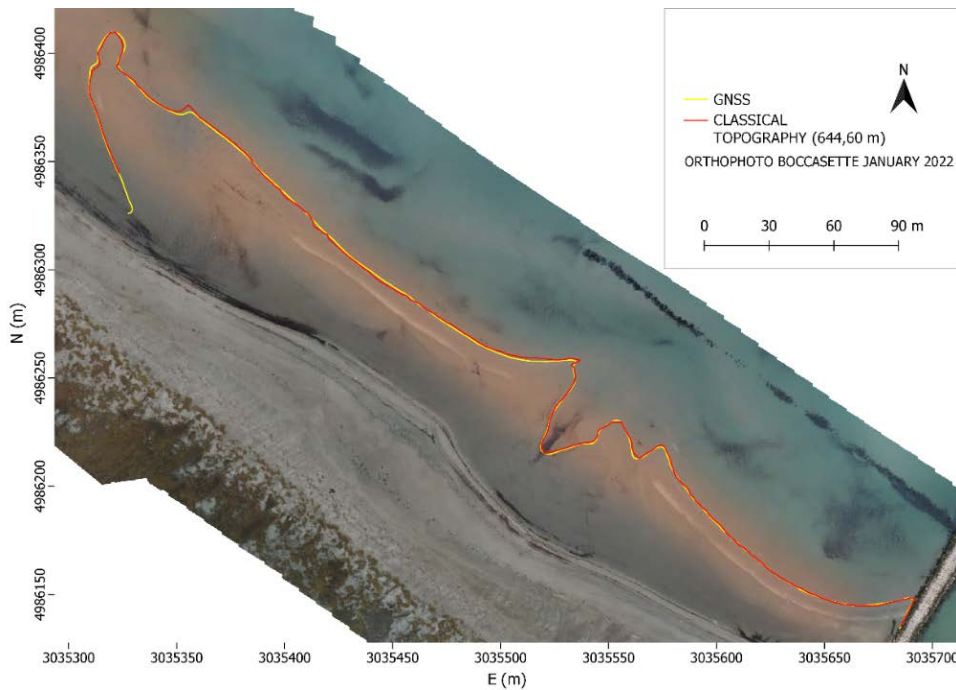


Figure 98 Variation between GNSS and Total Station.

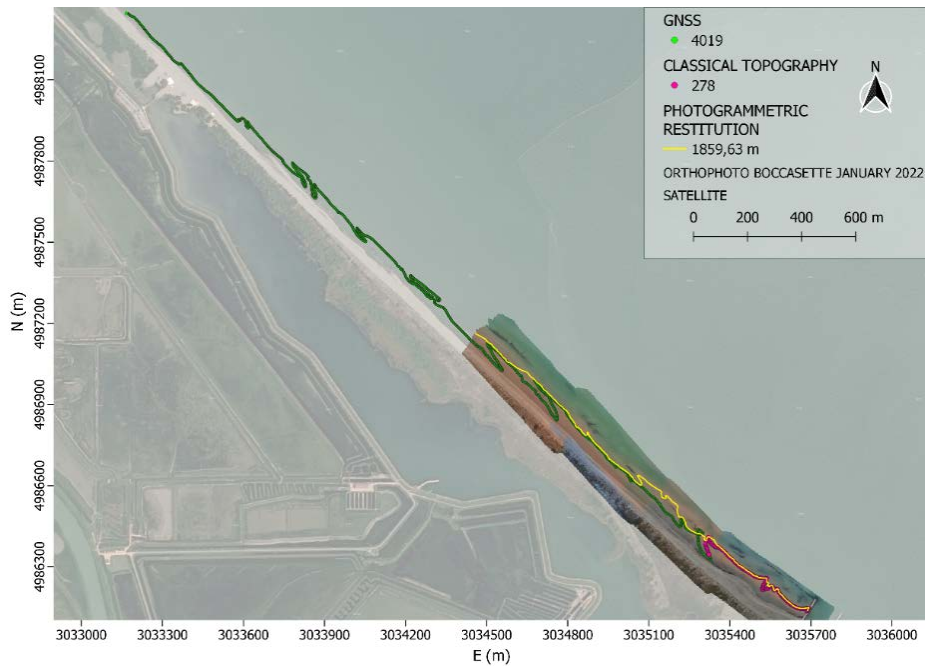


Figure 99 Cover length of different methods.

We can see from the tables a high accuracy, the distances between the points measured by classical topography and GNSS almost always remain under a meter except for some small areas. It is interesting to note in the image to follow that even at points where the geometry is not regular, the two methods returned very detailed measurements.

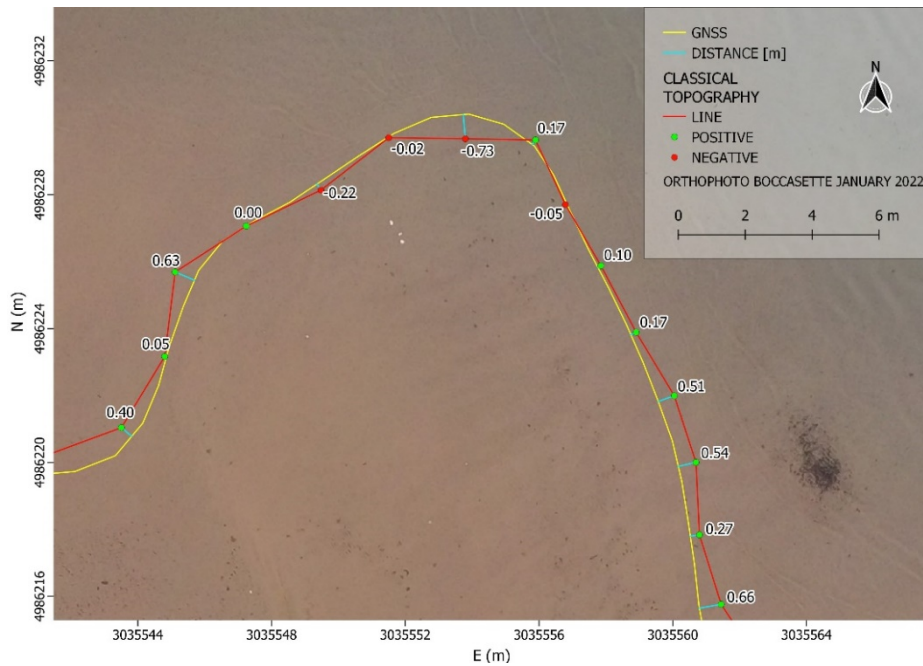


Figure 100 Excellent tracking between GNSS and Total Station.

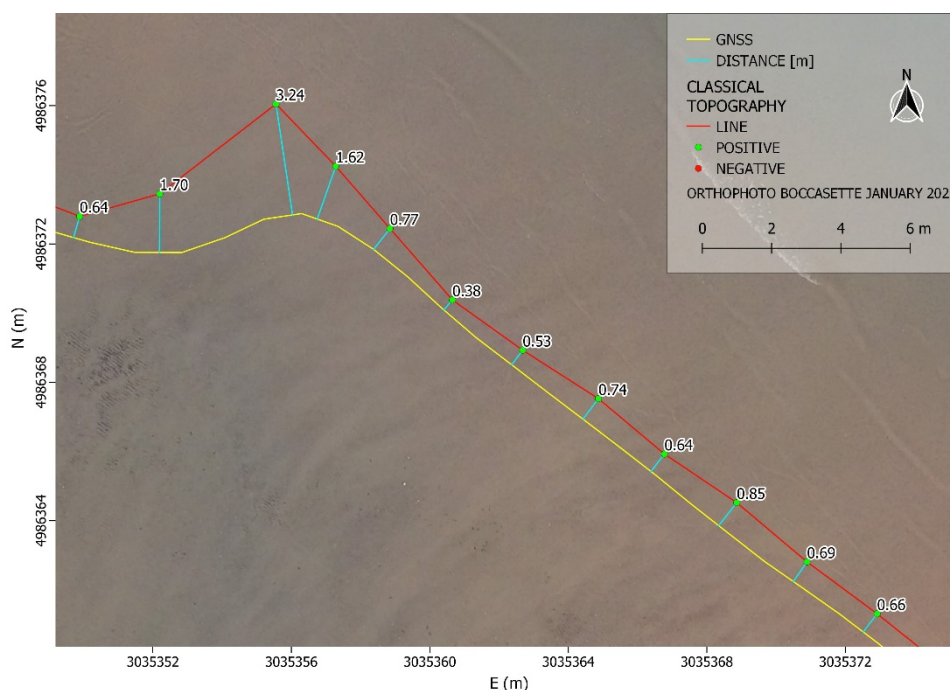
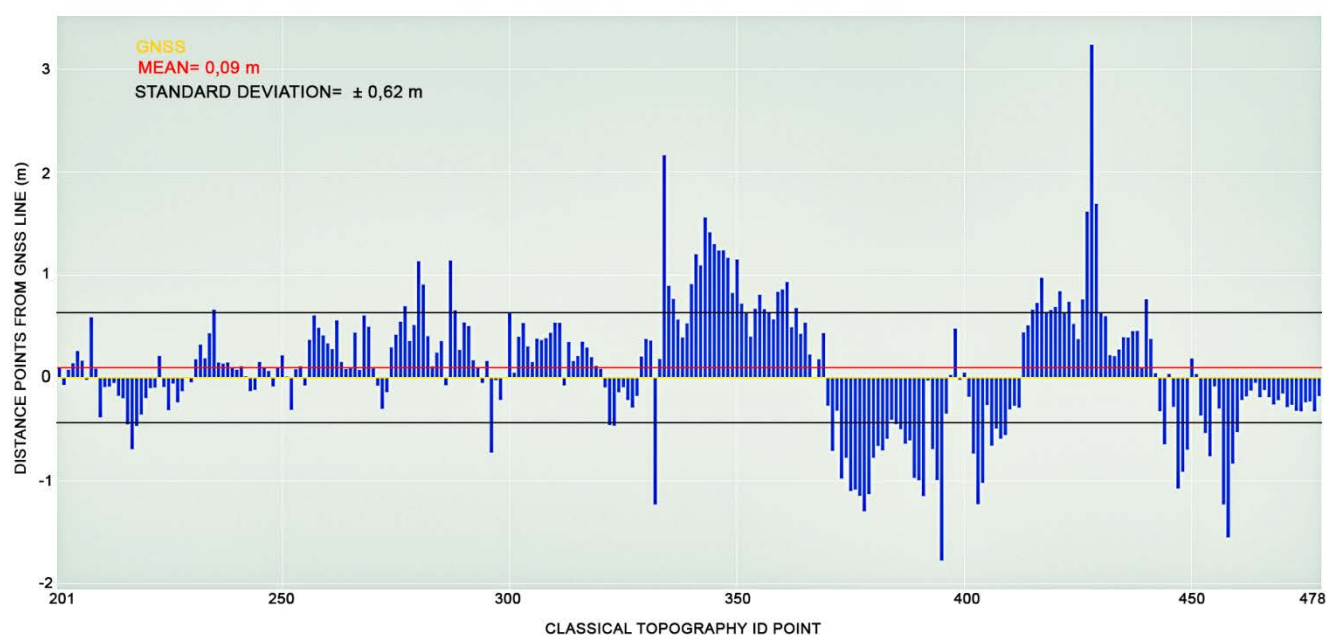


Figure 101 Localized points where deviation error increases.

These two methodologies show excellent applicability for detailed surveys as in the case of interest, bringing to light that the influence of the operator in identifying the coastline is a marginal factor since the results barring some small variations show very close values. Having clarified the various aspects without divulging further we can report the results obtained, in this case the points show an average distance of 0.096 m  $\pm$  0.62 m standard deviation. We thus note a significant improvement, with the average showing a deviation in the open sea direction (positive) of only 9 cm and a standard deviation of 62 cm, which is within the criteria of accuracy, keeping in mind that the coastline has a dynamic behavior related to wave motion. We again report on the following page the graph (2) containing the measurements and their results, highlighting the deviation of each individual point from the GNSS line considered as a reference for comparison. The analysis performed within QGIS on the 278 points obtained with classical topography (Total Station) indicates that 250 measurements are  $\leq$  1 m (89.92 % of the measurements) of the remaining 28 measurements only 7 exceed 1.5 m and only 2 are greater than 2 meters with values of 3.24 m and 2.17 m. We can therefore also conclude this second comparison by stating that, for Boccasette the best solution, considering the various aspects treated

and the objectives of interest was found to be the methodology with classical instrumentation and GNSS, the values in fact, even considering the influence of the operator and the variability of the wave motion, are contained and present a good spatial distribution thus allowing a detailed survey.



Graph 2 Comparison between GNSS and Total Station (Boccasette).

#### 5.2.1.4 GNSS and CLASSICAL TOPOGRAPHY (areas)

Similarly, to what we saw before for completeness, and in order to be able to better compare measurements across comparisons, we proceed to the verification with areas. In this case we can say from the outset that since the lines drawn by the connection of the points are very close, we have no particular problems, both methods (GNSS and classical topography) demonstrated excellent applicability with regular and well-defined geometries. Let us therefore look at the area images (Figure 102-103) in order to comment on the results. For this part we will focus on the area covered by GNSS and classical topography comparison, the remaining part for now is not comparable due to limited coverage with classical topography (Total Station).

High resolution geomatics techniques for coastline detection and monitoring:  
 Boccasette and Barricata case studies (Po River Delta, Rovigo, Italy).

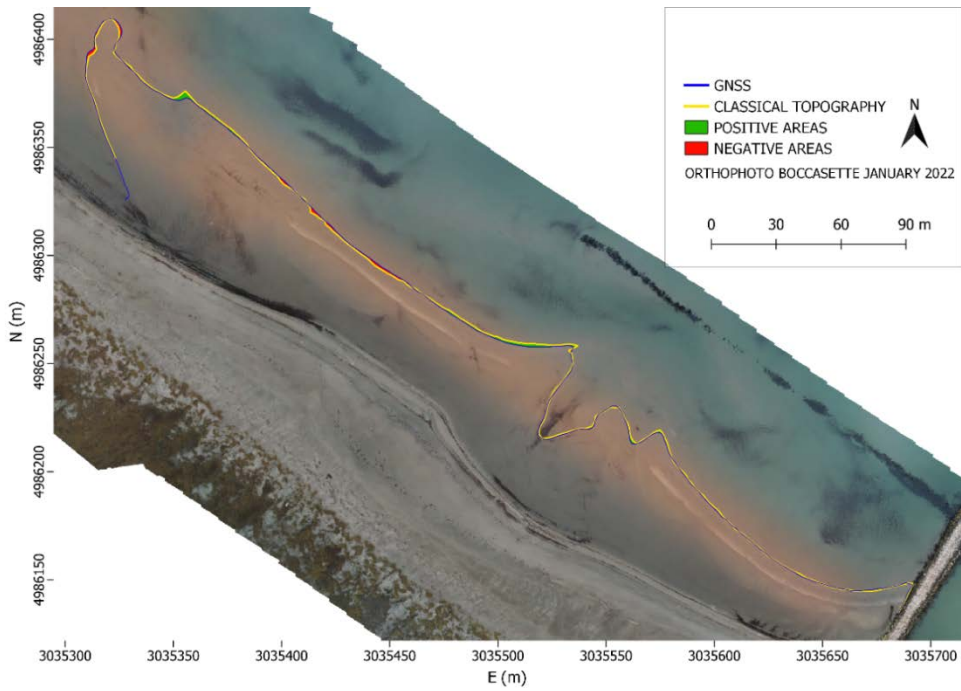


Figure 102 Positive and negative areas between GNSS line and classical topography.

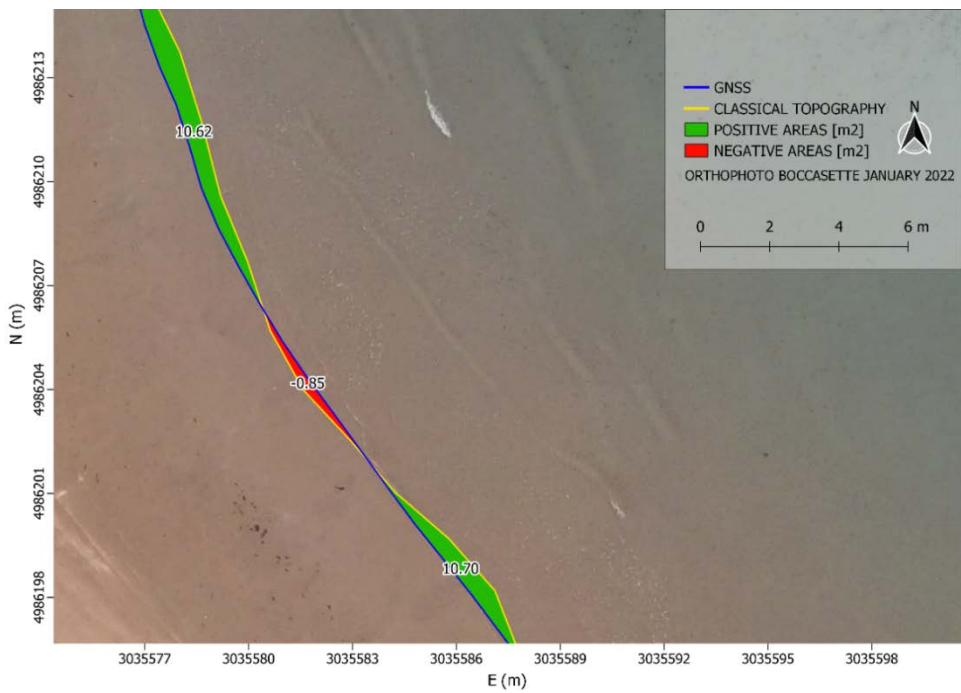


Figure 103 Small variations between the two lines.



In this comparison as with distances, areas also returned very detailed values, with an average of  $1.15 \text{ m}^2 \pm 15.10 \text{ m}^2$  standard deviation, with individual area values reaching as high as  $64.31 \text{ m}^2$ . If we now go to look at the previous comparison with photogrammetry, we already notice a rather significant difference. We can therefore state once again that for the Boccasette survey the least precise methodology turns out to be that by photogrammetric restitution, but beware, this does not mean that the methodology is not precise, but in these contexts due to the climatic conditions, and the low reflectivity of the marine environment as we have noted it is difficult to trace the coastline, with significant loss of accuracy to detail. This results in greater effectiveness for GNSS and classical topography methodologies. Let us now see the case of Barricata, and at the end we will go on to indicate the most suitable methodology for coastline identification, based on the results of both coastlines.

## 5.2.2 *Barricata results*

### 5.2.2.1 GNSS and PHOTOGAMMETRIC RESTITUTION (distances)

With Barricata we enter the second survey campaign. Here we directly try to bring to light the fundamental differences between the two surveys in such a way as to avoid a repetitive treatment, since the procedures performed are similar to those carried out for Boccasette, with the difference that in this case the climatic conditions were significantly better (Figure 105). We immediately notice from image 106 that the maximum coastline deviation is 6.56 m, which is considerably improved compared to the previous case where it was as high as 40 m. Another important aspect concerns the geometry of the line (Figure 104), in fact we observe that even in the cases of greater deviation, where it was more difficult to trace from the photos the beach shows a rather linear trend in comparison with Boccasette.

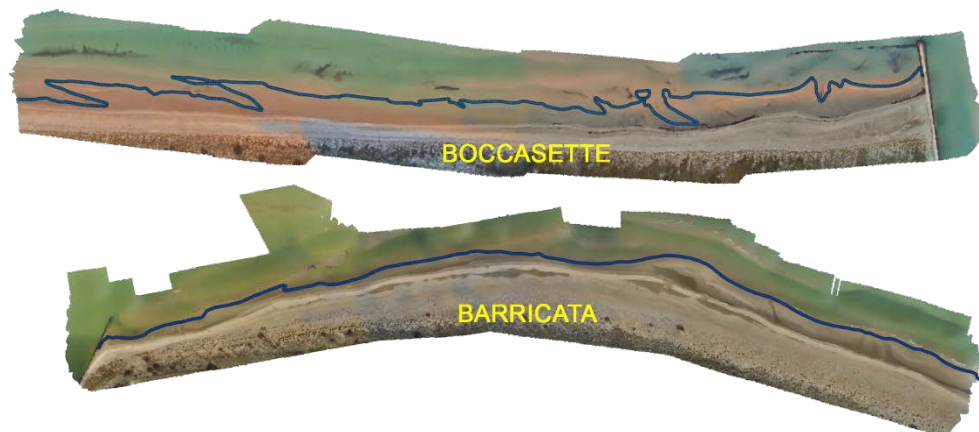


Figure 104 Different land-sea boundary geometry between Boccasette and Barricata, using GNSS points.

High resolution geomatics techniques for coastline detection and monitoring:  
Bocasette and Barricata case studies (Po River Delta, Rovigo, Italy).



Figure 105 Barricata weather conditions February 25, 2022.

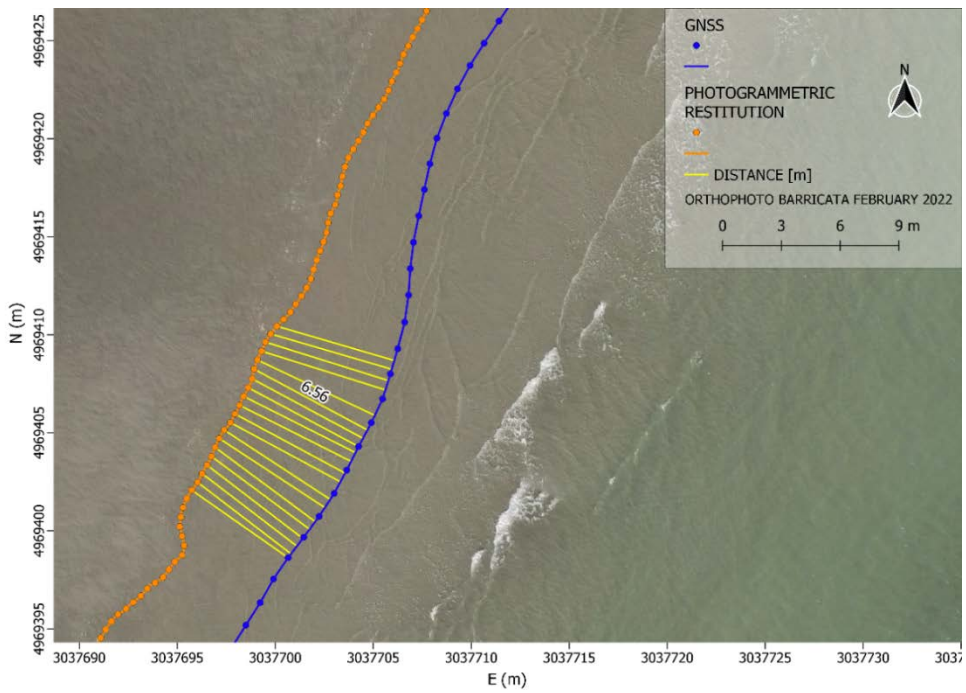


Figure 106 Maximum distance in restitution from photogrammetry to GNSS line.

If we now place our focus on the table with general framing that follows, it is immediately apparent that there is an excellent correspondence between the GNSS

line and the photogrammetric restitution, which for the scale of representation is almost coincident. Proof of this fact was confirmed by less difficulty in defining the coastline, which allowed a better restitution from the photos (Figure 107).



Figure 107 General framing coastline restitution lines (GNSS and photogrammetric restitution).

Despite a significantly better result to the previous case with same approach, we should not stop at the general scale, in fact, if we consider our goal, to obtain a detailed survey, we still do not reach the accuracy obtainable by surveying in the field with GNSS and Total Station. A notable constraint that is evident through the comparison of the images concerns the waves, which are not uniquely interpretable,

it is in fact difficult to identify an approach to follow for the whole tracking. We take a closer look in the following images (Figure 108-109) at the issues.

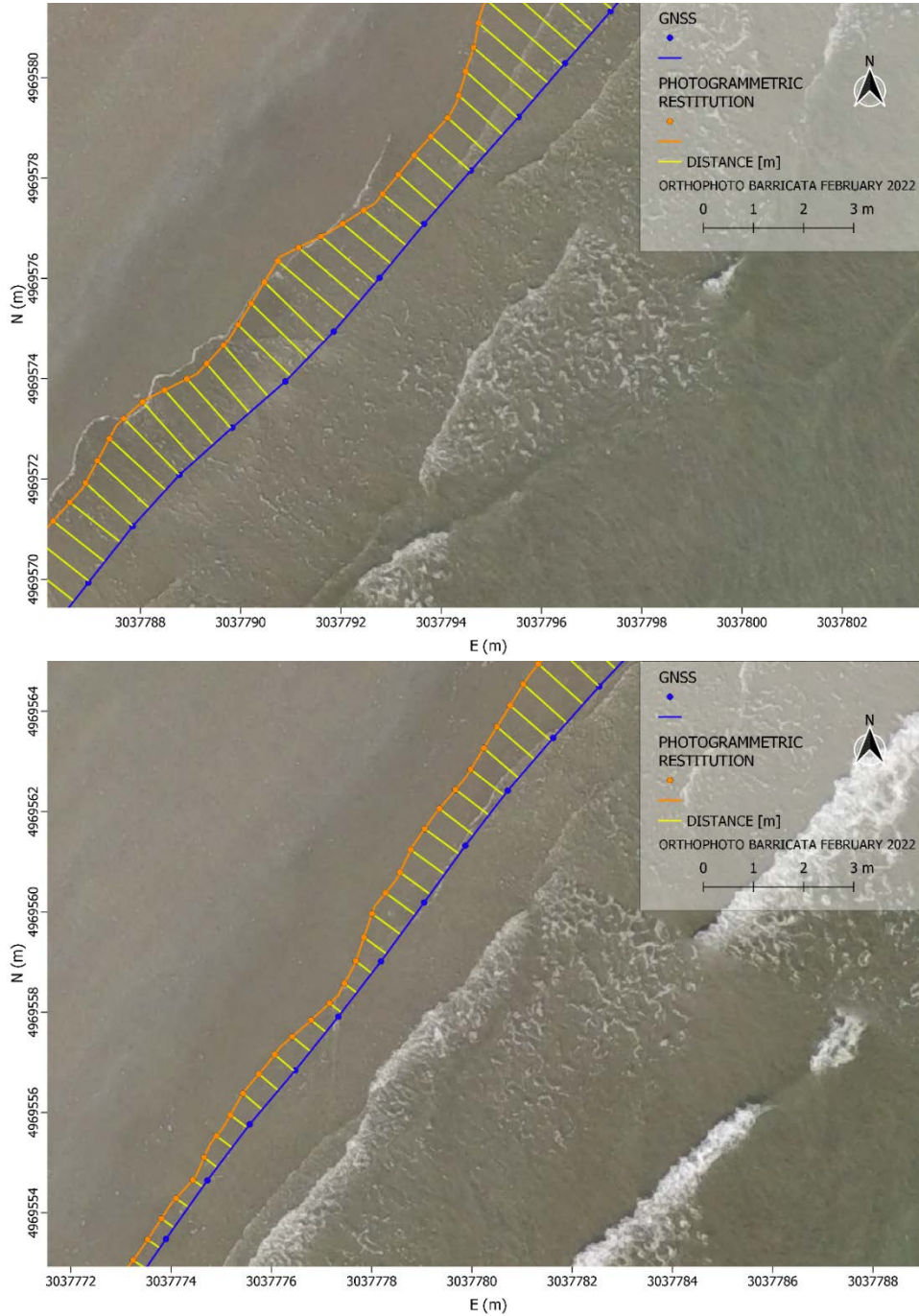


Figure 108 Wave behavior in line identification.

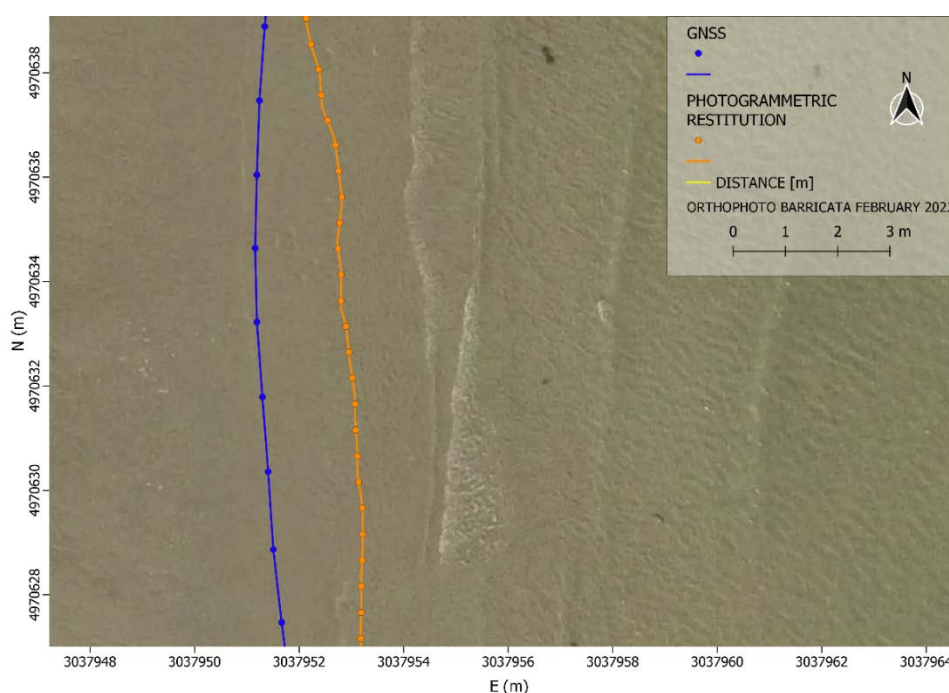


Figure 109 Wave behavior in line identification.

These three plates make us well understand graphically the difficulties in interpreting the coastline, from the photos, in fact, in the presence of waves it is not immediate to guess immediately position and direction. From the first image we notice the wave in a forward state and from it an attempt was made to interpret the line, we can certainly see a shift of the line toward shore, which leads us to think that perhaps it could have been plotted differently. Moving to the second image we notice right away how the similarities to the first one lead to a different line being drawn in each case. Another disturbing element concerns the “battigia”, which is clearly visible in the first two plates; we define it in such a way because we are not certain that the wave actually always goes that far, and it could be the effect of the lowering of the tide just before the measurements were taken. If we now move to the third table the situation is reversed again, in fact we notice a milder wave but at the same time a GNSS coastline that is further out than the photogrammetric restitution, exactly the opposite of the previous tables. Having reached this point one might think that where there are waves we adopt an approach that then changes in areas where the sea shows flatter, but unfortunately even this way of seeing on some points lapses in fact

from the following Figure 110, we see a very good restitution following the coastline using the approach followed for the previous table.

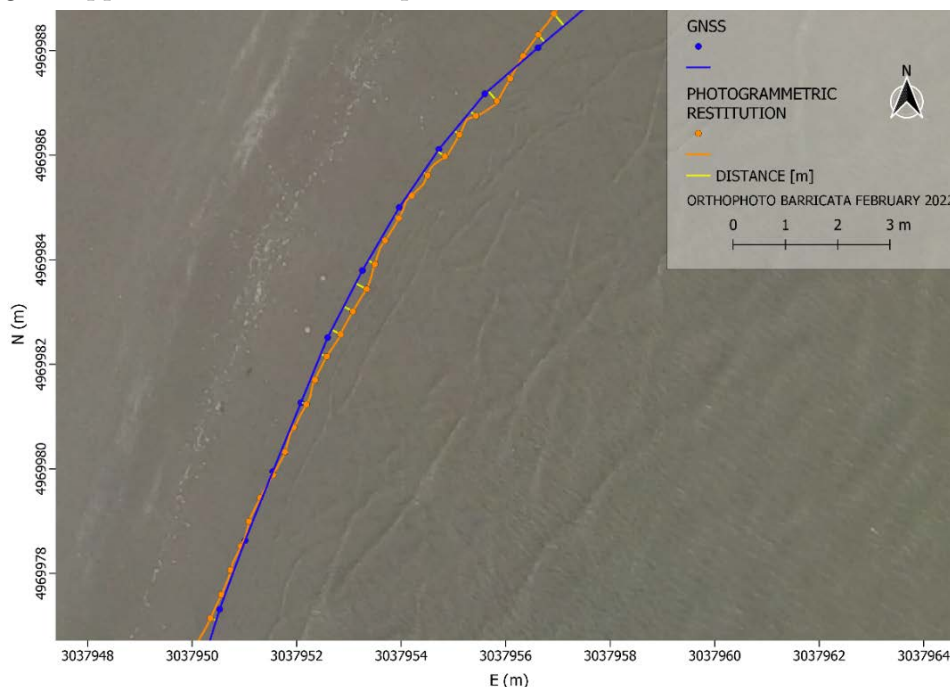
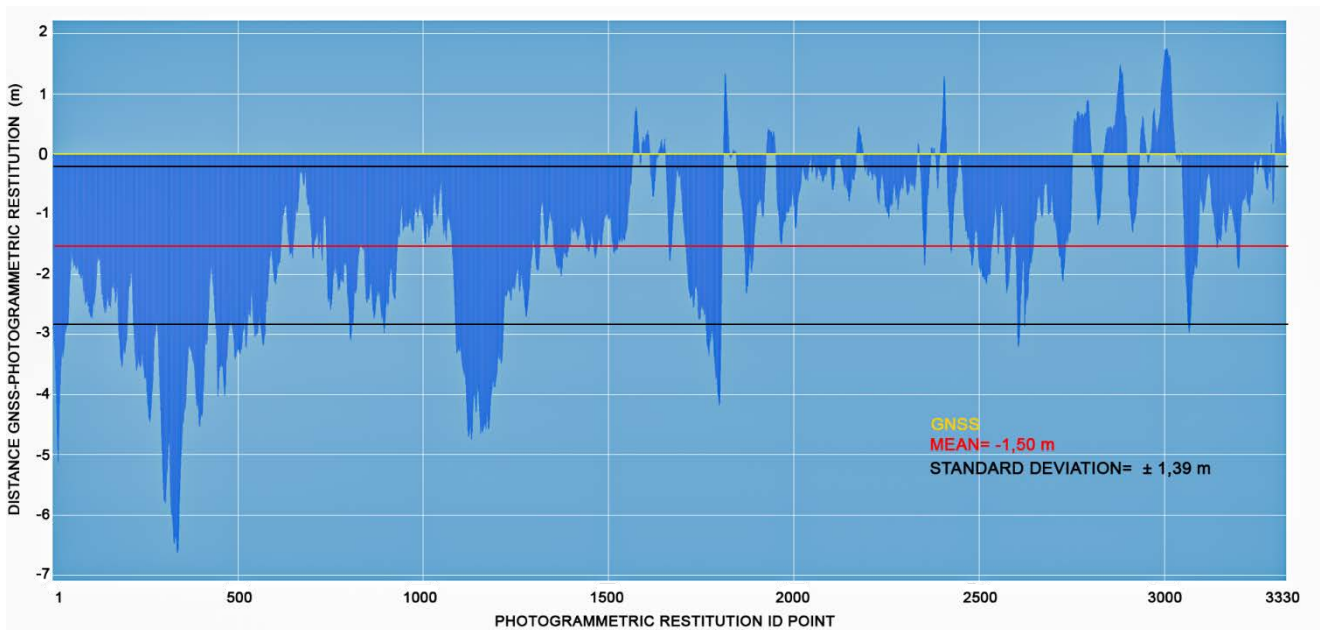


Figure 110 Good coastline identification.

So the points show an average distance of  $-1.50 \text{ m} \pm 1.39 \text{ m}$  standard deviation, with individual distance values reaching a maximum of 6.62 m. Since the mean is negative, it is clear that most of the return occurred in the direction of the beach relative to the GNSS line. Well, we can therefore confidently say that the results obtained considering the distances are certainly better than the Boccasette return, which, as we have seen, was characterized by various problems. On the other hand, given the results we cannot say that this methodology is suitable for a detail survey comparable with Total Station, but this statement certainly concerns the field of study, because as we know for certain urban areas and not only the photogrammetry technique offers very high results. Then depending on the scale of detail required one could always assess whether or not these parameters are within the field of interest. Once again to follow the graph (3) shown, it brings to light the deviation of each individual point from the GNSS line considered as a reference for comparison. Again, within QGIS, out of the 3330 points obtained along the photogrammetric restitution line at an interval of 0.50 m it turns out that only 1254 points have a

distance from the GNSS line  $\leq$  to 1 meter (37.65 % of the points), raising the tolerance to 2 meters results in 2257 values (67.77 %) being  $\leq$  to 2 meters, a value well over half. If we now do a reverse search and look for the largest values, for example, at 6 meters it follows that 20 points out of the total have distances  $\geq$  6 meters. We can therefore also conclude this comparison by saying that the results obtained show a marked improvement, but still far from the precision obtainable by GNSS and Total Station.



Graph 3 Comparison between GNSS and photogrammetric restitution (Barricata).

### 5.2.2.2 GNSS and PHOTOGAMMETRIC RESTITUTION (areas)

Having arrived at this point the results are quite clear, we now treat the procedure with areas in order to have a comparable figure with Boccasette, given the problems encountered with the distance method on the same. What we expect will be small areas, not at the level of the comparison with classical topography (Total Station) but not even the size seen on the same comparison for Boccasette.

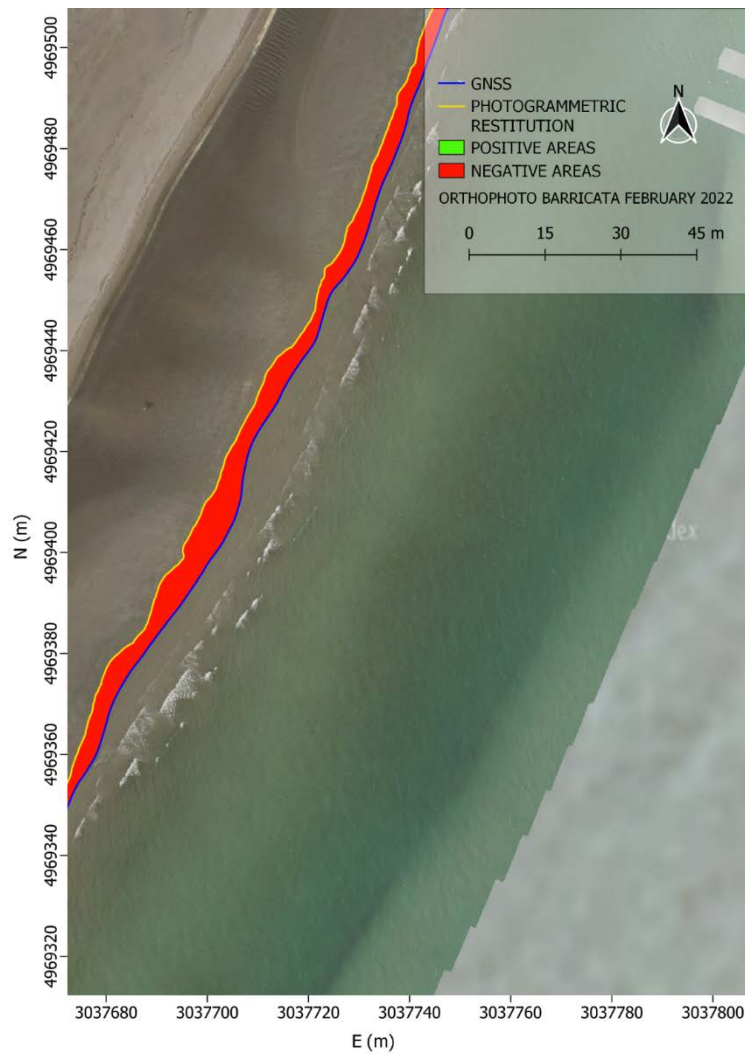


Figure 111 Areas with more intense wave motion.





Figure 112 Areas with milder wave motion.

Further confirmation on the disturbances can be seen from the figure above, in fact from image 111 it can be seen that along a band characterized by a more intense wave motion more difficulties were encountered, while in the next (Figure 112) the absence of waves allows for better restitution. So without divulging further let us now see the results obtained in this case; the whole areas present an average of  $-68.94 \text{ m}^2 \pm 313.78 \text{ m}^2$  standard deviation.

The results are certainly better than Boccasette but still far from the accuracy offered by the classical instrumentation used in comparison.

### 5.2.2.3 GNSS and CLASSICAL TOPOGRAPHY (distances)

Having reached this point, the approach of the study and the methodologies that are best suited for the survey under study are known. In the image to follow (Figure 113) we see that even for this measurement the classical topography (Total Station) gives a very good result, very close to the previous case, this confirms the preciseness of the method and the influence we can have in the measurements considering the aspects already discussed several times.

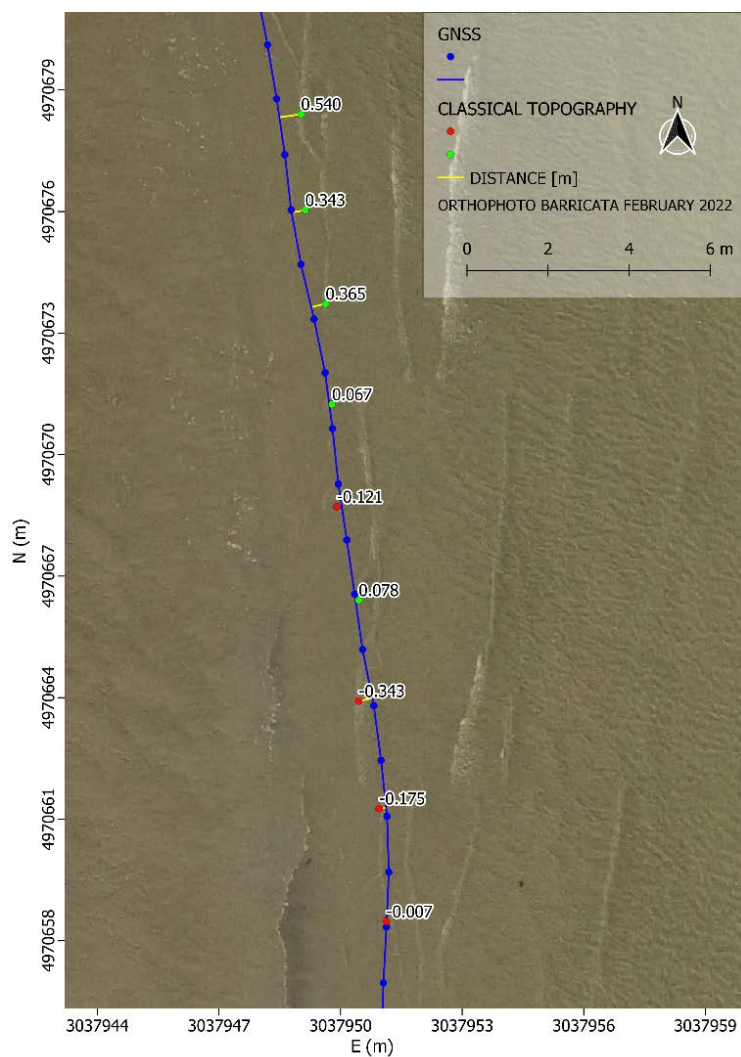


Figure 113 Excellent tracking between GNSS and Total Station.

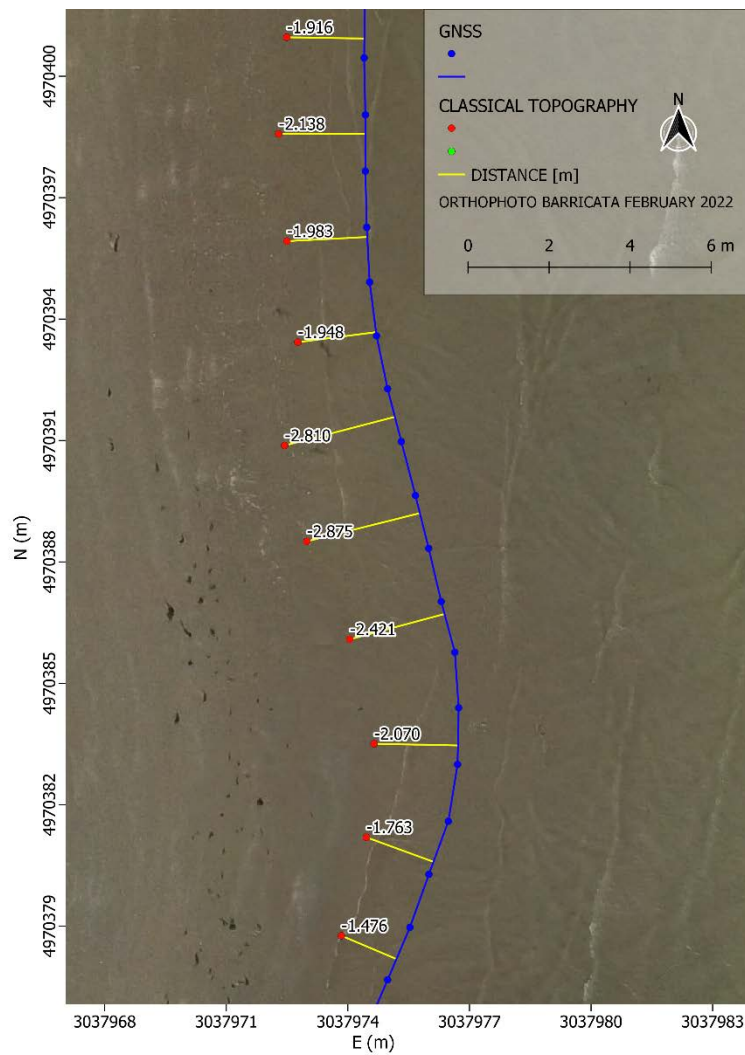


Figure 114 Localized points where deviation error increases.

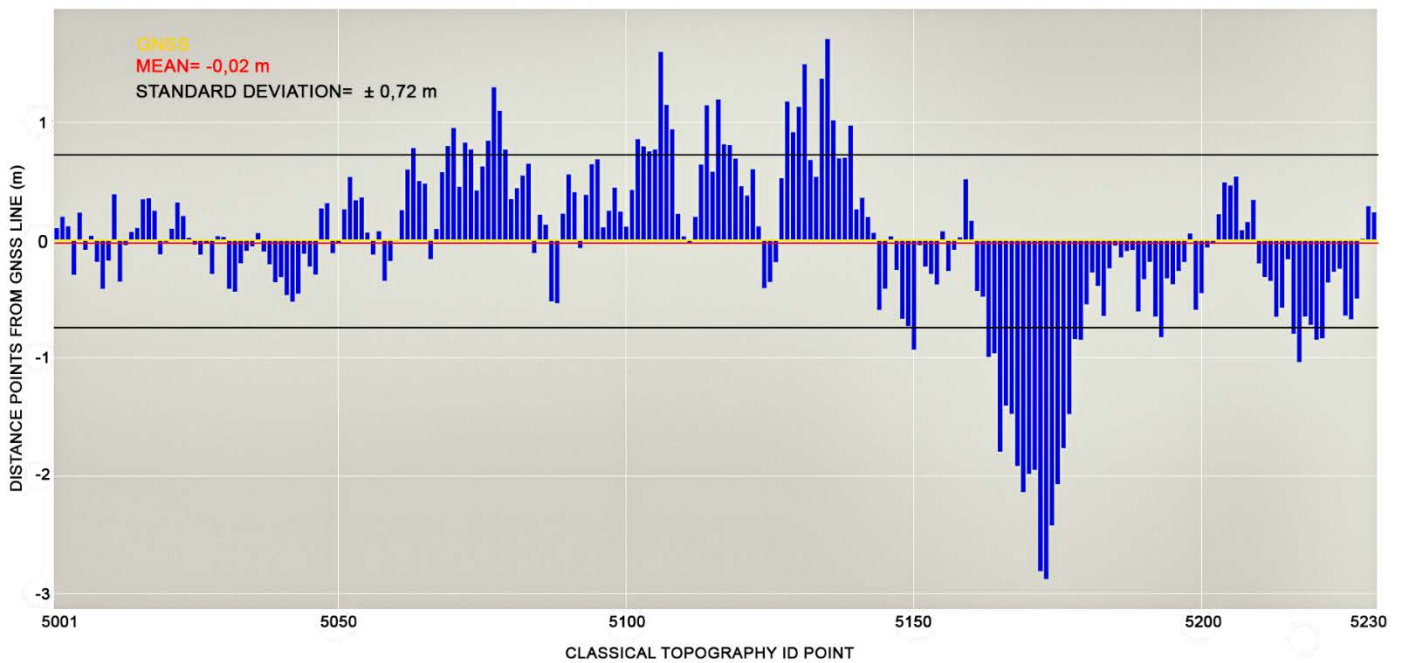
In the Figure 113 we see shown what are the minimum differences in the “second” image 114 the maximum deviation values.

In this comparison the points show an average in terms of distance of  $-0.02 \text{ m} \pm 0.72 \text{ m}$  standard deviation.

We report again on the following page the graph (4) containing the measurements and their results, highlighting the deviation of each point from the GNSS line considered as reference for the comparison. The analysis performed within QGIS on the 230 points obtained with classical topography (Total Station) indicates that 204

measurements are  $\leq 1$  m (88.69 % of the measurements) of the remaining 26 measurements 12 exceed 1.5 m and only 5 are greater than 2 meters with a maximum value of 2.87 m.

The results obtained in this case confirm the preciseness of the method for a detailed survey, showing values with low variability between Boccasette and Barricata, despite the fact that the measurements were made under different climatic conditions and operators.



Graph 4 Comparison between GNSS and Total Station (Barricata).

#### 5.2.2.4 GNSS and CLASSICAL TOPOGRAPHY (areas)

In this comparison as we expected the results are very good, with the set of areas showing a mean of  $-0.24 \text{ m}^2 \pm 15.99 \text{ m}^2$  standard deviation.

From the images to follow, specifically in figure 115 we see an area where the restitution shows a larger deviation and therefore returns a larger area, on the other hand in the areas with a slight deviation as in figure 116 we see very small areas for some cases approximating zero, indicating that the two survey lines are almost overlapping.

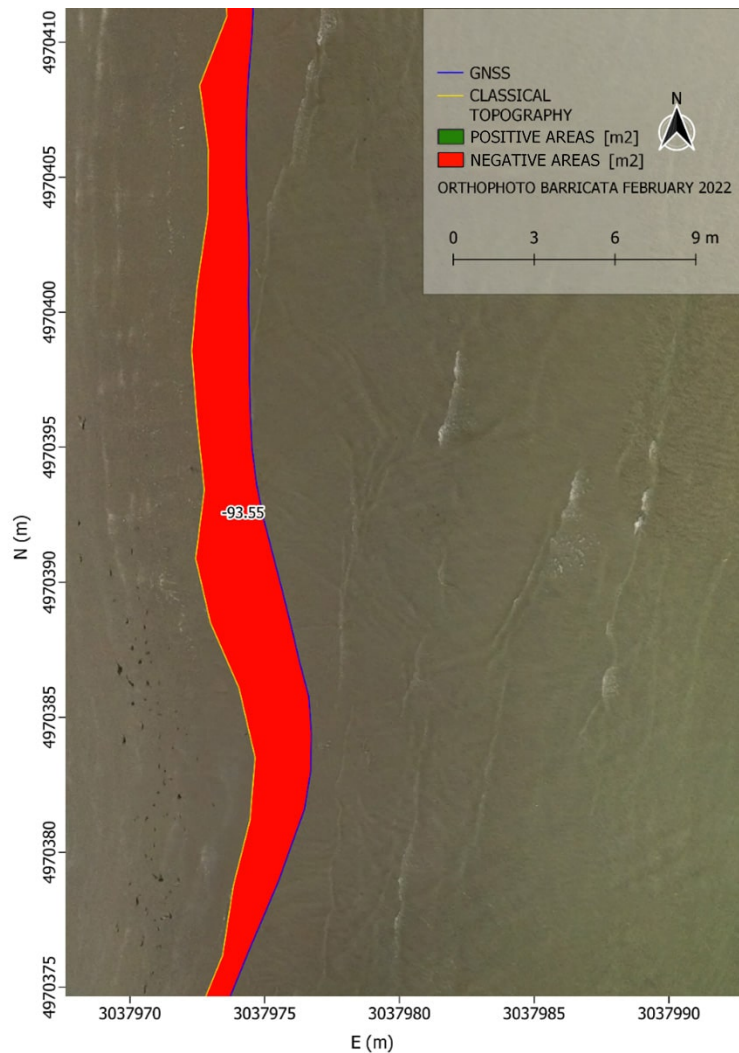


Figure 115 Negative area zone.

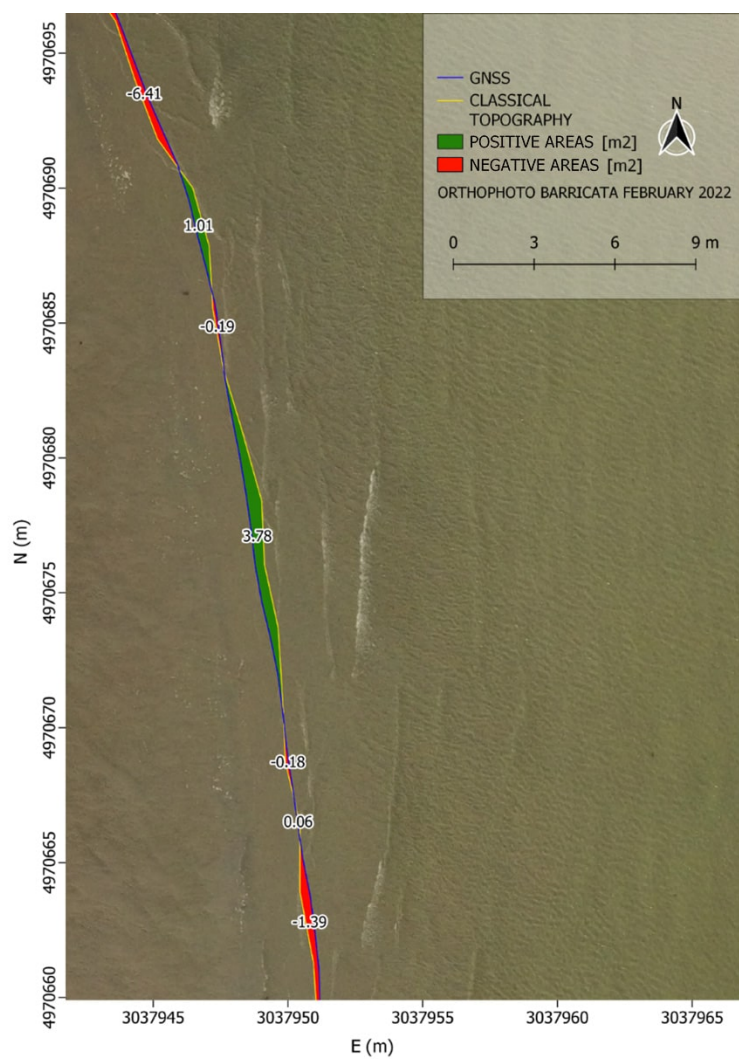


Figure 116 Area with good restitution.

### 5.3 Evaluation multitemporal analysis

In this section we focus on the location of the zero-line obtained with QGIS software through contour lines plotted on the DEM, and the zero-line obtained through LiDAR methodology from the year 2018. We are going to assess whether the areas under study are subject to significant coastal variation.

Next, we can see the graphical elaboration related to the comparison for Boccasette (Figure 117) and Barricata (Figure 118). From the legend on the tables, we distinguish in yellow color, the zero-line extracted from the LiDAR survey performed in the year 2018, in blue color instead, the zero line obtained using the DEM related to the Drone flight performed in January 2022. The area between the two lines represents the change in the area of interest. In this case we considered positive deposition (green area), when the zero line of 2022 is in the open sea direction compared to that of 2018, erosion the opposite case (red area).

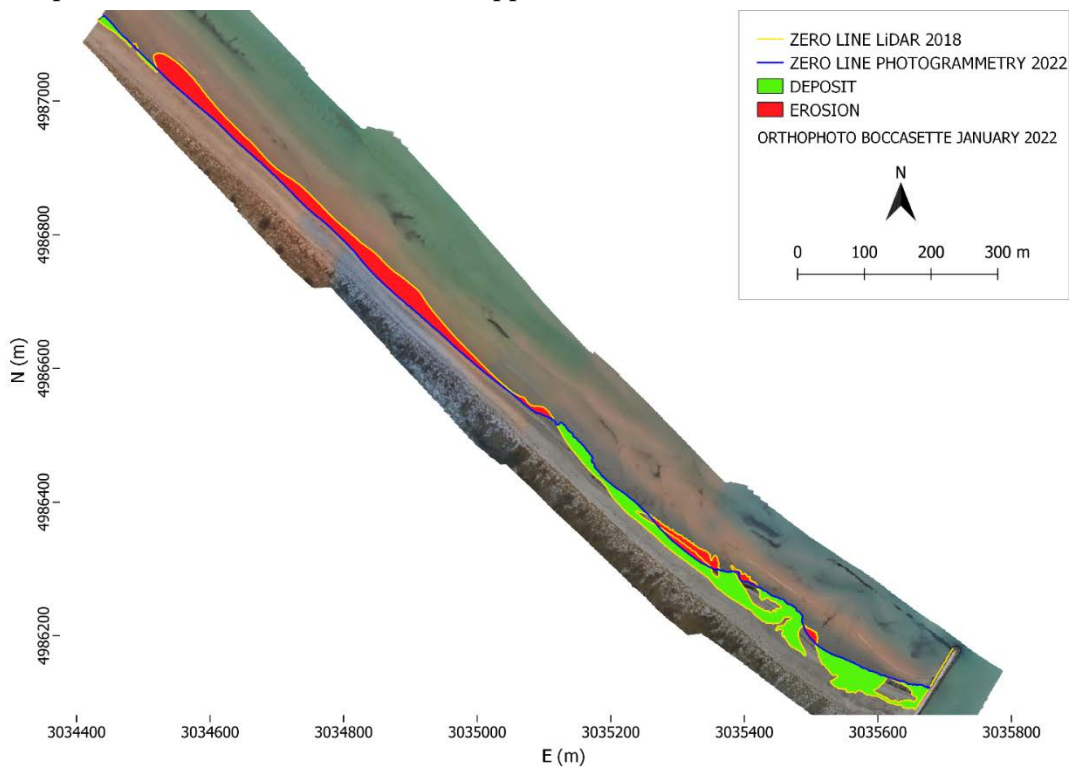


Figure 117 Multi-temporal study result for Boccasette.

For Boccasette beach (Figure 117) we found by calculation of areas an erosion zone of  $-14551.4 \text{ m}^2$ , and a deposition zone of  $13751.2 \text{ m}^2$ . So, through difference results a very slight erosion trend with a value of  $-800.2 \text{ m}^2$ .

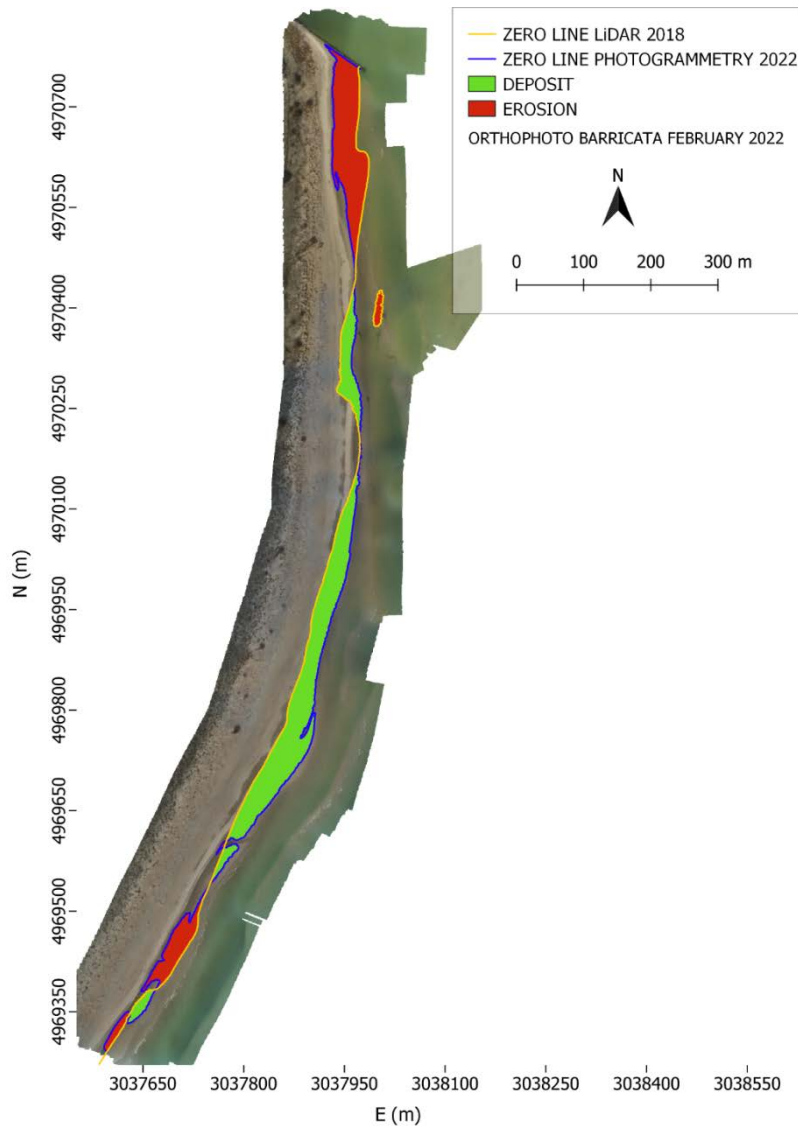


Figure 118 Multi-temporal study result for Barricata.

Similarly to what was seen for Boccasette, the areas in Barricata (Figure 118) were calculated, obtaining in this case a deposit of  $21782.9 \text{ m}^2$ , and an erosion of  $-14222.7 \text{ m}^2$ , it follows that there is a tendency to deposit material, especially as seen in the central part with a deposit area compared to 2018 of  $+7560.2 \text{ m}^2$ .



To conclude this partial analysis on the changes from the zero line we can consider the resulting results as a partial indicator. As can be seen the two areas under study provide us with two different results on one side we have an erosion trend (Figure 117) and on the other a deposition (Figure 118), it is therefore complicated, to express an account on the coastal variations of the two areas, also because the photogrammetric survey covers an area of less than half of the stretches for both Barricata and Boccasette, it follows therefore a limiting data. A description of coastal evolution requires analysis of fluvial and marine dynamics, in fact, the coasts receive most of the sediment that feeds the beaches via rivers from the lands that emerge. The sea is a major contributor to the formation of coastal structures through wave action and currents, fulfilling the threefold role of erosion, transport, and coastal sediment accumulation. Such oceanic modeling efforts can lead to coastal retreat when its erosional effects predominate, or coastal advancement if accumulation processes dominate, often both phenomena acting simultaneously on adjacent coastal areas. The extent of the coastal zone can be affected, sometimes significantly, by phenomena such as in the present case of subsidence. Subsidence as we have seen is a long-term process of slow lowering of the land, related to the natural compaction of fine sediments in floodplains, often aggravated by the extraction of water and hydrocarbons from underground. In addition, even abrupt changes in the coastline can be induced by tectonic movements, mostly associated with high-magnitude earthquakes.

The complexity of these issues is quite clear, thanks to the data obtained, comparisons in the coming years will make it possible to determine whether this phenomenon of erosion or deposition is in any way going to increase or decrease. For the moment what we can say especially for Boccasette, where the resulting area is small, is a substantial stability with variations probably related to sea currents.

High resolution geomatics techniques for coastline detection and monitoring:  
Boccasette and Barricata case studies (Po River Delta, Rovigo, Italy).

## 6 Conclusions and Future Developments

The thesis activity in this first phase led, thus to the composition of a picture, of the state of knowledge, at a higher scale of detail with respect to the erosion phenomenon and adaptation to climate change of the PRD coastline. As mentioned in the introduction section, the goal was to identify the topographic methodology most suitable for a detailed study of the coastline. Important element concerns the tide, in fact by carrying out the survey at low tide the sea surface is “flatter” and the coastline boundaries less dynamic, simplifying the survey, in identifying a line as accurate as possible. The comparison of the analyzed methodologies thus provided a basis for a more detailed study of the area, taking into consideration that in the near future one of the main factors that could increase the vulnerability of the coastal areas of the PRD including the protection structures are the effects of eustasy of the Adriatic Sea, in addition to the already known issue related to subsidence, thus increasing the risk of flooding. These large losses, in fact, could cause the rupture of the defense infrastructure, thus exposing fragile areas to the erosive activity of sea waves, resulting in an ever-increasing reduction of the margin of safety, thus bringing that area susceptible to frequent if not permanent sea flooding. Regarding the latter issue, although studies show that in recent years the phenomenon has been greatly reduced, it still results in a high subsidence compared to natural trends. As already mentioned sea level rise and anthropogenic activity, such as operations to make rivers navigable for tourism and fishing, certainly can only worsen this phenomenon, leading to the modification of natural processes.

It is important, therefore, to make as in this case a careful assessment since the considerable changes in the coastline have already caused the loss of vast areas of community importance in the Veneto Regional Park of the Po Delta. The choice of the two areas concerns their characteristics as we have seen in fact they are beaches that have not been remodeled by the hand of man, they have kept away from the establishments so as not to be affected by those works. The considerations on the results that will be discussed now will serve as a basis for an approach suitable for an increasingly accurate study, thus allowing, the adoption of mitigation measures in useful time to avoid significant changes in natural balances. In conclusion to this study we can therefore state that among the methodologies used the most limiting in

terms of coverage is the classical topography (Total Station), in fact as it could be seen from the images it allows a very high precision survey but over a very limited area. Is also a very expensive piece of instrumentation, requires positioning on a stable point and the intervention of two operators, one at the instrument and one at the prism, as we have seen from the photos, so it is not the most suitable for this type of survey. Then follows the SfM technique, which demonstrated superior coverage but several difficulties in drawing a line of detail, with a level of definition deemed insufficient to represent the phenomena of interest with the necessary accuracy. In fact, in the photogrammetric models, large differences arose, especially in the case of Boccasette, which greatly affected the final result. The problem exposed obviously is not to be attributed to the method but to the difficulty on the part of the operator in the phase of tracing the photos as we have been able to note, it results in fact from this study that the restitution of the detailed coastline on the photogrammetric models is not easy due to the clarity of the water in areas where the sea is calm and the bottom "flat.". Another disturbing element especially for Boccasette concerns the low illumination during the acquisition phase which greatly affected the quality of the final orthophoto, besides as already exposed several times the irregular geometry of the beach. Another interesting product obtained from photogrammetry concerns the multitemporal analysis for the study of zero line variation over the past 4 years compared with LiDAR 2018. The latter analysis would not have been possible so smoothly without a DEM. All this makes us realize that the product obtained through SfM allows multiple analyses through a single survey. It must be said, that the methodology of photogrammetry is very convenient compared to the others in that it allows photos to be taken on site and then measurements to be made directly in the office from them, thus allowing for simpler and less costly survey campaigns; it should also be considered that the instrumentation has a significantly lower cost than GNSS and Total Station.

Without divulging too much, it is therefore clear that the methodology that best appeals for a detailed survey of the coastline is the GNSS methodology in differential mode, which for the same amount of time allows a significantly higher coverage among the compared methods, perfectly following in the field the trajectory of the coastline without interruption. But even this methodology has a not inconsiderable cost and requires surveying directly in the field. However, it turned out to be an

interesting comparison to evaluate the spatial oscillation in acquisition by different operators at the instruments. Look at the results for GNSS and Total Station, they show values below one meter for almost all the measurements compared, which is the expected level of accuracy for a correct return of the coastline in the case of interest. For photogrammetry, on the other hand, there is still some work to be done before being able to obtain acceptable measurements, one might think of carrying out, coupled with the photogrammetric survey a thermal camera survey in order to be able to identify the temperature difference between sand and sea, short of the "battigia" area considered acceptable as wave-related variability. The thermal camera would also provide excellent support for all those areas of irregularities present in Boccasette that heavily affected the final error due to complex identification from photos.

The GNSS method favored in this study for selected areas in the PRD can be applied to multiple areas in order to obtain as much information as possible and create datums on the coastline that can then be compared years later to assess planimetric changes in detail. By then intersecting these results with research on sea rise, it will then be possible to assess which of the phenomena mentioned most affects the vulnerability of this area. As already mentioned an additional product obtained in this study concerns the multi-temporal analysis through the use of the DEM photogrammetric product, which allowed the extraction of the zero line for a comparison on the planimetric variations of the same with respect to the year 2018 who show us a substantial stability in the last 4 years.

The possibilities of analysis and possible future developments allow in this case increasingly accurate planimetric monitoring preventing and limiting damage to the local population including buildings, infrastructure, and land, improving the safety of the area through more sustainable urban development.

High resolution geomatics techniques for coastline detection and monitoring:  
Boccasette and Barricata case studies (Po River Delta, Rovigo, Italy).

## 7 Bibliography

- [1] Massimo Fabris, *Coastline evolution of the Po River Delta (Italy) by archival multi-temporal digital photogrammetry*, Geomatics, Natural Hazards and Risk, Department of Civil, Environmental and Architectural Engineering, University of Padova, Padova, Italy, February 2019, pp. 1007-1027.
- [2] Nicola Cenni, Simone Fiaschi, and Massimo Fabris, *Monitoring of Land Subsidence in the Po River Delta (Northern Italy) Using Geodetic Networks*, Department of Geosciences, University of Padova, UCD School of Earth Sciences, University College Dublin, Department of Civil, Environmental and Architectural Engineering—ICEA, University of Padova, April 2021, pp. 1-21.
- [3] Massimo Fabris, *Monitoring the Coastal Changes of the Po River Delta (Northern Italy) since 1911 Using Archival Cartography, Multi-Temporal Aerial Photogrammetry and LiDAR Data: Implications for Coastline Changes in 2100 A.D.* Department of Civil, Environmental and Architectural Engineering, University of Padova, 2021, pp.1-23.
- [4] Massimo Fabris, Vladimiro Achilli, Nicola Cenni, Simone Fiaschi, Mario Floris, Andrea Menin, Michele Monego, Paolo Riccardi, *Integrazione di dati SAR e GNSS per lo studio della subsidenza nel Delta del Po*, ASITA 2018, pp. 473-480.
- [5] ISTITUTO GEOGRAFICO MILITARE, Servizio Geodetico, *Nota Per Il Corretto Utilizzo Dei Sistemi Geodetici Di Riferimento All'interno Dei Software Gis*, Updated January 2022.
- [6] Pietro Colombo Lino Tosini, Giancarlo Mantovani, Gianfranco Zanetti, Annalaura Tezzon, Maurizio e Mauro Tezzon, *Sessant'anni di bonifica nel delta del Po*, Consorzio di Bonifica Delta Po Adige, 2009, pp.126-185.
- [7] Angela Barbano, Stefano Corsini, Massimo Paone, Claudio la Mantia, *Definizione della linea di costa italiana e delle opere di difesa*, APAT, Dip. Tutela delle Acque Interne e Marine, pp 1-6.

- [8] Mario Biolcati, *Piano Degli Interventi Proposta Di Trasformazione Urbanistica, Valutazione Di Incidenza Ambientale*, Comune Di Porto Tolle Provincia Di Rovigo, 2016, pp.7-8.
- [9] MATTM-Regioni con il coordinamento tecnico di ISPRA, *Linee Guida per la Difesa della Costa dai fenomeni di Erosione e dagli effetti dei Cambiamenti climatici*, Documento elaborato dal Tavolo Nazionale sull'Erosione Costiera, 2018.
- [10] Istituto Idrografico Della Marina, *Linee Guida Per Lo Studio E La Descrizione Ai Fini Cartografici Della Zona Costiera*, 2017, pp. 7-10-12-13.
- [11] Sara Carli, Luigi E. Cipriani, Deborah Bresci, Chiara Danese, Pierluigi Iannotta, Enzo Pranzini, Lorenzo Rossi, Lilian Wetzel, *Tecniche di monitoraggio dell'evoluzione delle spiagge*, Dipartimento di Scienze della Terra dell'Università degli Studi di Firenze; Regione Toscana - Direzione Generale delle Politiche Territoriali e Ambientali.
- [12] Regione del Veneto, *Piano di gestione – Delta del Po*.
- [13] Massimo Fabris, *slides of the course LAND SURVEYING AND GEOGRAPHICAL INFORMATION SYSTEM (GIS)*, 2020-2021.
- [14] AgisoftMetashape, *User Manual: Professional Edition, Version 1.5*, 2019.
- [15] QGIS Project, *QGIS Desktop 3.16 User Guide*, 2022.
- [16] Zanichelli, Cannarozzo, *Principi\_e\_strumenti\_fotogrammetria*, 2012.
- [17] Roberto D'Apostoli, Francesco Giampaolo, *Guida pratica al rilievo topografico con GPS e stazione totale*, 2018.



- [18] «Porto Brricata» [Online]. Available: <https://portobarricata.it/territorio/>. [Consulted April 2022].
- [19] «studioeidos» [Online]. Available: <https://www.studioeidos.it/index.php/barricata-nel-parco-delta-del-po-diventato-riserva-della-biosfera-unesco/> [Consulted April 2022].
- [20] «mokabyte» [Online]. Available: <http://www.mokabyte.it/2019/03/geolocmobile-1/> [Consulted April 2022].
- [21] «Autodesk» [Online]. Available: <https://www.autodesk.it/solutions/cad-software#:~:text=Il%20CAD%2C%20ovvero%20Computer%2DAided,manual e%20con%20un%20processo%20automatizzato.> [Consulted May 2022].
- [22] «openoikos» [Online]. Available: <https://www.openoikos.com/blog/le-basi-di-qgis-la-rappresentazione-della-terra-ed-i-sistemi-di-riferimento/> [Consulted May 2022].
- [23] «openoikos» [Online]. Available: <https://www.openoikos.com/blog/le-basi-di-qgis-i-sistemi-di-riferimento-piu-usati-in-italia/> [Consulted May 2022].
- [24] «3dmetrica» [Online]. Available: <https://3dmetrica.it/occhio-alla-quota/> [Consulted May 2022].
- [25] «3dmetrica» [Online]. Available: <https://3dmetrica.it/trasformazione-di-coordinat/> [Consulted May 2022].
- [26] «paolapozzolo» [Online]. Available: <https://paolapozzolo.it/deviazione-standard/> [Consulted May 2022].
- [27] «rhino3d» [Online]. Available: <https://www.rhino3d.com/it/features/> [Consulted May 2022].

High resolution geomatics techniques for coastline detection and monitoring:  
Boccasette and Barricata case studies (Po River Delta, Rovigo, Italy).

- [28] << agriregionieuropa>> [Online]. Available:  
*<https://agrireregionieuropa.univpm.it/it/content/article/31/37/cuneo-salino-fattore-limitante-il-delta-del-po>* [Consulted May 2022].



